STRESS MANAGEMENT USING PHYSIOLOGICAL SIGNALS AND AUDIO STIMULATION

by

Rateb Majd Katmah

A Thesis Presented to the Faculty of the
American University of Sharjah
College of Engineering
in Partial Fulfillment
of the Requirements
for the Degree of

Master of Science in
Biomedical Engineering

Sharjah, United Arab Emirates

November 2021

Declaration of Authorship

I declare that this thesis is my own work and, to the best of my knowledge and belief, it does not contain material published or written by a third party, except where permission has been obtained and/or appropriately cited through full and accurate referencing.

Signature ……Rateb Majd Katmah…….

Date……28-October -2021……..……

The Author controls copyright for this report.

Material should not be reused without the consent of the author. Due acknowledgement should be made where appropriate.

© Year 2021

Rateb Majd Katmah

ALL RIGHTS RESERVE

Approval Signatures

We, the undersigned, approve the master's thesis of Rateb Majd Katmah

Thesis Title: Stress Management Using Physiological Signals and Audio Stimulation

Date of Defense: 10-November-2021

Name, Title and Affiliation	Signature
Dr. Hasan Al-Nashash Professor, Department of Electrical Engineering Thesis Advisor	
Dr. Usman Tariq Associate Professor, Department of Electrical Engineering Thesis Co-Advisor	
Dr. Fares Yahya Postdoc, Department of Electrical Engineering Thesis Co-Advisor	
Dr. Gerassimos Barlas Professor, Department of Computer Science and Engineering Thesis Committee Member	
Dr. Hasan Mir Professor, Department of Electrical Engineering Thesis Committee Member	
Dr. AbdulRahim Shamayleh Program Coordinator Biomedical Engineering Graduate Program	
Dr. Lotfi Romdhane Associate Dean for Graduate Affairs and Research College of Engineering	
Dr. Sameer Al-Asheh Interim Dean College of Engineering	
Dr. Mohamed El-Tarhuni Vice Provost for Research and Graduate Studies	

Acknowledgements

First and foremost, I would like to express my heartfelt thanks to my supervisors, Prof. Hasan Al Nashash and Dr. Usman Tariq, for giving me this invaluable research opportunity and for guiding me through the many stages of the research. Their vast knowledge and skills inspired me to strive harder and try new things.

I would really like to thank Dr. Fares Al Shargie for being a helpful research mentor and for taking the time to answer all of my inquiries without hesitation. His contributions were critical in developing the study methodology, and his ideas were vital in molding and enhancing this thesis.

I am grateful to the Biomedical Engineering Graduate Program for providing me with a graduate scholarship to complete my master's degree. Special appreciation to the Biosciences and Bioengineering Research Institute for sponsoring this research endeavor. I would also like to thank all of the volunteers who gave up some of their time to participate in our research experiment.

Lastly, I would like to thank all of the field researchers who helped pave the road for our work. Their comments were invaluable as a guide and a source of inspiration.

Dedication

This thesis is dedicated to my family, who instilled in me the virtues of perseverance and commitment and relentlessly encouraged me to strive for excellence.…

Abstract

Stress has a significant role in the development of a wide variety of mental, psychological, emotional, behavioral, and physical illnesses. Additionally, there is substantial evidence in the literature that stress impairs vigilance. Thus, early stress detection, vigilance enhancement, and stress mitigation may aid in the prevention of a wide range of diseases and improve human health. The purpose of this thesis is to examine the effects of binaural beat stimulation (BBs) on increasing alertness and reducing mental stress in the workplace. We devised an experiment in which participants were subjected to time pressure and negative feedback while completing the Stroop Color-Word Task (SCWT). Then, we used 16 Hz BBs to improve vigilance and reduce stress levels. Functional Near-Infrared Spectroscopy (fNIRS), salivary alpha-amylase, behavioral data, and subjective reactions were used to determine the levels of stress. We quantified the level of stress using statistical analysis, functional connectivity based on Partial Directed Coherence (PDC), Graph Theory Analysis (GTA) and Convolution Neural Network (CNN). We discovered that BBs substantially increased target detection accuracy by 11.05% ($p<0.001$), decreased effort and temporal demand, boosted performance, and decreased cortisol levels. The deep learning results indicated that the CNN technique combined with PDC features is capable of discriminating between four distinct mental states (vigilance, enhancement, stress, and mitigation) with an average accuracy of 70.62%, a sensitivity of 68.39%, and a specificity of 90.76%.

Keywords: ***Mental stress; Vigilance enhancement; Stress mitigation; Stroop Color-Word Task (SCWT); Functional connectivity; Cortisol level; Functional near infrared spectroscopy (fNIRS); Partial Directed Coherence (PDC); Convolutional Neural Network (CNN)*****.**

Table of contents

List of Figures

List of Tables

List of Abbreviations and Symbols

BBS	Binaural Beats Stimulation
CNN	Convolutional neural networks
DNN	Deep neural networks
DOI	Difference of influence
ECG	Electrocardiogram
EEG	Electroencephalogram
EOG	Electrooculogram
fMRI	Functional Magnetic Resonance Imaging
fNIRS	Functional near infrared spectroscopy
GC	Granger Causality
GCE	Global cost efficiency
HRV	Heart Rate Variability
KNN	K-Nearest Neighbors
LDA	Linear Discriminant Analysis
MVAR	Multivariate auto regressive model
MVARM	Multivariate Auto-Regressive Model
OMST	Orthogonal minimal spanning trees
PC	Personal Computer
PDC	Partial Directed Coherence
PDC	Partial directed coherence
PFC	Prefrontal cortex
PLV	Phase-Locking Value
RSFC	Resting state functional connectivity
SCWT	Stroop Color-Word Task
SVM	Support Vector Machine
SVM	Support Vector Machines
TLS	NASA Task Load Index
TOT	Time on Task
VR	Virtual reality

Chapter 1. Introduction

In this chapter, we introduce the topic of stress assessment and mitigation. Following an overview of mental stress types, causes and associated illnesses, we introduce the thesis objectives and research contribution. Finally, the overall structure of the thesis is described.

1.1 Overview

Mental stress is widely considered to be one of the most challenging health problems. It is described as the human body's response, which is governed by the sympathetic nervous system (SNS) and the hypothalamus-pituitary-adrenocortical axis (HPA axis), to mental, physical, and emotional stimuli [1, 2]. This term can refer to internal (personality structure) or external (problem solving) issues that cause different physiological and negative emotional alterations [3]. Mental stress, in particular, has direct physiological consequences that contribute to a variety of illnesses such as cognitive difficulties, stroke, cardiovascular disease, speech abnormalities, and depression [4]. Furthermore, this complicated phenomena has indirect impact on the human body at several levels, including skin problems, lifestyle, insufficient sleep, and decision making [5-7]. Acute stress, episodic stress, and chronic stress are the three stress categories based on the duration of exposure to the stressor. Acute stress is caused by brief exposure and is not considered detrimental. Episodic stress occurs when the stimulus is more frequent over a shorter period of time [8]. Chronic stress is caused by long-term stresses and is thought to be the most damaging form [9]. Hence, early diagnosis of mental stress is an important component in the therapeutic intervention to prevent numerous health issues.

1.2 Thesis Objectives

Assessing mental stress is a difficult task because everyone handles stress differently [10]. The available techniques for detecting subjective experiences of mental stress are influenced by many systemic flaws, such as response bias (participants tend to respond properly using their preferred way). Similarly, the observed behavioral stress responses, such as body gestures and facial expressions, have some limitations due to conscious monitoring (purposed or slight). Neurologically, it is necessary to deliver appropriate

energy sources to muscles and nerve cells in order to serve adaptability to stress circumstances. As a result, the HPA axis (neuroendocrine unit consists of the hypothalamus, pituitary gland, and adrenal glands) stimulates the production and secretion of the three principal stress hormones (epinephrine, norepinephrine, and cortisol). Hence, according to Hellhammer et al.[11], cortisol levels are an acknowledged biomarker for quantifying stress levels.

Significant relation between physiological signals and body vital functions such as electrocardiogram (ECG), blood volume pulse (BVP), electrodermal activity (EDA), and electromyogram (EMG) has been investigated [12, 13]. However, in terms of consistency, validity, and efficacy in evaluating mental stress, these biosignals are heavily influenced by a variety of circumstances (including stress) such as illnesses, humidity, and ambient temperature. As more than just a result, they are unable to build the best method for predicting stress levels. Therefore, different neuroimaging methods provide an important tool for estimating neurophysiological activity associated with stress stimuli. One of the most discussed neuroimaging modalities is electroencephalography (EEG). It measures brain electrical activity in milliseconds and reflects it in real time. Nevertheless, insufficient spatial resolution on the scalp, poor detection of brain activity below the top cortical layers, and the inability to detect the precise sites at which various neurotransmitters are present are regarded as the primary drawbacks of EEG [14, 15]. In contrast, functional near infrared spectroscopy (fNIRS) gives better spatial resolution than EEG (but temporal resolution is more limited) and better temporal resolution than fMRI (but spatial resolution is more limited) [16, 17].

The other research challenge in stress management is stress mitigation which refers to the intentional use of medical, therapeutic, or technological interventions to improve behavioral performance and cognitive processing [18]. Stress mitigation and performance enhancers can be applied in two ways. The first one involves disabled function that is treated by therapeutic methods. The second one is used to improve the cognitive capacities for subjects.

As a result, this thesis covers two major issues that have a substantial impact on people's health. The first is detecting mental stress through physiological stress response analysis using fNIRS system. The second issue is determining the efficacy of using

binaural beat stimulation as a therapeutic factor in altering the cerebral hemodynamic response, which leads to vigilance enhancement and stress alleviation.

1.3 Research Contribution

The purpose of this study is to analyze the changes in cerebral connectivity of fNIRS signals between different brain regions as a result of using a stress-induced test. This mechanism, in particular, is based on variations in haemoglobin concentrations (brain connectivity) during various stress conditions. We propose that fNIRS signals could be utilized to categorize mental stress by detecting hemodynamic responses from the pre-frontal cortex (PFC) which is very sensitive to stress, according to Arnsten et al. [19]. To put the theory to the test, a computerized version of the Stroop Color-Word Task (SCWT) is used to raise stress levels. Additionally, we hypothesize that binaural auditory beat stimulation might reduce mental stress. In this regard, we will investigate binaural beat stimulation at 16 Hz as a stress-reduction approach for synchronization of a specific brain rhythm. To quantify functional coupling between brain regions under the stress phases, a PFC hemodynamic signal is examined using an autoregressive model, which is the partial directed coherence (PDC) with graph theory analysis (GTA). Hence, the directionality of information flow between the two hemispheres under separate stress states would be reflected by analyzing the PDCs. The proposed procedure is depicted in Figure 1.1 as a flow chart.

1.4 Thesis Organization

The rest of this thesis is organized as follows:

Chapter 2 provides an overview for the different methods that have been used in detecting and mitigating mental stress. Several behavioural, psychological and physiological techniques are discussed in addition to the fNIRS method and its relation to the other neuroimaging techniques in analysing brain activity.

The proposed methodology is discussed in Chapter 3, specifically the experimental protocol to stimulate stress levels, the approach to recruiting and selecting subjects, the experiment apparatus to record fNIRS signals, the pre-processing algorithm, and the fNIRS data analysis based on functional connectivity.

The fourth chapter presents a thorough analysis of the data linked to alpha amylase levels, behavioral data, subjective data, connectivity strength/directionality of

information flow, graph theory analysis measures, and applied deep learning. Full-scale GTA at the global level is performed in various auditory situations to investigate potential enhancement and mitigation effects.

This thesis is concluded in Chapter 5 with a review of significant research findings and recommendations for future study areas.

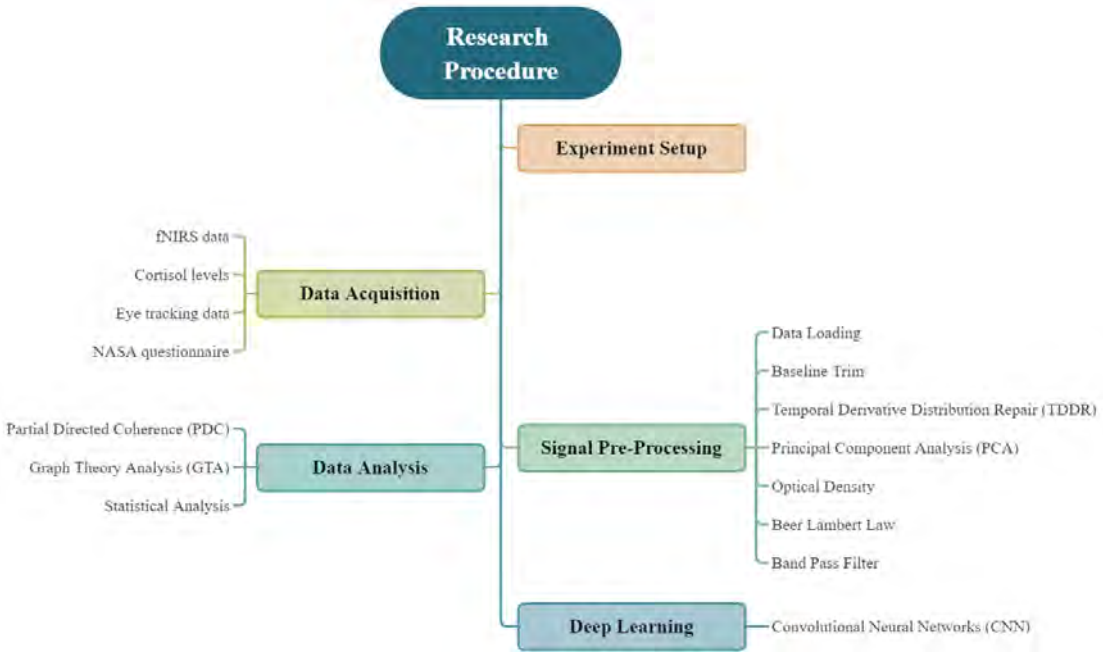

Figure 1.1: Flow chart of the various steps used for stress detection and fNIRS analysis.

Chapter 2. Background and Literature Review

This chapter provides a comprehensive description of the approaches utilized in the identification and alleviation of mental stress. First, a general overview of several psychological, behavioural, and physiological approaches is provided. Then, a comparison of Functional Near-Infrared Spectroscopy (fNIRS) and other neuroimaging techniques is performed. Following that, a full overview of several strategies for cognitive enhancement and stress mitigation is explored. Finally, a variety of fNIRS research domains and criteria will be described.

2.1 Mental Stress Assessment

Several studies have been conducted to explain and analyze human bodily responses, including nervous system adaptation to deal with an impending threat (stressor). Many scholars have recently focused on acute stress and its consequences on psychological and mental aspects. Self-report questionnaires [20] such as the perceived stress scale [21], are the most commonly used approach for quantifying stress level. Various research have established questionnaire scores and self-report ratings as a ground truth that is used as a reference to explore the precise stress state level. The necessity for such testimony stems from some participants' subconscious behaviour (they cannot accurately identify their stress level) [22]. As a result, the fundamental drawback is its reliance on the participant (subjective technique) [23, 24].

Furthermore, different physical measurements, such as body motions, skin temperature, thermal infrared imaging, electromyogram, respiration rate, electrodermal activity, heart activity, and blood pressure, have been shown to indicate stress levels. According to various scholars, experiencing stressful conditions causes decreased movement of the upper limbs as well as greater head mobility and shaking [25-27]. Marazziti et al. [28] investigated higher temperature during stress phases, whereas Kaufman et al. [29] discovered that observed temperature varies among body sections. Recent research has used infrared thermal cameras to measure increased facial temperature, which is strongly influenced by increased blood flow during stress [30, 31]. Likewise, Pavlidis et al. [32] examined temperature variations in the periorbital region, whereas Hong et al. [33] and Engert et al. [34] offered different metrics for the forehead and nose, respectively.

Additionally, elevated stress levels stimulate the sympathetic nervous system (SNS), which regulates muscle activation and contraction. An electromyogram (EMG) could be used to measure muscular tension by detecting the action potential of the stimulated muscle [35]. Healey et al. [13], Lundberg et al. [36], Cacioppo et al. [37] and Wijsman et al. [38] have demonstrated enhanced muscular response due to triggered stress phases using Stroop Color-Word Task (SCWT) and mental arithmetic task by employing detectors placed on trapezius or forehead muscles.

Similarly, monitoring the rate or amount of air that may be exchanged by the lungs is thought to be an indicator of mental stress [39]. Depending on the level of stress (relaxation or tenseness), this scenario will increase, reduce, or produce stoppage and arbitrary variations in respiration and breath rate [40-42]. In particular, Hosseini et al. [43] discovered that integrating breath rate data with other physiological markers improves stress detection accuracy.

Electrodermal activity (EDA) is another physical measure used in stress detection that evaluates skin electrical activity in order to distinguish the conductivity level (CL) and conductivity response (CR). During stress recognition procedures, these two characteristics exhibit regular fluctuations. Several studies revealed effective increases in CL and CR levels during stress phases as a result of increased epidermal moisture [44-46].

As previously stated, mental stress triggers the SNS, which initiates the fight-or-flight response, resulting in increased blood flow and heart activity. The electrocardiogram (ECG) and its central contraction peak (QRS), which represent ventricular contraction, depict this activity. In the meantime, ECG analysis is performed by calculating heart rate (HR) (number of beats per minute) and heart rate variability (HRV) (the distribution of RR interval over time). Several studies used these simple and reliable magnitudes and found increased rhythm for HR and HRV [47-50]. Cardiac muscle contraction causes high pressure to build up in the arteries, which is measured by systolic (SBP) and diastolic blood pressure (DBP). Activated SNS during stressors causes vasoconstriction and increased cardiac output, indicating elevated blood pressure (hypertension). The main disadvantage is that it is highly sensitive to numerous

conditions (such as cardiovascular illness), making pressure measurement dependent on the type of stressor [51, 52].

Since stress originates in the amygdala, which influences the autonomic nervous system response, these assessments may yield positive results [53]. Nonetheless, physiological markers are influenced by a variety of factors (including stress), for example, measuring hormone levels (such as cortisol) is affected by circadian rhythm (its concentration changes throughout the day) [54, 55], physical activity affects salivary alpha amylase level [56, 57] and EDA is sensitive to skin disease and humidity [58].

On the other hand, many neuroimaging techniques, such as electroencephalography (EEG), positron emission tomography (PET), and functional magnetic resonance imaging (fMRI) are used for this purpose, but all of them have implementation difficulties in order to obtain accurate results, particularly when dealing with real-life stress monitoring [59-61]. EEG is one of the most often discussed neuroimaging technique. It measures the electrical activity of the brain in milliseconds and reflects it in real time. However, the main limitations of EEG are regarded to be low spatial resolution on the scalp, poor detection of neural activity that occurs below the upper cortex layers, and the inability to detect the exact places at which distinct neurotransmitters are located [14, 15]. Meanwhile, fMRI delivers striking views of cortical activity. Despite the high spatial resolution of fMRI, the images produced and the statistical methods utilized must be carefully analysed to avoid false positives. Moreover, fMRI is a relatively expensive technique with a low temporal resolution that has difficulty discriminating several events in a short period of time [62, 63]. In comparison, functional near infrared spectroscopy (fNIRS) promises an alternate method of detecting mental stress because it has better spatial resolution than EEG and better temporal resolution than fMRI [16, 17]. Conversely, only few researches have used this technique individually [64], while the majority have combined it with EEG and ECG [65, 66].

2.2 Functional Near Infrared Spectroscopy (fNIRS)

FNIRS is a non-invasive technique for observing brain activity. It works by measuring changes in the cerebral hemodynamic response (blood flow and oxygenation) of an intact skull after infrared light with a wavelength of (650 – 950 nm) is applied to the

head via multiple light emitters [67, 68]. This wavelength range is chosen due to the prominent absorption of oxygenated (ΔHbO) and deoxygenated (ΔHbR) haemoglobin, which can be determined by measuring light scattering across brain areas as a result of specific neuronal activity [69]. The received signal strength will be determined in particular by photodetectors and emitters that establish channels for converting the fNIRS signal to changes in concentration of ΔHbO and ΔHbR [16]. In comparison to other neuroimaging techniques such as EEG, fMRI and PET, fNIRS has the fewest limitations and hence has the potential to be used as a substitute neurophysiological strategy for stress phase detection. Additionally, fNIRS systems have less needs, particularly for preparation and calibration, than conventional EEG systems [70]. Amidst having a higher temporal resolution than fMRI and PET, EEG measurements have a low spatial resolution [71]. Meanwhile, EEG mobility characteristics are fair in comparison to fMRI and PET mobility challenges, which need a highly regulated laboratory environment and strict criteria for study participation [72]. On the contrary, fNIRS is classified as a major system to analyse the cortex of the brain under mental stress and workload with reduced calibration efforts, high spatial resolution and low sample frequency (less than 20 Hz) [73-75]. The adaptability of various head positions with the customized fiber optics results in a minimal fNIRS setup effort [16]. It is also worth noting that although EEG signals are very susceptible to motion artifact (and hence require extra filtering, processing, and analysis), fNIRS motion artifact resistance ensures that the signal quality remains stable, while reducing the influence of artifacts [75]. Table 2.1 compares fNIRS, EEG and fMRI results based on past research.

2.2.1 FNIRS studies

There have been numerous neuroimaging studies that have used fNIRS as the principal method for identifying cortical activity utilizing a variety of characteristics, stressors, and brain areas. Using several virtual training scenarios, Shi et al. [80] explored the impact of mental stress on workers and found that there was a large increase in the prefrontal cortex connectivity, which was then used to detect stress at a rate of 80% accuracy. Meanwhile, Mucke et al. [81] used fNIRS and the Trier Social Stress Test (TSST) as a stressor to examine the impact of psychosocial stress on cognition. Furthermore, the results of Gurel et al. [82], Al-Shargie et al. [2, 83] and Shirvan et al. [84] convincingly proved the fNIRS's capability as a crucial tool for early diagnosis

Table 2.1: Comparing fNIRS, EEG and fMRI neuroimaging techniques [75-79].

	fNIRS	**EEG**	**fMRI**
Spatial resolution	Moderate	Poor	Good
Temporal resolution	Moderate	Good	Poor
Restriction of bodily movements	Good	Moderate	Poor
Continuous, long-time measurement	Good	Moderate	Poor
Application cost	Good	Good	Poor
Mobility	Mobile	Mobile	Not mobile

and stress quantification based on statistical analysis after utilizing an arithmetic task as a stressor. Likewise, other research used the fNIRS system in conjunction with an EEG system to enhance classification performance when identifying mental stress [85] and Alzheimer disease [86]. Similarly, the fNIRS approach has been used with people of various ages, such as monitoring new-born language development [87-89] or assessing employees' stress levels, decision making, and cognitive reaction in a construction site [90-92]. Meanwhile, a variety of research discussed cognitive testing [93], multimodal validations [94], clinical studies [95] and pediatric populations [96]. Besides that, some studies encountered problems, particularly for task conditions including range of motion [97] and real-world testing [98]. Additionally, one of the key stressors in correctly generating stress is the use of virtual reality (VR) technology, which is adaptable to a variety of events and tests [99-101]. Table 2.2 highlights several of these reviews that used the fNIRS approach to assess brain activity for various reasons. The table depicts the stressor used to induce stress, the neuroimaging technique used in conjunction with fNIRS, the brain region of interest, and the features used to analyze fNIRS signals. The outcomes of the study [80] established a negative correlation between individuals' performance and neurophysiological parameters such as gaze movement patterns. Amiyangshu et al. [102], on the other hand, discovered a positive link between cognitive load and attained performance score. Furthermore, the

strategy presented by Chan et al. [103] improved the differentiation approach for diagnosing Alzheimer's disease. The study [82] used a combination of fNIRS and photo-plethysmography and discovered many improvements in the categorization of different stressors. Meanwhile, Parent et al. [104] combined fNIRS and ECG to achieve the highest accuracy in measuring mental workload. According to one research [105], spatial overlapping is not required for maximal activation of the cortex and functional coherence.

2.2.2 FNIRS connectivity features

Feature extraction is a critical step in obtaining meaningful information about a signal, since it identifies required characteristics or feature vectors that represent a pattern vector [106, 107]. The fNIRS signal is composed of information from a dense network of linked neurons. Studying brain connections may thus give an accurate view of the brain's structure and how various areas communicate with one another. There are two types of brain connectivity: functional and effective [108, 109]. Functional connectivity (FC) is a term used to describe the connections between different parts of the brain based on the temporal coherence between the activities of multiple neurons. The cross correlation between the spike trains of neurons may be used to identify it. Numerous techniques for estimating functional connectivity have been developed, and all of them lead to the same conclusion: whether two or more brain units communicate or not. Effective connectivity, on the other hand, is the most basic circuit for describing a neuron's ability to maintain the same temporal relationship between two neurons as has been shown in experiments. It describes how the nervous system affects the rest of the body [110]. Functional connectivity has a non-directional and correlative character, while effective connectivity examines the directed effects between various brain areas. As a result, understanding functional connections across brain regions helps us understand functional connectivity under stress and under non-stress circumstances [111]. Brain activity could be represented as a network using fNIRS connectivity analysis, with nodes (vertices) linked through connections (edges) [112]. When doing a channel-by-channel analysis, the nodes correspond to the fNIRS channel and the connections correspond to the calculated connectivities between pairs of channel signals. Depending on the connectivity metric used, the edges may be either directed or undirected. Graphs or adjacency matrices may be used to represent functional networks.

The effectiveness of each of these techniques of visualization is determined on the analysis's goals. Topological connections may be shown using graphical techniques because they retain information about the relative spatial positions of the nodes. Adjacency matrices, on the other hand, are more suited for vast networks, but they do away with any spatial characteristics [112]. It is worth noting that undirected edge networks contain symmetric adjacency matrices. To save just the most important edges, thresholding may be used once the connectivity network is constructed (either directed or undirected). After then, various graph-theoretic metrics may be used to describe the network's topological properties.

2.3 Mitigation of Stress

Because there aren't any well-established procedures for dealing with stress, stress management has remained marginal in medical practice despite the grave implications on the human body, particularly on the Autonomic Nervous System (ANS). Therefore, the purposeful use of medicinal, therapeutic, or technological interventions to improve behavioural performance and cognitive processing is referred to as stress mitigation [18]. Several studies in the literature have explored numerous cognitive enhancers that reduce mental stress. Some of these stress-reduction techniques are commonplace and are frequently incorporated into everyday living routines such as sports [113, 114], diet and herbal extracts [115], meditation [116], odor exposure [117, 118], yoga [119, 120], chewing gum [121], and caffeine [122]. The use of unusual methods for mitigating stress has also been documented in research like those that used cognitive workload modulation [123], video games [124, 125], transcranial current stimulation [126, 127], haptics [128-130], pharmaceuticals [131], and stress alleviating biofeedback [132, 133]. Thus, as an alternative, we can manage physiological changes and monitor stress mitigation in real time using the biofeedback (BFB) method. However, neurofeedback (NFB) method employs real-time recordings of brain activity to improve self-regulation of certain brain processes associated with behavior [134, 135]. EEG, fMRI, and fNIRS are the most widely utilized NFB methods [136]. The basic idea is that by brain training with such feedback, one may entrain, alter, and regulate neural activity. Nevertheless, due to a lack of efficient regulation of brain training activities, the majority of BFB and NFB research were scarcely transferred from cognitive neuroscience lab to real-life

practices. While these types of mitigation approaches provide real-time input, they are not appropriate for use in the workplace.

Many studies have focused on utilizing auditory stimulation using binaural beats to enhance neural connectivity and reduce stress levels. Binaural beat stimulation (BBS) has been used in studies [137-139] to improve alertness. Meanwhile, Isik et al. [140] and Beauchene et al. [141] have shown that synchronization of brain signals and BBS causes particular changes in the mental and cognitive state. Similarly, Reedijk et al. [139] showed that BBS had a substantial influence on subject control and visual attention, whereas Lorenza et al. [142] discovered that BBS with a high frequency (40 Hz) tend to diminish participants' attentional processing. High-frequency binaural beats are associated with alertness, while low-frequency beats are associated with mental relaxation, according to Vernon et al. [143]. Alternatively, Goodin et al. [144] discovered no improvement in the mental state or performance after using BBS.

The purpose of this research is to analyse the changes in cerebral connectivity of fNIRS signals between different brain regions as a result of using a stress-induced test. This mechanism, in particular, is based on variations in haemoglobin concentrations (brain connectivity) during various stress conditions. We propose that fNIRS signals could be utilized to categorize mental stress by detecting hemodynamic responses from the pre-frontal cortex (PFC) which is very sensitive to stress, according to Arnsten et al. [19]. To put the theory to the test, a computerized version of the Stroop Color-Word Task (SCWT) is used to raise stress levels. Additionally, we hypothesize that binaural auditory beat stimulation might reduce mental stress. In this regard, we will investigate binaural beat stimulation at 16 Hz as a stress-reduction approach for synchronization of a specific brain rhythm. To quantify functional coupling between brain regions under the stress phases, a PFC hemodynamic signal is examined using an autoregressive model, which is the partial directed coherence (PDC) with graph theory analysis (GTA). Hence, the directionality of information flow between the two hemispheres under separate stress states would be reflected by analysing the PDCs.

Table 2.2: Previous fNIRS related studies.

Ref	Year	Research field	Stressor	Method	Region of Interest	Features	Notes
[145]	2021	Stress-related Exhaustion Disorder (ED)	Stroop-Simon test	fNIRS	Prefrontal cortex	Statistical analysis	ED patients perform similarly on behavioural measurements, they process information differently in the prefrontal cortex.
[146]	2021	Stress effect on patients with Major Depressive Disorder (MDD)	Trier Social Stress Test (TSST)	fNIRS Heart rate Cortisol	Bilateral dorsolateral prefrontal cortex (DLPFC), bilateral inferior frontal gyrus (IFG) and superior parietal lobule (SPL).	Statistical analysis	Prefrontal hypoactivity in stress mediates the development of affect-driven rumination in MDD subjects.
[147]	2021	Impact of COVID-19 restrictions on mental health	Videos	fNIRS	Frontal and occipital cortex	General Linear Model (GLM)	COVID-19 contributes in decreasing brain hemodynamics.
[148]	2021	Workplace design-related stress	Montreal Imaging Stress Task (MIST)	fNIRS EEG	Prefrontal cortex	Functional connectivity: Intersite phase clustering (ISPC)	Decreased inter-hemispheric connectivity for non-ergonomic workstation group.
[149]	2021	Effects on noisy workplace on brain activity	Montreal Imaging Stress Task (MIST)	fNIRS EEG	Prefrontal cortex	Statistical analysis	Decreased oxygenated haemoglobin with high noise levels.
[150]	2020	Mental stress for athlete	Stimulation film	fNIRS	Prefrontal cortex	Statistical analysis for the hemodynamic response	-

[151]	2020	Quality analysis of HR derived from fNIRS in stress assessment	MIST	fNIRS ECG	Prefrontal cortex	Statistical analysis Independent Component Analysis (ICA)	The extracted HR from fNIRS is brain-related response and it indicates mental stress
[152]	2020	Workplace design-related stress	MIST	fNIRS EEG	Prefrontal cortex	Canonical correlation analysis (CCA)	CCA identified workstation types with a maximum accuracy of 98.8% with an improvement with 9.4% for fNIRS
[80]	2020	Mental stress for workers	Virtual training scenarios	fNIRS eye tracking	L/R dorsal lateral prefrontal. L/R primary motor. L/R premotor	Functional connectivity: - Covariance of ΔHbO - Correlation coefficients	Significant increases in connectivity strength. Random Forest classification 80.38%
[103]	2020	Alzheimer	Verbal fluency test (VFT)	fNIRS	Prefrontal cortex	Functional connectivity: Pearson correlation (OMST, GCE)	-
[102]	2020	Cognitive lagging in working memory	Visuo-spatial task	fNIRS	Prefrontal cortex	Mean; variance; skewness; kurtosis of ΔHbO. Correlation (r)	Ensemble classifier
[82]	2019	Mental stress	rest, mental arithmetic, and N-back memory	Headband NIRS	Prefrontal cortex	Statistical: - ANOVA	Random forest classifier

						- Benjamini-Hochberg	
[2]	2019	Mental stress	MIST	fNIRS	Right/dorsolateral Prefrontal cortex	P-value / t-test topographical map	-
[86]	2019	Alzheimer	Digit verbal span task	fNIRS EEG	-	Statistical analysis: GLM Connectivity: Phase Lag Index (PLI)	Connectivity within the beta frequency range showed greater suppression in the AD group than in the healthy group.
[104]	2019	Mental stress and workload	n-back task Mental arithmetic	fNIRS ECG	Lateral/medial prefrontal cortex	64 fNIRS features from: Average changes and slopes for HbO2 and HHb	Naive Bayes classifier 47%
[84]	2018	Mental stress	Mental arithmetic task	fNIRS	-	linear features (statistical). Non-linear: approximate entropy, fractal dimension, detrended fluctuation.	-
[105]	2018	Cortical activation/ connectivity	Visuospatial working memory task	fNIRS	Front-parietal	Wavelets transform coherence	Coherence was greater within the parietal compared to prefrontal.
[153]	2017	Reduce false discovery in static modes	-	fNIRS	-	Correlation, Prewhitened wavelet	-

						coherence, Preweighted correlation, Numerical Simulations	
[154]	2017	Study brain network	Finger-tapping task.	fNIRS	Premotor, dorsolateral, orbitofrontal, motor	Effective connectivity: Time-resolved partial directed coherence	Specify the direction of the link between two regions of interest (gives info about dynamic, not only mean connectivity)
[155]	2017	Mental workload	Aircraft piloting tasks	fNIRS	Prefrontal cortex	correlation analyses, ANOVA … Averaging	-
[85]	2016	Mental stress	MIST	fNIRS EEG Salivary	Prefrontal cortex	Amplitudes of ΔHbO & ΔHb Topographical maps	- Concentration change in O2Hb returns to their baseline at the end of rest condition. - SVM: 84.1%
[156]	2016	Evaluate the feasibility of NIRS-based EC BCIs	Mental arithmetic	fNIRS	Prefrontal cortex	Mean, average slope of the ΔHbO & ΔHb	LDA 75.60% closed eyes 77.00% Open eyes
[157]	2016	Compare the classification accuracies	Mental arithmetic	fNIRS	Prefrontal cortex	Mean, variance, skewness, kurtosis of ΔO2Hb	SVM (89.80%) ANN (89.50%) KNN (69.70%)

[158]	2015	BCI/fNIRS relation	Mental arithmetic	fNIRS	Prefrontal cortex Motor cortex	Mean and slope of O2Hb	-
[159]	2014	BCI/fNIRS relation	Mental arithmetic	fNIRS	Prefrontal cortex	Mean value of O2Hb, HHb and Ht	LDA (70.00%)
[160]	2014	Hemodynamic activity	SCWT	fNIRS	Prefrontal cortex	Functional connectivity: Wavelets transform coherence (WTC)/ Spearman correlation. Effective connectivity: Granger causality	Correlation results: greater negative correlation between response time and the left PFC
[161]	2014	Mental workload	Computer-based piloting task.	fNIRS HRV	Prefrontal cortex	Mean HbO2 concentrations. ANOVA [processing load (low vs. high) and control difficulty (easy vs. hard)].	-
[162]	2010	Resting state functional connectivity (RSFC)	Motor-localizer task	fNIRS	Sensorimotor and auditory cortexes	RSFC: -Seed-based correlation analysis - Data-driven cluster analysis.	-

Chapter 3. Methodology

This chapter goes into great depth and details the experimental procedure and how to elicit and alleviate stress. It also gives details on the technique used to choose and recruit individuals, the kind of stressor, the experimental equipments used to capture and record fNIRS and behavioral data, and the data analysis methods.

3.1 Experimental Protocol

3.1.1 Subjects

Thirty healthy volunteers from the American University of Sharjah were recruited for the study (5 females and 25 males; aged between 20 and 41 years old). Eligible participants were healthy right-handed people with normal vision, hearing and color perception who have not used any long-term medicine or had any evidence of drug addiction, and who have not had any coffee, energy drinks or alcohol for at least 12 hours before to the experiment. Everyone was seated in a plush chair in a cool area with plenty of ventilation. In addition to the detailed information on the task's purpose, each participant also saw PowerPoint slides with a brief summary of the experiment's process, as well as a statement stating that they had the right to quit the session at any time. Prior to the test, the individual signed a typed word file consent form with their name as a signature. To avoid the effects of circadian rhythm on cognitive function, the experiment was only conducted between 1 and 5 p.m [163]. The American University of Sharjah's Institutional Review Board authorized the study's protocol, which was created in accordance with the Helsinki Declaration.

3.1.2 Mental stress task

Stroop Color-Word Task (SCWT) was utilized as a stressor. It is based on the monitoring of six different color words that are shown in a random sequence ('Magenta', 'Green', 'Yellow', 'Red', 'Cyan', and 'Blue'). The displayed word on the computer screen was printed in a different color ink than the meaning of the word, and the correct response is the color of the typed word (for example, the word "Blue" is written in yellow, therefore the correct answer is "yellow" word). In this incongruent example, subjects were supposed to call the ink color rather than reading the word. Hence, participants experienced this conflicting mental state by doing a less automatic activity (identifying the font color) while concealing the doubt generated by a more automated

one (naming the word) [164, 165]. Several literature reviews have applied SCWT to detect different cognitive functions such as processing speed [165], awareness [166], control/executive assessment [167], working memory [168] and cognitive flexibility [169]. Moreover, functional brain imaging investigations found that pre-frontal cortex (PFC) is the main influenced area by SCWT because of its functional asymmetry property [170].

In details, the SCWT was divided into two levels of complexity, each of which had the same length but related to a distinct level of stress. Vigilance level, included slow presentation for the questions/trials in which the respondent needs to reply as fast as possible but without automatically flipping the question. The recorded average time in answering the questions was lowered by 10/20% in the stress level which is utilized to put time pressure on the subject. SCWT was created and tracked using MATLAB software (R2020b, Natick, MA, USA). Figure 3.1 depicts the key phases that were presented during the task procedure. Each trial consists of a single word (with a random backdrop color) and six options from which to choose (answers and background are in different colours). Participants' responses should be rapid and precise (by left-clicking the mouse on one of the six answering buttons). Failure to answer or replying wrong within the allotted time would result in feedback to the participants on their performance, such as a message on the screen that said "Correct", "Incorrect", or "Time is out". Therefore, a dummy user performance indicator was displayed with each trial, suggesting poor performance by the participants in comparison to their peers. Consequently, while completing the SCWT, behavioral data such as detection accuracy and average reaction time was gathered. This data was collected in order to determine the levels of stress and stress mitigation. We used various markers to indicate the beginning and finish of the SCWT in each block and experiment condition.

3.1.3 Salivary alpha amylase

Many studies have found a link between mental stress and the levels of salivary alpha amylase (SAA). Catecholamines are present in SAA concentrations where Epinephrine (EPI) and Norepinephrine (NE) are the two most important catecholamines. During the

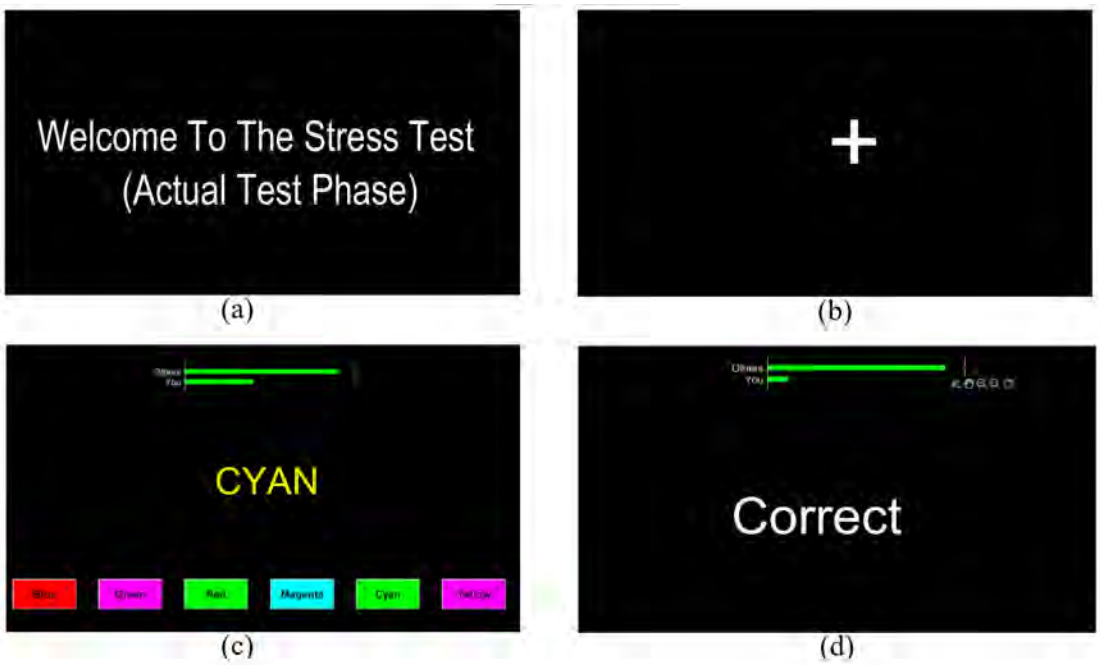

Figure 3.1: Phases of stroop color-word task. (a) welcoming message, (b) resting period, (c) stroop stimulus, (d) post-trial feedback.

"fight or flight" response, EPI and NE are released into the circulation and saliva. This release generates a quantifiable quantity that can be extracted from SAA samples [171]. According to Chatterton et al. [171], salivary amylase concentrations predict plasma catecholamine levels and can be used as a stress indicator. Meanwhile, the findings of Rohleder et al. [172] revealed that when individuals were exposed to TSST stressors, their SAA levels rose and then decreased after waking.

The amylase activity was measured using a hand-held monitor (COCORO meter, NIPRO, Osaka, Japan). The monitor measures amylase activity by evaluating reaction time. A disposable test strip plus a monitor comprise the hand-held monitor. The test strip is made up of a collection paper and an amylase reagent paper. Saliva was collected by dipping a salivary-sampling strip in saliva and placing it under the tongue for 40 seconds. The strip was then immediately placed in an automated saliva transfer system, where it was compressed and converted into alpha-amylase test paper. The salivary intensity reading was then computed, and the level of stress was determined. We collected salivary alpha-amylase samples to ensure that the task generated stress was experienced by all individuals. Throughout the trial, each subject had five samples of salivary alpha-amylase collected. As a baseline sample, the first sample was taken prior

to the start of the experiment. The remaining four samples were taken immediately after each stress period.

3.1.4 Binaural beat stimulation

In this work, we employed binaural beat stimulation (BBS) to mitigate mental stress. We used stereo headphones (RZE-BT200H, Toshiba, Sharjah, United Arab Emirates) to simulate/present pure tones of 250 Hz and 266 Hz to the right and left ears of participants. The pure tones were interpreted as a 16 Hz binaural beat. Figure 3.2 illustrates the auditory stimulation effects using binaural beats [173]. The tones were generated with the MATLAB program (R2020b, Natick, MA, USA) and played continuously during the SCWT stimuli. The volume of the audio stimuli was adjusted by the participants at the start of the experiment. Additionally, the sound intensity was adjusted to 60 decibels (dB), which is comparable to 48 decibels (dB) of normal hearing. In each block, the 16 Hz BB was shown continuously along with the 30 second SCWT. To guarantee that the maximum stimulus frequencies are considerably below the Nyquist rate, the audio tone was produced at a sampling rate of 48 kHz.

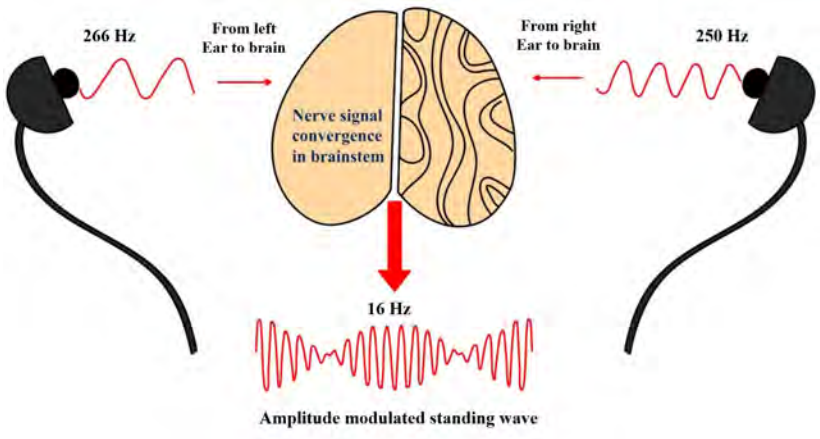

Figure 3.2: Application of binaural beats.Carrier sinusoidal tones of 250 and 266 Hz generate a 16 Hz beat [174].

3.1.5 FNIRS recording system

During the experiment sessions, brain activity (oxygenated and deoxygenated haemoglobin) was measured using fNIRS system NIRSport2 (NIRx Medical Technologies, NY, USA) with 20 channels (8 sources and 7 detectors). Emitters and detectors were designed to have a 3 cm distance between each other. Figure 3.3 depicts the experiment environment that included data collection and task configuration setup.

The infrared signal was produced at two wavelengths (760 nm and 850 nm) and captured using detectors with a sampling frequency of 10.17 Hz. Additionally, Figure 3.4 illustrates the distribution of fNIRS optodes on the scalp (sources in red and detectors in green). To capture the fNIRS signals and verify that the NIRScap was appropriately placed on the participant's head, the Aurora acquisition program (Aurora 2020.07, NIRx Medical Technologies, NY, USA) was utilized in a way that all sources and detectors are positioned as defined in the selected configuration similar to the Figure 3.4.

An automatic signal optimization approach was applied before starting the test to ensure excellent signal quality and to establish the ideal brightness of the source for each channel. A number of variables were determined by the optimization step. These included signal level, source brightness, dark noise, and coefficient of variation (see Figure 3.5). Poor signal quality can be caused by a variety of factors, including the presence of hair, poor optode-skin contact, inappropriate cable positioning, and inadequate source-detector pair design. While data was being collected, changes in ΔHbO and ΔHbR concentrations were observed in real-time using several display modes. A parallel port interface was established between the fNIRS acquiring PC and the stimulus monitoring PC to get markers on the recorded signal to represent stress task state when switching between resting phase and questions phase.

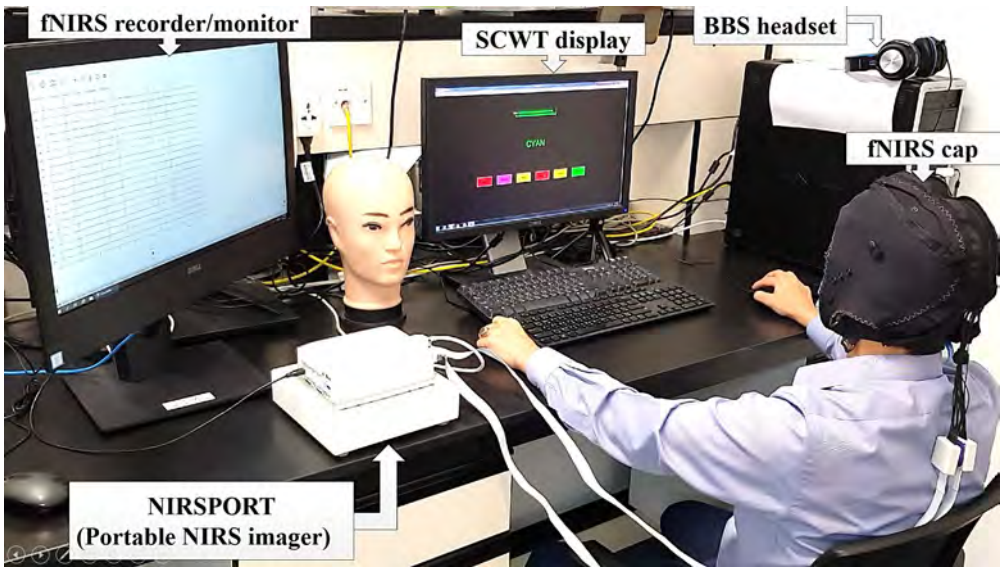

Figure 3.3: Experimental and data acquisition setup. The setup consists of two computers, one for monitoring and recording fNIRS signals and the another is to display the stroop task, NIRS device with

sources and detectors, NIRS cap with black cover cap and headphones.

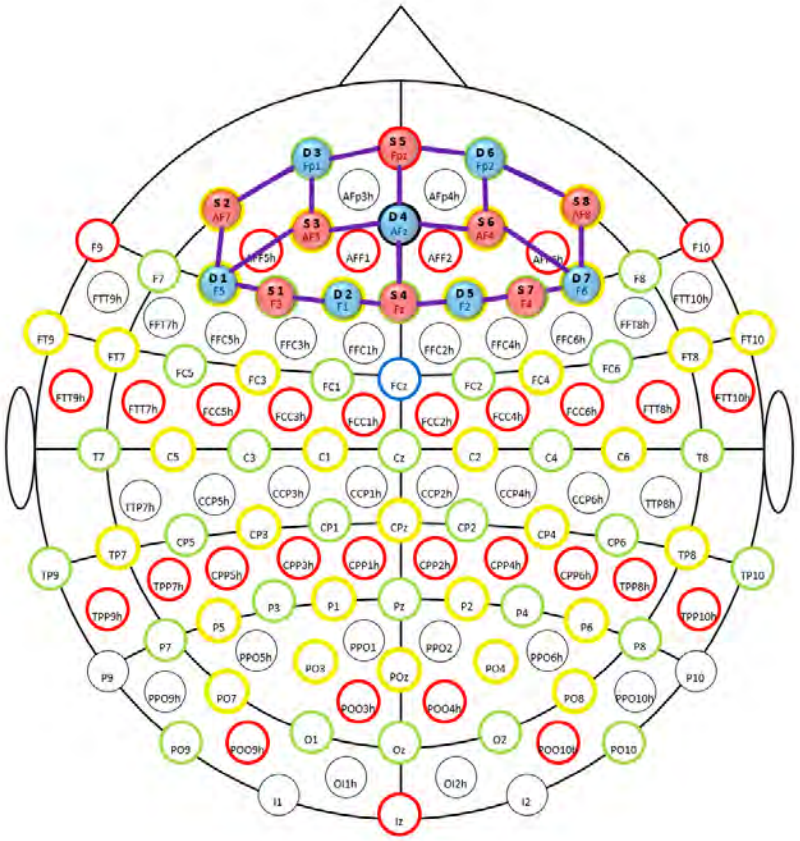

Figure 3.4: Selected channel configuration. Eight sources (red) and seven detectors (blue) forming 20-channels with six regions of interest over pre-frontal cortex area.

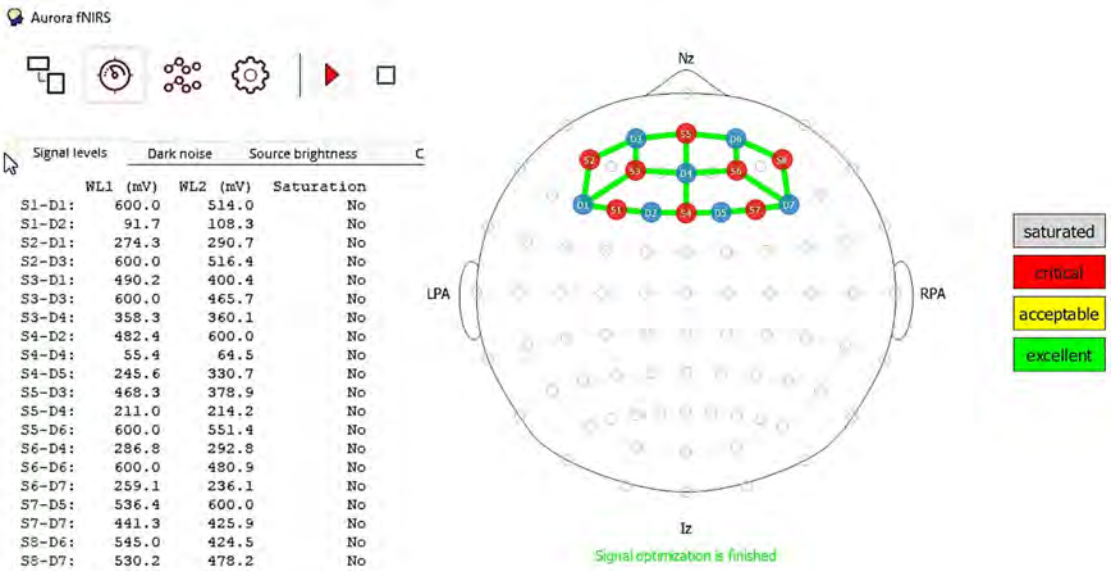

Figure 3.5: fNIRS signal optimization by Aurora software.The average voltage level in each channel from a certain source to the detector can be marked as excellent (green), acceptable (yellow) or low (red).

3.2 Data Acquisition

The research protocol was prepared in accordance with COVID-19's suggested preventive precautions and safety measures. Cleaning and preparing medical equipments (including fNIRS) necessitated adherence to a hygiene regimen suggested by the local institution and mandated by the local health authority. Meanwhile, the producer declared the efficacy of these disinfectants, as well as the exposure duration and concentration. To keep COVID-19 from spreading, participants and instructor maintained a social/physical distance of at least one meter. As a result, each subject was received a comprehensive description of how to conduct the experiment so that he/she would complete the entire experiment without direct interference from the researcher. The experiment took place at the American University of Sharjah's Biomedical Laboratory. Given that the experiment settings had a well-controlled environment with consistent temperatures and lighting conditions. Figure 3.6 shows the experiment protocol and the blocks arrangement for each level of the SCWT.

At the beginning of the experiment, participants were encouraged to carefully read a script word file comprising an introduction and explicit instructions on how to complete the task. Candidates then went through the approval procedure and filled out health history forms. To increase the stability of the fNIRS signal, participants were asked to accomplish the stress task with minimal head and body movements. This experiment was completed in five main sessions. Subjects did the SCWT for 5 minutes without fNIRS recording in the first session (training phase) to become acquainted with the task, and feedback on performance was provided upon completion. fNIRS was acquired during the second session (vigilance phase) while participants performed a 10-minutes stroop task that consisted of 10 blocks of questions (each for 30 seconds) separated by resting periods (20 sec each). During this phase, participants were instructed to respond as quickly as possible (there is no time limit per question). In the third session (enhancement phase), participants were instructed to utilize the headphones to listen to the binaural beats while repeating the vigilance phase. Following that, the vigilance phase's average time to answer each question was decreased by 10/20% (negative feedback and time constrain). Here as consequence, the fourth session (stress phase)

was structured similarly to the vigilance phase (10 minutes of recording time) with restricted time per question. In the fifth session (mitigation phase), participants were asked to use the headphone to have binaural beats stimulation while repeating the stress phase. The four phases were presented randomly, with half of the participants starting with the Vigilance phase and the other half with the Stress phase.

Complete procedures were scheduled on consecutive days, and the entire projected time for each participant, including introduction, preparation, and recording, was roughly one hour. Overall, each participant spent 15 minutes being introduced and trained, 10 minutes completing out questionnaires and capturing salivary cortisol, and 40 minutes performing the SCWT while recording the fNIRS signal. This study's questionnaire was based on NASA's Task Load Index (TLX) [175]. Before and after each SCWT, all participants filled out a questionnaire. The TLX evaluated workload using five 7-point scales. For each point, increments of high, medium, and low estimates result in 21 gradations on the scales. "Mental Demand," "Physical Demand," "Temporal Demand," "Performance," "Effort," and "Frustration" are among the items examined.

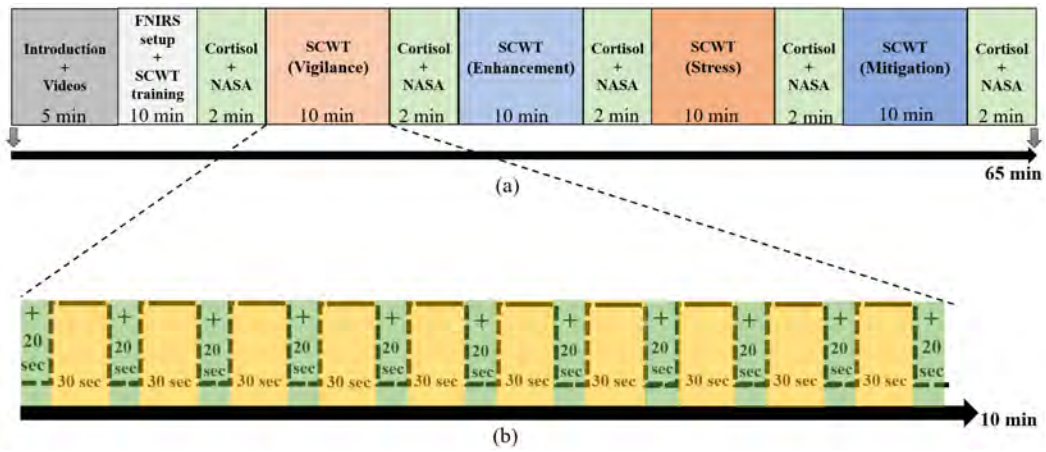

Figure 3.6: Experiment procedure of mental stress detection study.(a) A complete experiment with almost one-hour duration including four levels of recordings (b) One stress level with 10 blocks, including questions for 30 sec and resting periods for 20 sec.

3.3 Data Analysis

3.3.1 Behavioral performance

During the task, behavioral parameters such as the average reaction time and detection accuracy were estimated. The response time was determined by the amount of time each subject spends between the time the stimulus is displayed and their response is

given [80, 169]. Additionally, the monitored accuracy was calculated by dividing the number of right answers by the total number of color word questions that were displayed. It was important to assess the difference in the stroop effect between the various stress conditions in order to determine the association between brain activity, behavioral performance, and stress-related processing [160].

3.3.2 FNIRS pre-processing

MATLAB NIRS Brain AnalyzIR Toolbox (developed by Atlassian Corp and Neuroimaging Tools & Resources Collaboratory) was used to extract the fNIRS data and translate them into a change in optical density [176]. The concentration variations of the HbO and HbR were then determined using Beer-Lambert law (MBLL) [177]. For movement artifact correction of sharp peaking signals, we employed Temporal Derivative Distribution Repair (TDDR) and principal component analysis (PCA). Hence, fNIRS signals were subjected to several pre-processing stages in order to eliminate signal drift, false-positive rates, arterial pulsation, noise, and motion artifacts. These stages included removing motion artifacts, filtering the signal with a bandpass filter (0.009 - 0.8 Hz), baseline rectification, and moving average. Furthermore, by determining the power spectral density of the fNIRS signals, 30 frequency values ranging from 0.01 to 0.3 Hz were recorded.

3.3.3 Functional connectivity

Partial directed coherence (PDC) is a multivariate auto regressive model (MVAR) that is used to estimate the time-dependent auto regressive (AR) coefficients that contribute to the directed effects of Granger causality on the information flow among fNIRS signals. Rather than merely describing mutual synchrony across brain areas, PDC informs us about the functional connectivity of the two brain regions under investigation. A sophisticated network will be established to depict the direction and weight of information flow between the fNIRS channels. As a result, a multivariate (complex network characteristics) level is favoured over a bivariate (connectivity between pairs of regions) and univariate (intra-regional connectivity). Assuming $\boldsymbol{X}(t)$ is fNIRS signal with 20 channels (N) defined by $\boldsymbol{X}(t) = [x_1(t), x_2(t), \dots, x_{20}(t)\,]^T$, then the multivariate model of N fNIRS channels can be defined by Eq.1:

$$\boldsymbol{X}(t) = \sum_{r=1}^{r=p} \boldsymbol{A}_r(t)\, \boldsymbol{X}(t-r) + \boldsymbol{W}(t) \tag{1}$$

where, $\boldsymbol{W}(t)$ is a zero-mean white Gaussian noise, $\boldsymbol{A}_r(t)$ is a matrix of time-varying MVAR parameters and p is the model order which is set to be 6 in this analysis. More details about the PDC and model order can be found in the previous EEG studies [178], [169]. The appropriate model order p was calculated by Akaike information criterion (AIC) represented by Eq.2:

$$AIC(p) = 2\, log\left[det\left(\sum\ \right)\right] + \frac{2\, N^2 P}{N_{total}} \tag{2}$$

where $det(\sum\ )$ is the determinant of the covariance matrix of noise vector and N_{total} is the total number of fNIRS samples in all trials. The $i \times j$-coefficient matrix $\boldsymbol{A}_r$ at the time lag r is given by Eq.3:

$$\boldsymbol{A}_r = \begin{bmatrix} a_{11}(r) & \dots & a_{1j}(r) \\ \vdots & \ddots & \vdots \\ a_{i1}(r) & \dots & a_{ij}(r) \end{bmatrix} \tag{3}$$

where the MVAR coefficient a_{ij} represents the effect of the time-series signal $X_j(t-r)$ on $X_i(t)$. Once the coefficients of the MVAR model are adequately estimated, the difference between the N-dimensional identity matrix I and the Fourier transform of the coefficient series $\boldsymbol{A}_r$ can be used to create a representation of Granger causality in the frequency domain, as follows:

$$\bar{\boldsymbol{A}}(f) = \boldsymbol{I} - \boldsymbol{A}(f) = \boldsymbol{I} - \sum_{r=1}^{P} \boldsymbol{A}_r e^{-j2\pi f r} \tag{4}$$

Knowing that, $\boldsymbol{A}(f)$ is the frequency domain equivalent of the coefficient matrix $\boldsymbol{A}_r$ that is produced by applying the Fourier transform on each $a_{ij}(r)$ of the matrix $\boldsymbol{A}_r$. Then, PDC that indicates the direction and weight of information flow at frequency f from channel j to channel i within each time block (here, we have 10 blocks) was estimated by Eq.5:

$$PDC_{i,j}(f) = \frac{\left|\bar{A}_{i,j}(f)\right|}{\sqrt{\sum_k \bar{\boldsymbol{A}}^*_{kj}(f)\bar{\boldsymbol{A}}_{kj}(f)}} \tag{5}$$

where $\overline{\boldsymbol{A}}_{i,j}(f)$ is the $(i,j)^{th}$ element of $\overline{\boldsymbol{A}}(f)$. The PDC matrix data format is 4 × 30 × 10 × 30 × 20 × 20, reflecting the stress phase × subjects × time blocks × frequencies × channels × channels, respectively. The PDC has a value between 0 and 1, with larger values indicating greater interaction between the two nodes. Figure 3.10 shows a block diagram of the many procedures involved in the analysis of fNIRS data, including pre-processing and functional connectivity.

3.3.4 Graph theory analysis

Graph theoretical analysis (GTA) offers quantitative measures for analyzing the topological architecture of functional connectivity networks. There are N nodes and W weighted edges in a specified network or graph G; the graph theory analysis produces global and local network metrics. In our research, the nodes were the fNIRS channels, and the connections were determined by the PDC connectivity metric. The brain network parameters were calculated based on the matrices generated by PDC for each individual. Furthermore, neuroimaging data that estimates weak network connections may be noisy or inaccurate. As a result, network thresholding was often used before GTA in order to remove any weak spots and to bring attention to the connections that are significant [179]. When comparing networks with similar global densities across groups or circumstances, it was essential to compare networks with similar global densities [180]. As a result, the observed phenomena will not be skewed by an unequal distribution of network connections. Thresholds were used to maintain a specified number of the most important edges [181, 182]. Before the GTA, there was no standard for determining what a person should be paid. Instead, a 0–1 range with a 0.1–step was investigated. The graphical analytic measures in this study are based on the notions of node degree, node strength, clustering coefficient, and efficiency. The definitions and mathematical expression of these metrics are presented in further detail below.

Nodal Degree (ND): ND is a metric of centrality that assesses the relevance of network nodes [183]. The local node degree d_i is defined mathematically as the number of edges directly related to a certain node (excluding self-loops) normalized by the number of available edges:

$$d_i = \frac{1}{N-1} \sum_{j \neq i \in N} a_{ij} \tag{6}$$

where a_{ij} denotes the edge status between node i and node j (i.e., $a_{ij} = 1$ if the edge weight $w_{ij} \neq 0$), and N is the total number of nodes in the network. A network's global node degree (the arithmetic mean of all node degrees) represents the overall density of connections and is commonly used to compare various networks.

Nodal Strength (NS): It is the total of the edge weights that connect a node to the other nodes in a weighted network and is calculated using Equation (7). The network's average node strength is the arithmetic average of the strengths of all individual nodes in the network. In this example, node strengths aid in determining a specific region's participation and information flow in a functioning brain network [184].

$$s_i = \frac{1}{N-1} \sum_{j \neq i \in N} w_{ij} \tag{7}$$

Knowing that s_i is the local node strength and w_{ij} is an element weight of the PDC matrix.

Clustering Coefficient (CC): It is a network segregation metric that measures how well nearby nodes form full networks or cliques [183]. The local clustering coefficient C_i is determined for node i as the ratio of the sum of geometric means of all existing weighted triangles to the total number of triangles feasible. C_i, in particular, evaluates how efficiently the cluster of nodes interacts, and a high C_i value corresponds to a high local efficiency of information transport. This may be represented mathematically in an undirected and weighted network as [184]:

$$C_i = \frac{\sum_{j \neq i \in N} \sum_{h \neq (i,j) \in N} \left(w_{ij} w_{jh} w_{hi}\right)^{1/3}}{s_i(s_i - 1)} \tag{8}$$

Network Efficiency (NE): The local node efficiency is a measure of functional integration that measures the extent to which individual nodes aggressively integrate specialized information from other dispersed nodes within the network [183]. This feature is defined by the idea of a route between nodes. Shorter routes indicate a greater possibility for integration and, as a result, a higher efficiency of information flow. The local efficiency E_i is determined mathematically as the average of the reciprocal of the shortest routes between all nodes in the network [185]:

$$E_i = \frac{1}{N(N-1)} \sum_{i \neq j \in N} \frac{1}{L_{ij}} \quad (9)$$

Knowing that L_{ij} is the length of the shortest path between nodes i and j. The Dijkstra method was used to find the shortest path between two nodes, with the total of the lengths of its constituent edges reduced [186, 187]. Edge lengths are the inverse of edge weights. Paths between unconnected nodes are often characterized as having unlimited lengths.

Statistical analysis was carried out between the vigilance and stress levels, as well as between those phases and their respective BBS phases (vigilance/enhancement and stress/mitigation). We utilized paired t-tests to assess the connection metrics between stress and mitigation using the following criteria. To begin, we examined the connectivity measures d_i, s_i, C_i, and E_i across vigilance and stress levels. Second, we compared the connectivity metrics in d_i, s_i, C_i, and E_i between the vigilance and enhancement phases, as well as the stress and mitigation phases. If the test rejects the null hypothesis at the 5% level of significance, the result h is 1, otherwise it is 0. Additionally, the confidence interval and structural stats providing information on the test statistic are returned by the test.

3.4 Classification Analysis

A neural network is an adaptable system that learns through the use of linked nodes or neurons arranged in a layered structure similar to that of the human brain. The human nervous system has roughly 86 billion neurons that are linked by approximately $10^{14} - 10^{15}$ synapses. In Figure 3.7, a real neuron and a commonly used mathematical model are shown. Each neuron receives input signals through its dendrites and transmits them via its axon. The axon ultimately forks and links to the dendrites of neighboring neurons through synapses. As illustrated in the Figure 3.7, the signals traveling up the axons (e.g., x_0) interact multiplicatively (e.g., $w_0 x_0$) with the dendrites of the other neuron, depending on the synaptic strength at that synapse (e.g., w_0). The theory is that synaptic strengths (weights w) can be learned and that they govern the intensity of effect (and its direction: executory (positive weight) or inhibitory (negative weight)) exerted by one neuron on another. Dendrites transmit the signal to the cell body, where it is summed. If the total sum is more than a certain value, the neuron may fire, sending a

spike down its axon. It is assumed in the computational model that the exact timings of the spikes are irrelevant and that just the frequency of the firing transmits information. We simulate the neuron's firing rate using an activation function f, which indicates the frequency of spikes along the axon, based on this rate coding interpretation [188]. Numerous activation functions, such as sigmoid, tanh, and ReLU, are encountered in practice. Sigmoid compresses a real-valued input to a range between 0 and 1 (Eq.10). Tanh compresses a real-valued input to the range [-1, 1] (Eq.11). Rectified Linear Unit is abbreviated as ReLU. It accepts a real-valued input and sets the threshold to zero (in other words, it substitutes negative values with zero) (Eq.12).

$$\sigma(x) = \frac{1}{1 + e^{-x}} \tag{10}$$

$$\tanh(x) = 2\sigma(2x) - 1 \tag{11}$$

$$f(x) = \max(0, x) \tag{12}$$

Moreover, a neural network may be taught to detect patterns, categorize data, and predict future occurrences using data. Its behavior is determined by the manner in which its constituent components are linked and the strength, or weight, of those linkages. These weights are changed automatically during training in accordance with a defined learning rule until the artificial neural network successfully accomplishes the intended job. A neural network, which takes inspiration from biological nerve systems, utilizes basic components working in parallel to create many processing levels. An input layer, one or more hidden layers, and an output layer comprise the network. Each layer has multiple nodes, or neurons, and the nodes in each layer utilize the outputs of all nodes in the preceding layer as inputs, ensuring that all neurons communicate with one another through the various levels. During the learning process, the weight of each neuron is changed, and changes in the weight affect the intensity of the output from that neuron. As with other machine learning techniques, neural networks may be used for both supervised learning (classification, regression) and unsupervised learning (pattern recognition, clustering) [189].

Deep learning, on the other hand, is a subset of machine learning, which is a subset of artificial intelligence and statistics. In machine learning, the learning system establishes correlations between the data. Data is entered together with the associated outcomes.

This is the system's training. The machine learning system establishes relationships between the data and the outcomes and generates rules that become part of the system. When fresh data is provided, it is possible for new findings to emerge that were not included in the training set. Meanwhile, deep learning is a term that refers to neural networks that have several layers of neurons. The term "deep learning" connotes something more profound, and in popular literature, it is interpreted as implying that the learning system is a "deep thinker." In Figure 3.8, a single-layer and multilayer network are shown. Multilayer networks, it turns out, can learn things that single-layer networks cannot. A single layer multiplies the inputs by weights and then adds them together after going through a threshold function. The second layer of a multilayer or deep learning network is used to mix the inputs before they are output. There are more weights, and the network's increased connectivity enables it to learn and solve more complicated issues. Due to its ability to automate feature extraction, deep learning has become more prominent in the field of image and signal processing. Feature extraction with end-to-end deep learning algorithms, that extract features and learn classifiers jointly, is used in signal processing for better classification accuracy. Deep learning models, often outperform humans. Models are trained utilizing a huge amount of labelled data and multilayer neural network topologies [191, 192].

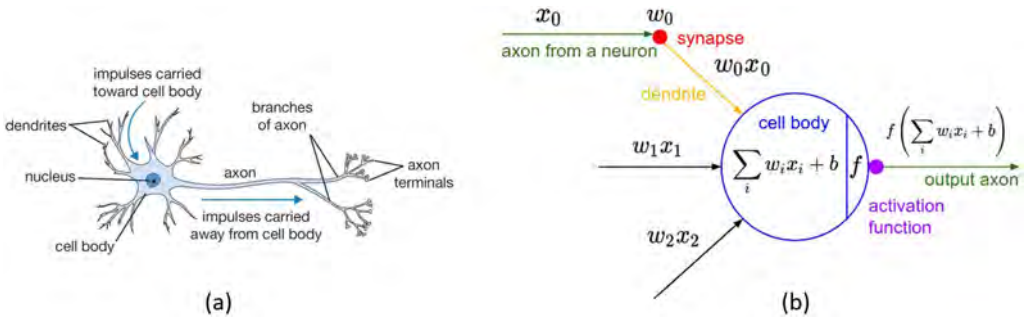

Figure 3.7: A cartoon illustration of a biological neuron (a) and its mathematical representation (b).[190]

Several machine learning techniques, including k-nearest neighbors (KNN), linear discriminant analysis (LDA), and support vector machine (SVM), have been utilized in fNIRS research to differentiate between two distinct situations as stress/vigilance conditions [193-195]. The major limitations of these algorithms are the manual extraction and selection of features, which introduces uncertainty regarding the feature's suitability for the stated task.

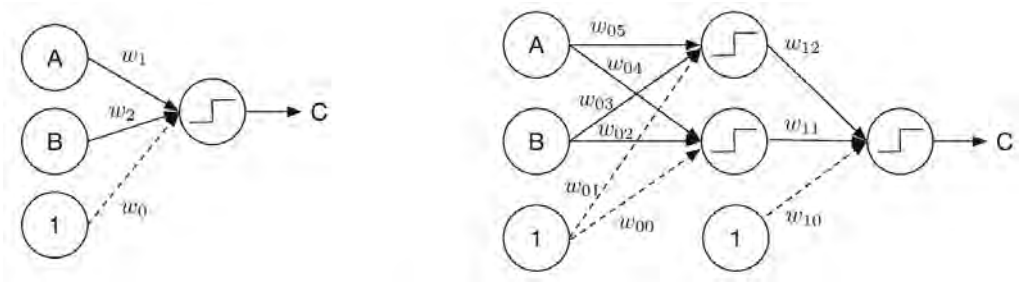

Figure 3.8: Two neural networks. (a) Single-layer network, (b) Multilayer network (deep learning network).[192]

Deep convolutional neural networks (CNN) are one of the popular deep neural networks. CNNs remove the requirement for manual feature extraction, which eliminates the necessity to identify image classification features. The CNN algorithm works by directly extracting characteristics from images. By automating the feature extraction process, deep learning models, such as those used in object categorization, become very accurate. Using tens or hundreds of hidden layers, CNNs learn to identify various characteristics in a picture. Each hidden layer enhances the complexity of the image features that have been learnt. For instance, the first hidden layer may learn how to identify edges, while the last one may learn how to detect more complicated forms that are unique to the geometry of the item being recognized [196, 197].

Furthermore, CNNs are intended to utilize a signal's spatial correlation, and since PDC matrices include information in the second dimension as well, the adoption of a 2D-CNN architecture enables full exploitation of the features present in PDC matrices. A new CNN's architecture must be defined before it can be built and trained. The network design varies according on the kind and number of layers. The kinds and number of layers depends on the individual application or data. Classification networks, for example, often include a softmax layer and a classification layer, but regression networks must have a regression layer at the network's conclusion. A network with less than one or two convolutional layers may be adequate to learn from a modest quantity of grayscale picture data. On the other hand, with more complex data including millions of coloured images, a network with numerous convolutional and fully linked layers may be required. The following is a quick description of the most often employed layers [198, 199]:

- The **image input layer** feeds pictures into a network and normalizes the data.

- The two-dimensional **convolutional layer** applies sliding convolutional filters to the two-dimensional input and is composed of the following components:
  - A collection of weights that is applied to an area in the picture is termed a **filter**. The filter iterates vertically and horizontally along the input picture, doing the same calculation for each area. To put it another way, the filter convolves the input.
  - The step size with which the filter travels is termed a **stride**.
  - **Dilated convolution** is a kind of convolution in which the filters are extended by inserting gaps between the filter components. Increase the receptive field (the region of the input that the layer can view) of the layer using dilated convolutions without increasing the number of parameters or computation.
  - As the filter traverses the input, it utilizes the same set of weights and bias for convolution, resulting in the formation of a **feature map**. Each feature map is the product of convolution with a unique weight set and bias. As a result, the total number of feature maps equals the total number of filters.
- A **batch normalization layer** individually normalizes a subset of data across all observations for each channel. To speed up training of the convolutional neural network and lower the susceptibility to network initialization, it is better to utilize batch normalization layers between convolutional layers and nonlinearities, such as ReLU layers.
- A **ReLU layer** does a threshold operation to each input element, setting any value less than zero to zero.
- A **2-D max pooling layer** provides downsampling by splitting the input into rectangular pooling zones, then determining the maximum of each region.
- A **2-D average pooling layer** provides downsampling by splitting the input into rectangular pooling areas, then calculates the average values of each zone.
- In a **fully connected layer**, the input is multiplied by a weight matrix and then a bias vector is added. As the name indicates, all neurons in a completely linked layer connect to all the neurons in the preceding layer. This layer aggregates all of the features (local information) gathered by the preceding layers throughout the image to detect the broader patterns. For classification challenges, the final fully connected layer combines the characteristics to categorize the images.

- A **softmax layer** converts the input to a softmax function.
- The cross-entropy loss for classification and weighted classification tasks involving mutually exclusive classes is computed by a **classification layer**.

The architecture of our proposed 2D-CNN is shown in Figure 3.9. It consists of three convolutional layers with batch normalization (BN), a global average pooling (GAP), and one fully connected layer. After each convolution layer, a Rectified linear unit (ReLU) layer is added as a nonlinear activation function [200]. Finally, a fully connected layer and binary Softmax regression are employed for classification. As shown in Figure 3.9, three convolution layers (CL) each include fifteen filters with dimensions of 1×3, 3×2, and 1×1, respectively. Following each CL, a batch normalization layer (BNL) is used to minimize the internal covariance shift. This decrease improves training speed and decreases the likelihood of data overfitting. The BNL output is then translated to positive real numbers using the ReLU layer, which is utilized to activate or deactivate nodes depending on the mapped value. The suggested network's design, configuration, and other trainable characteristics are described in Table 3.1. The proposed network's training parameters are set to their default settings as follows: the squared gradient decay factor is 0.999, the gradient factor is 0.9, the ADAM optimizer's denominator offset is 1×10^{-8} and the gradient threshold is 1, while the initial learning rate is 1×10^{-3}; the learn rate drop factor and period are set to 0.4 and 5, respectively. Finally, the Softmax layer classifies each input into one of the C mutually exclusive classes using the cross-entropy (CE) loss function.

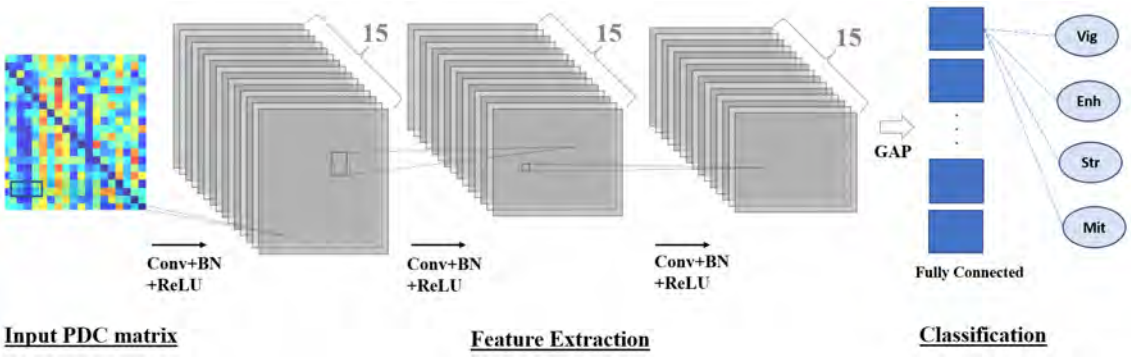

Figure 3.9: CNN architecture for feature extraction and classification of PDC matrices for the four phases. Conv: Convolution, Vig: Vigilance, Enh: Enhancement, Str: Stress, Mit: Mitigation.

Table 3.1: The architecture of the proposed CNN network.

Layer	Name	Type	Activations	Learnables	Total Learnables
1	imageinput 20×20×1 images with 'zerocenter' normalization	Image Input	20×20×1	-	0
2	conv_1 15 1×3 convolutions with stride [1 1] and padding 'same'	Convolution	20×20×15	Weights 1×3×1×15 Bias 1×1×15	60
3	batchnorm_1 Batch Normalization	Batch Normalization	20×20×15	Offset 1×1×15 Scale 1×1×15	30
4	relu_1 ReLU	ReLU	20×20×15	-	0
5	conv_2 15 3×2 convolutions with stride [1 1] and padding 'same'	Convolution	20×20×15	Weights 3×2×15×15 Bias 1×1×15	1365
6	batchnorm_2 Batch Normalization	Batch Normalization	20×20×15	Offset 1×1×15 Scale 1×1×15	30
7	relu_2 ReLU	ReLU	20×20×15	-	0
8	conv_3 15 1×1 convolutions with stride [1 1] and padding 'same'	Convolution	20×20×15	Weights 1×1×15×15 Bias 1×1×15	240
9	batchnorm_3 Batch Normalization	Batch Normalization	20×20×15	Offset 1×1×15 Scale 1×1×15	30
10	relu_3 ReLU	ReLU	20×20×15	-	0
11	gap Global Average Pooling	Global Average Pooling	1×1×15	-	0
12	fc 4 fully connected layer	Fully Connected	1×1×4	Weights 4×15 Bias 4×1	64
13	softmax Softmax	Softmax	1×1×4	-	0
14	classoutput crossentropyex	Classification Output	-	-	0

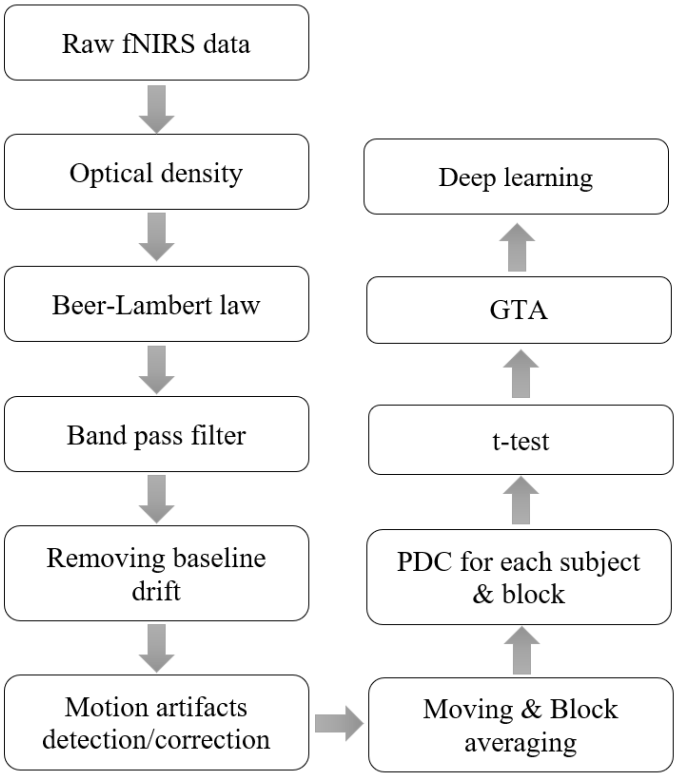

Figure 3.10: The processing flows of the approaches used to analyze fNIRS data.

Chapter 4. Results and Discussion

This chapter studies the role of fNIRS in quantifying mental stress and the influence of auditory stimulation on individuals' behavioral performance and cortical connectivity while conducting the SCWT. The purpose of this study was to determine whether stimulation with binaural beats (BBS) could improve brain connectivity, vigilance performance, and stress reduction. The PDC connectivity maps were created under four different stress conditions, two of which included BBS. To recap, the Vigilance phase is the SCWT with slowly displayed questions that have been shown to cause low levels of stress. The Enhancement phase incorporates BBS into the preceding phase in order to determine its effect on vigilance enhancement. SCWT's Stress phase is represented by faster questions that induce stress. Mitigation phase involves the application of BBS in order to determine its influence on stress mitigation. Thus, we used statistical analysis to examine if auditory stimulation resulted in significant improvements in the cortical functional connectivity. Meanwhile, the effects of induced mental stress on alpha amylase levels, behavioral data, and subjective data were further explored.

4.1 Alpha Amylase Levels

Each subject had five salivary alpha-amylase samples taken throughout the experiment. The first sample was taken as a baseline sample before to the experiment's start. The remaining four samples were collected immediately following each phase. Figure 4.1 depicts the results of salivary cortisol samples obtained five minutes before the experiment and immediately after the Vigilance, Enhancement, Stress, and Mitigation phases. The level of salivary cortisol increased from the Baseline to Vigilance and from the Enhancement to Stress phases, demonstrating that the SCWT elicited high levels of mental stress. By contrast, the phases containing BBS exhibited decreased amylase levels (Enhancement and Mitigation phases). To determine the significance of the differences between phases, a paired t-test was used. In particular, when compared to the Baseline phase (the phase with cortisol sample prior the experiment), the Vigilance and Stress phases demonstrated a statistically significant difference ($p<0.001$). This indicates SCWT's stress-inducing capability. Meanwhile, the ability of BBS to enhance vigilance was observed with $p<0.001$, and the same effect was observed for BBS to

alleviate mental stress (p<0.01). The recorded t-test results are displayed on the Figure 4.1 with one and two asterisks indicating p<0.01 and p<0.001, respectively.

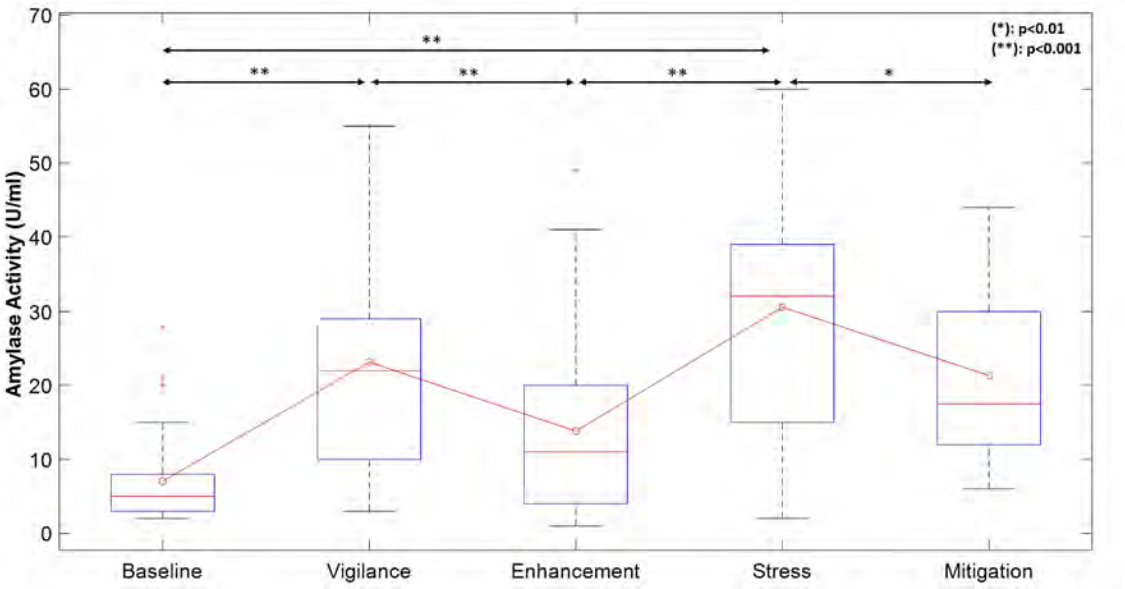

Figure 4.1: Salivary cortisol level based on alpha amylase concentration. The asterisks indicate a significant difference between two phases (*:p<0.01, **:p<0.001).

4.2 Behavioural Data

The accuracy in response to the SCWT stimuli was measured to assess participant's performance during the four phases. The behavioral data was collected during each 10 min SCWT for the 30 subjects. The study indicated that the percentage of accuracy decreased considerably during the Stress phase but increased or remained high throughout the Vigilance, Enhancement, and Mitigation phases, as shown in Figure 4.2. The mean accuracies of answering SCWT questions were 94.99%, 95.96%, 60.52%, and 71.57% for the Vigilance, Enhancement, Stress, and Mitigation phases, respectively. Paired t-test between the Vigilance and Enhancement phases showed no change in performance (no effect for the BBS on enhancing vigilance with p=0.126). In contrast, statistical analysis between the Stress and Mitigation phases showed significant decrements under the BBS condition (p < 0:001). Also, differences between the accuracies scored under the vigilance and stress phases were notable with a significant decrease in answering accuracy (p<0.001). This shows that the SCWT used in conjunction with time pressure and negative feedback was effective in raising stress levels.

As a result, there is an evidence that binaural beat stimulation improves the behavioral performance in the form of properly answering questions by 11.05% between Stress and Mitigation phases. Meanwhile, this improvement was not seen in enhancing vigilance.

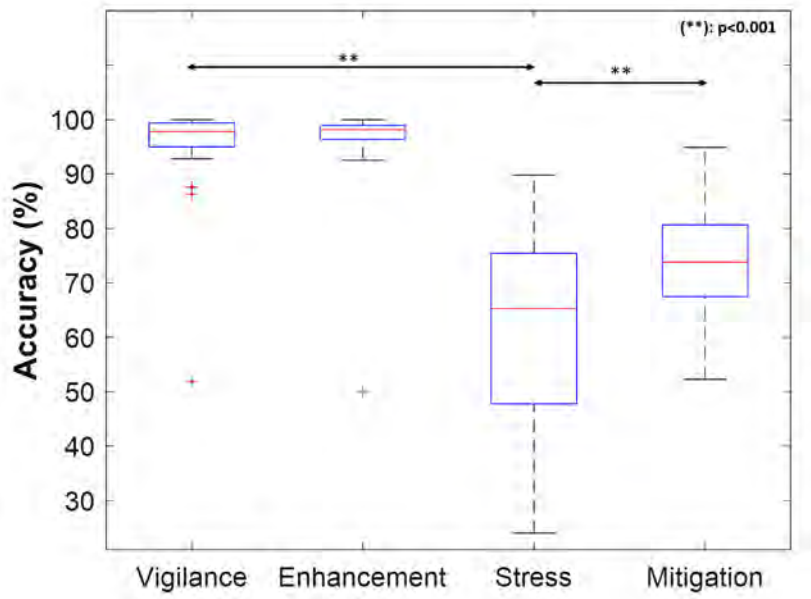

Figure 4.2: The recorded accuracies in answering SCWT's questions for the four stress phases. The asterisks indicate a significant difference between each two phases (**:p<0.001)

4.3 Subjective Data

NASA-TLX consisted of six subjective subscales, each of which should be reviewed prior to rating. As a result, participants were evaluated on a 100-point scale with 5-point increments for each task. The task load index was then calculated using these ratings. It was important to read the descriptions for each measurement to assist participants in responding correctly. NASA's Task Load Index scores were used to examine the subjective evaluation of stress level, and the results revealed a strong correlation between the task difficulty and the perceived stress level (pre- vs. post each phase). In general, high scores on all subscales (excluding Performance) were associated with high levels of stress, as evidenced by the Stress phase. Low subscale values, on the other hand, represented low levels of stress, which are considered as a result of BBS.

This study found that SCWT had a great ability to inflict stress by recording the substantial increases ($p<0.001$) in the mental demand, temporal demand, effort, and frustration criteria between the baseline and stress phases. On the other hand, the effect

of BBS on enhancing vigilance was demonstrated by a significant decrease ($p<0.05$) in the temporal demand. Meanwhile, between the Stress and Mitigation phases, the effort and performance criteria showed significant decreases ($p<0.05$) and increases ($p<0.01$), respectively. Table 4.1 summarizes the total TLX mean assessment ratings after the four stress stages. A considerable change in mental demand, physical demand, temporal demand, performance, effort and frustration is shown in Figure 4.3 as the statistical analysis results illustrate.

Table 4.1: Average TLX scores (Mean ± Standard deviation) for the four stress phases and the baseline phase.

	Mental Demand	**Physical Demand**	**Temporal Demand**	**Performance**	**Effort**	**Frustration**
Baseline	20±16.12	19.06±21.54	28.75±21.01	64.68±34.37	33.75±27.53	20.62±14.47
Vigilance	35.62±12.23	28.43±24.54	37.18±18.52	82.5±21.90	48.75±22.39	28.75±21.17
Enhancement	33.12±21.36	29.68±29.00	25±20.16	86.87±21.97	43.12±25.48	26.25±26.04
Stress	67.18±23.16	50.62±33.05	77.18±22.05	44.68±18.75	77.18±14.60	68.12±23.93
Mitigation	61.56±24.81	50.31±28.89	67.81±25.09	71.56±17.00	67.5±20.33	55.93±31.04

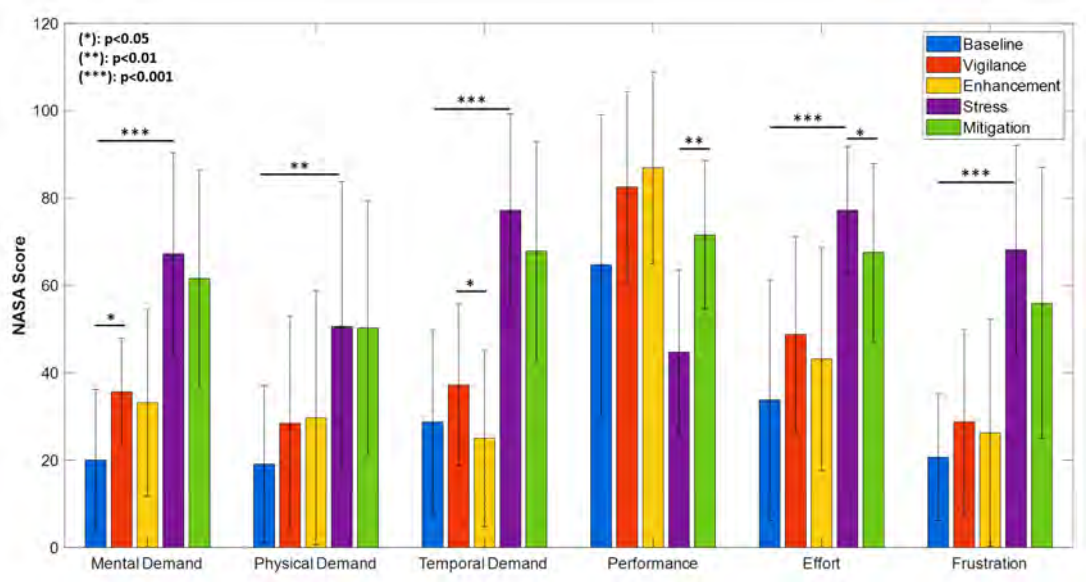

Figure 4.3: The average score for each NASA-determined criterion throughout the course of five phases. The asterisks indicate a significant difference between two phases (*:$p<0.05$, **:$p<0.01$, ***:$p<0.001$).

4.4 PDC Functional Connectivity

Partial directed coherence was used to reconstruct cortical connectivity networks in four different mental states. The subsequent subsections focus on detecting the induced stress by comparing the Vigilance and Stress phases, as well as on examining the BBS's proposed effect on boosting vigilance (by comparing the Vigilance and Enhancement phases) and on alleviating stress (comparing Stress and Mitigation phases). Figure 4.4 depicts the connectivity network plots to demonstrate the variations between the four mental states in terms of functional connectivity for the 20 fNIRS channels. The edges denoted the grand average PDC weights over frequencies (30 frequencies ranging from 0 to 0.3 Hz), blocks (10 SCWT blocks for each phase), and subjects (30 subjects). The decrease in PDC revealed a reduction in the network connecting the frontal lobes of the brain. PDC increases correlated with increased connection between frontal brain areas, and vice versa. As a result, the 1 PDC value at the top of the color bar represented an

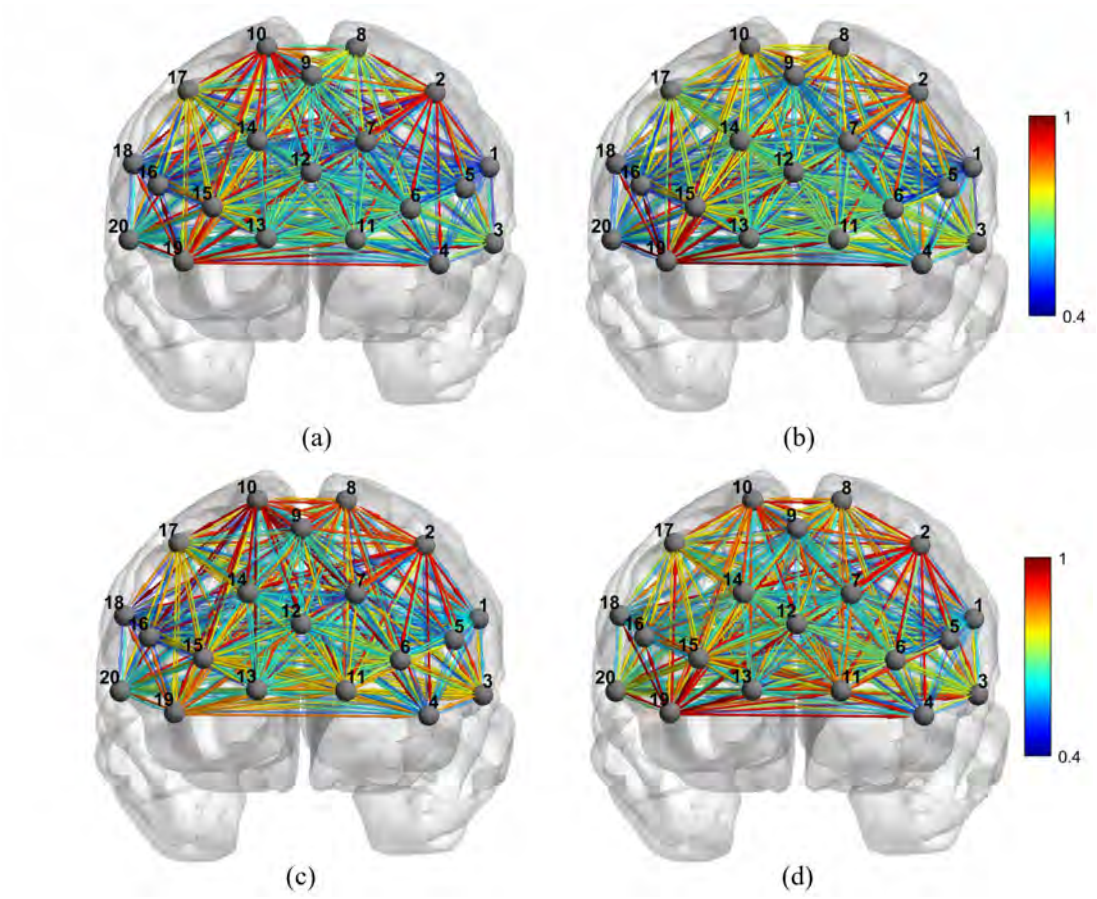

Figure 4.4: The average PDC connectivity map for the (a) Vigilance phase, (b) Enhancement phase, (c) Stress phase and (d) Mitigation phase.

increase in the weight of the information flow, while the PDC<1 suggested a drop in this flow. Many changes in connectivity between the four phases were apparent at first glance. Where exactly these significances occur will be determined by a subsequent statistical investigation.

Following that, between each of the two phases, a PDC connectivity map was constructed by subtracting the PDC maps. As a result, examining these maps provided a clear explanation for the rise or decrease in connectedness and information flow. In addition, a paired t-test was used to find the h matrix, which depicted the matrix of null hypothesis values, between each of the two stages ($p<0.05$). Each PDC node (which represented the intersection of a sender fNIRS channel and a receiver fNIRS channel) was subjected to this statistical analysis in order to determine its involvement in connectivity under varying levels of stress. The three connectivity maps depicted in Figures 4.5, 4.6, and 4.7 were created for (Vigilance-Enhancement), (Stress-Mitigation), and (Vigilance-Stress), respectively. In Figure 4.5, an increased alertness was observed primarily for channel 14, as evidenced by greater connectivity for this channel following BBS application, whereas the other channels demonstrated little or no connectivity change. Additionally, Figure 4.6 shows that BBS plays an important role in stress reduction by increasing PDC values during the Mitigation phase as compared to the Stress phase. According to Figure 4.7, the Stress phase had lower connectivity compared to the Vigilance phase, which was due to the time limits imposed by the SCWT. This map revealed variations in the PDC values between the two periods, while the t-test indicated that these differences were not statistically significant for the majority of nodes.

The influence of connectivity threshold was next examined in order to determine which crucial threshold values best describe the connectivity change between the four stress stages. As the threshold for PDC changed, so did the general pattern seen in Figure 4.8 for the average PDC. The phases that comprised BBS (Enhancement and Mitigation) demonstrated the highest PDC values across all thresholds up to 0.7. Likewise, the Stress phase showed the lowest PDC levels across the same threshold range. As soon as the 0.7 threshold was crossed, all four phases' mean PDC values were the same, and no longer significant differences in stress could be seen. Statistical analysis was created

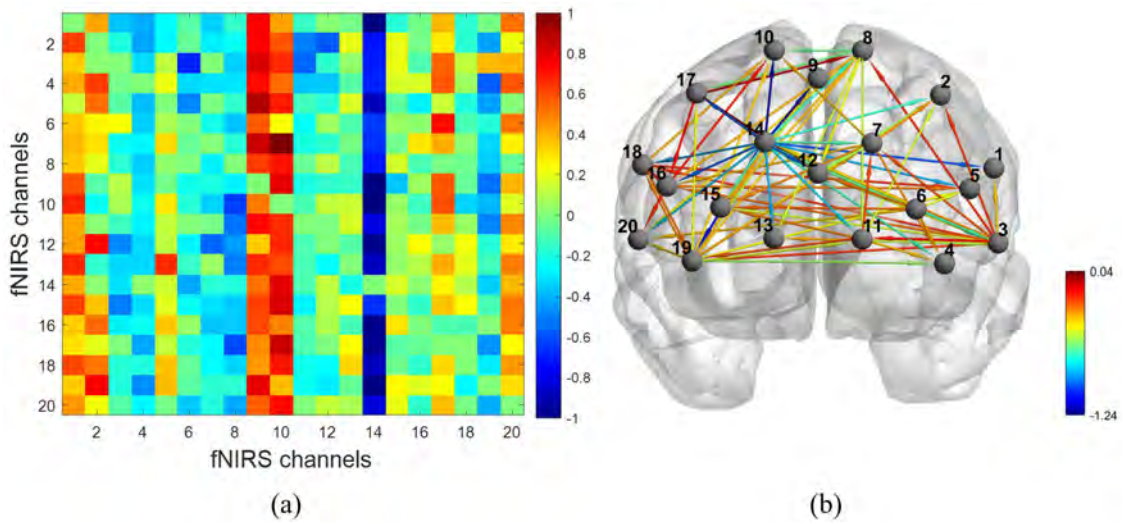

Figure 4.5: The functional connectivity difference. (a) subtraction PDC map for Vigilance-Enhancement with the hypothesis test results for each node, (b) the significant connectivities between the two phases.

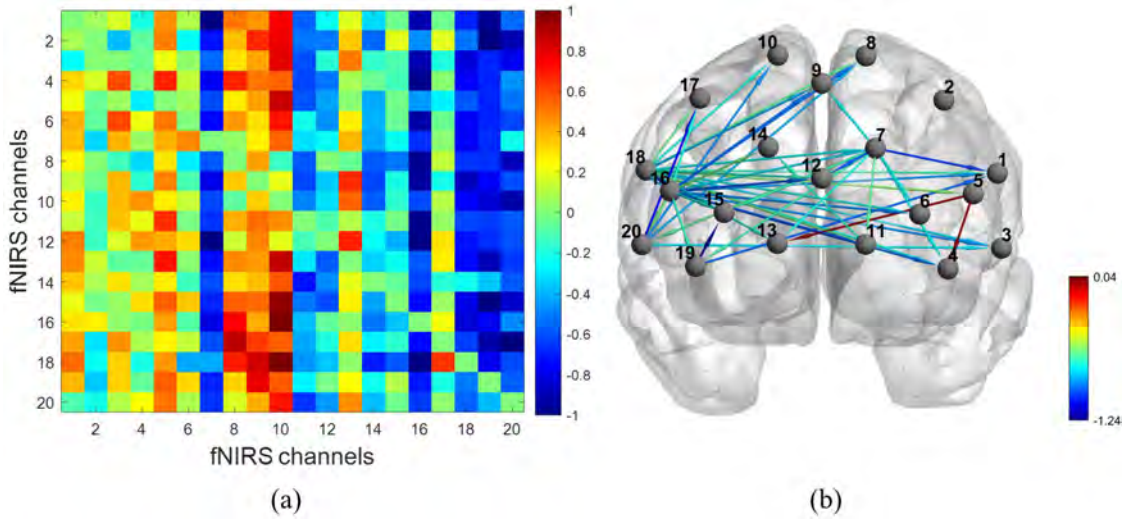

Figure 4.6: The functional connectivity difference. (a) subtraction PDC map for Stress-Mitigation with the hypothesis test results for each node, (b) the significant connectivities between the two phases.

on each PDC node because, as earlier mentioned, it is vital to evaluate the influence of each fNIRS channel on sending and receiving information ($p<0.05$). There were 400 intersection nodes in the connectivity network due to the 20 fNIRS channels being connected together. Figure 4.9 demonstrates the change in the number of crucial nodes between each two phases as a function of the applied threshold. Prior to and following application of the BBS, the maximum number of important nodes was observed (Vigilance Vs Enhancement, Stress Vs Mitigation). Between Vigilance and Enhancement Phases, the number of significant nodes dropped significantly, suggesting that most PDC values were fluctuating between thresholds of 0.1 and 0.2. Following

the previous approach, Figures 4.10, 4.11, and 4.12 show the difference in PDC connectivity between (Vigilance-Enhancement), (Stress-Mitigation), and (Vigilance-Stress). Specifically, in addition to the paired t-test for every node, a threshold of 0.7 was added to each map ($p<0.05$). As can be shown, the BBS played an important role in enhancing vigilance by recording elevated connectivity values for several ventrolateral channels, whereas channel 14 in the dorsolateral region showed lower connectivities with BBS. Similarly, the BBS in the right PFC showed considerable stress mitigation (high connection) compared to low connectivity values in the left ventrolateral area.

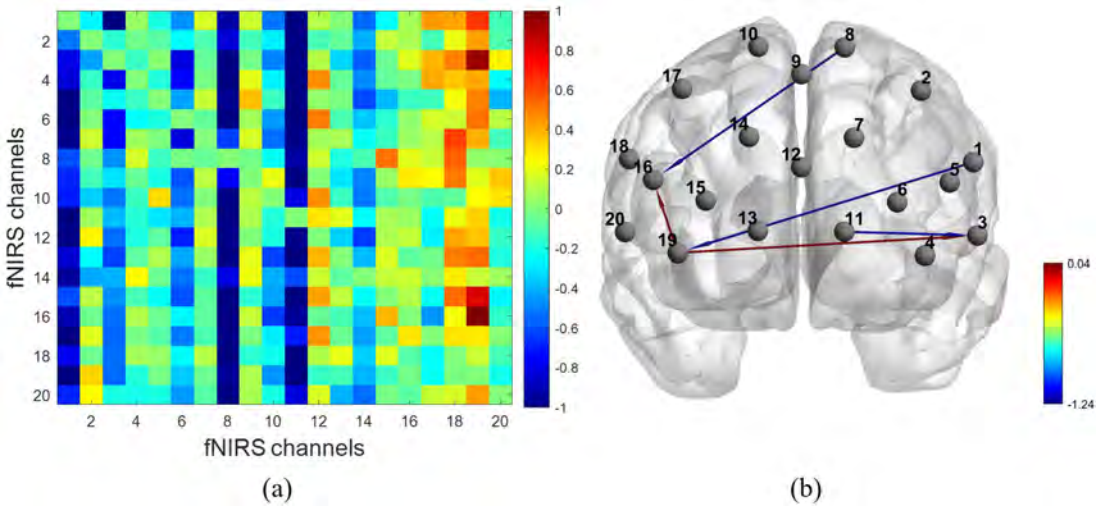

Figure 4.7: The functional connectivity difference. (a) subtraction PDC map for Vigilance-Stress with the hypothesis test results for each node, (b) the significant connectivities between the two phases.

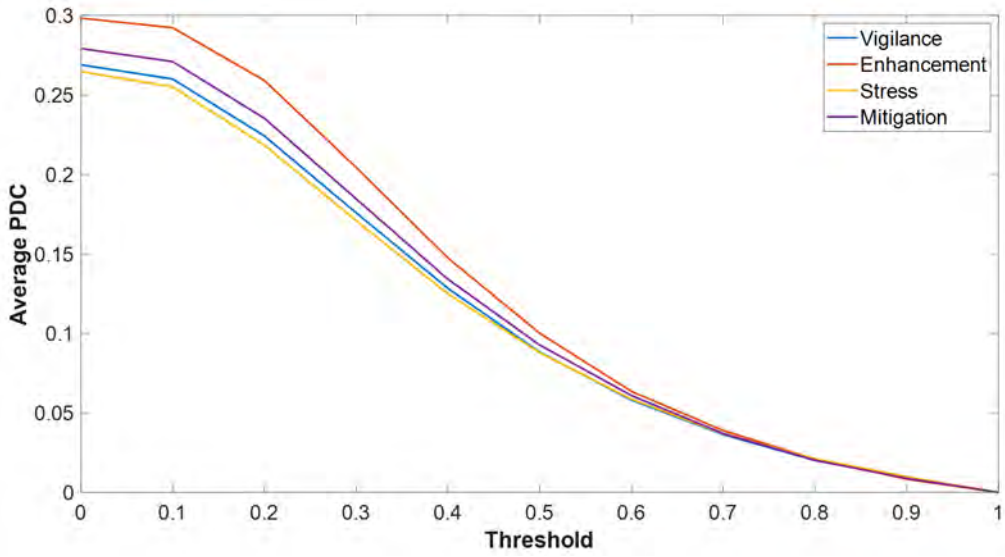

Figure 4.8: The average PDC behavior with respect to the PDC threshold increases.

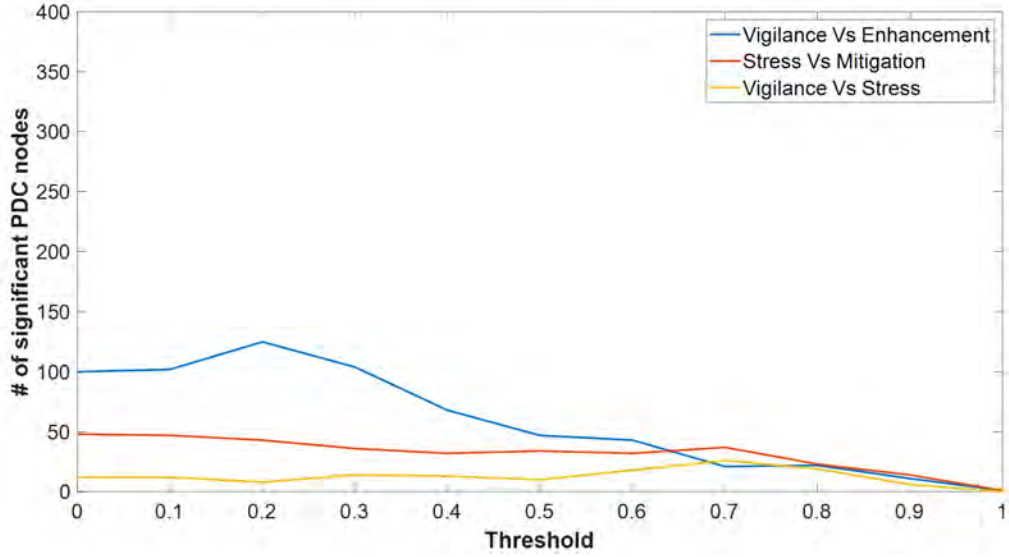

Figure 4.9: The number of significant PDC nodes between each two stress phases in relation to the PDC threshold grows.

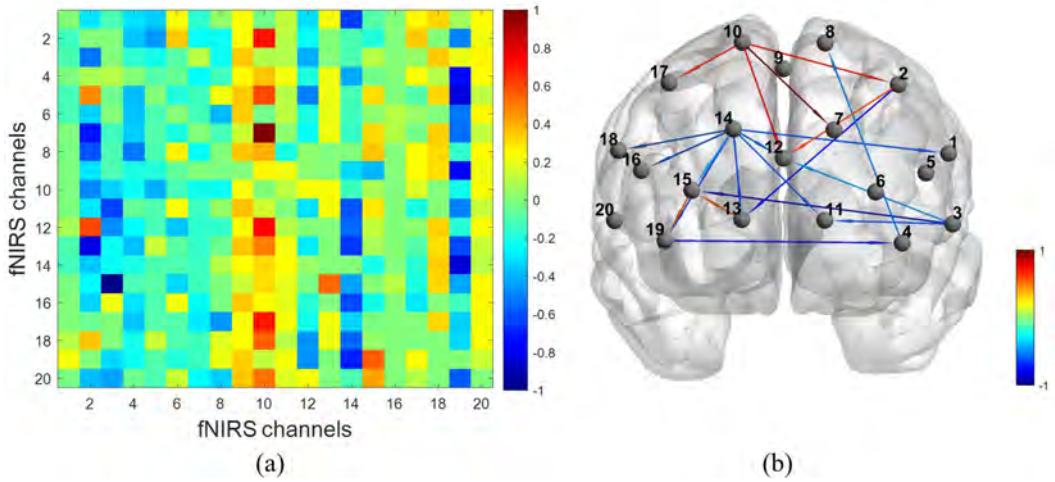

Figure 4.10: The functional connectivity difference with PDC threshold of 0.7. (a) subtraction PDC map for Vigilance-Enhancement with the hypothesis test results for each node, (b) the significant connectivities between the two phases.

4.5 Graph Theory Analysis

For the purpose of examining and quantifying cortical functional connectivity, a network graph theoretical analysis (GTA) was used. Networks of nodes and weighted edges were constructed using the PDC matrices. The global and local topology of functional connectivity networks were characterized using GTA depending on the concepts of node degree (ND), node strength (NS), clustering coefficient (CC), and efficiency (NE). To get the global versions of the nodes in the network's topology, we used the arithmetic means of their local versions. As a consequence, the comparison of the Alertness and Enhancement phases provided insight into BBS's capability to

improve vigilance. Furthermore, by comparing the Stress and Mitigation phases, the efficacy of BBS to reduce mental stress could be analyzed. Finally, the differences between the Vigilance and Stress phases were examined in order to validate the efficacy of SCWT to induce stress and the ability of fNIRS to measure it.

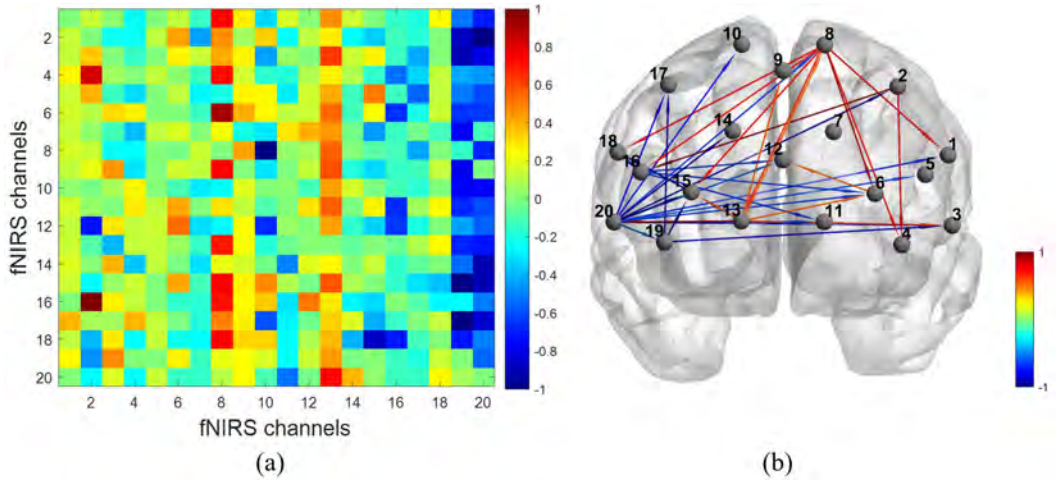

Figure 4.11: The functional connectivity difference with PDC threshold of 0.7. (a) subtraction PDC map for Stress-Mitigation with the hypothesis test results for each node, (b) the significant connectivities between the two phases.

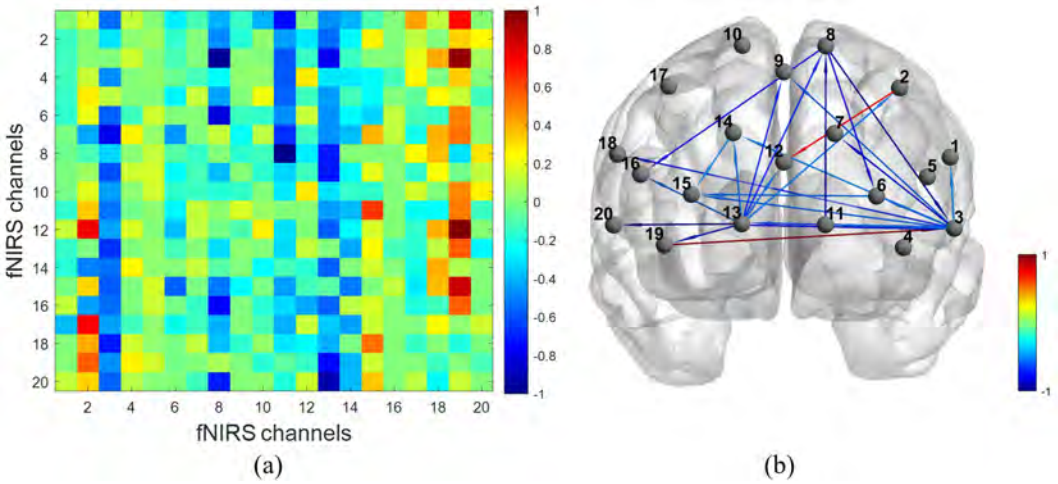

Figure 4.12: The functional connectivity difference with PDC threshold of 0.7. (a) subtraction PDC map for Vigilance-Stress with the hypothesis test results for each node, (b) the significant connectivities between the two phases.

4.5.1 Global network analysis

Figures 4.13–4.16 compare the global ND, NS, CC, and NE of full-scale functional networks under the four stress conditions. The mean values are shown, with error bars representing the standard error around the mean. Meanwhile, to examine the influence of network threshold level, the estimated metrics were displayed against a complete threshold range of 0 to 1 with a 0.1 step. A paired sample t-test was used at each

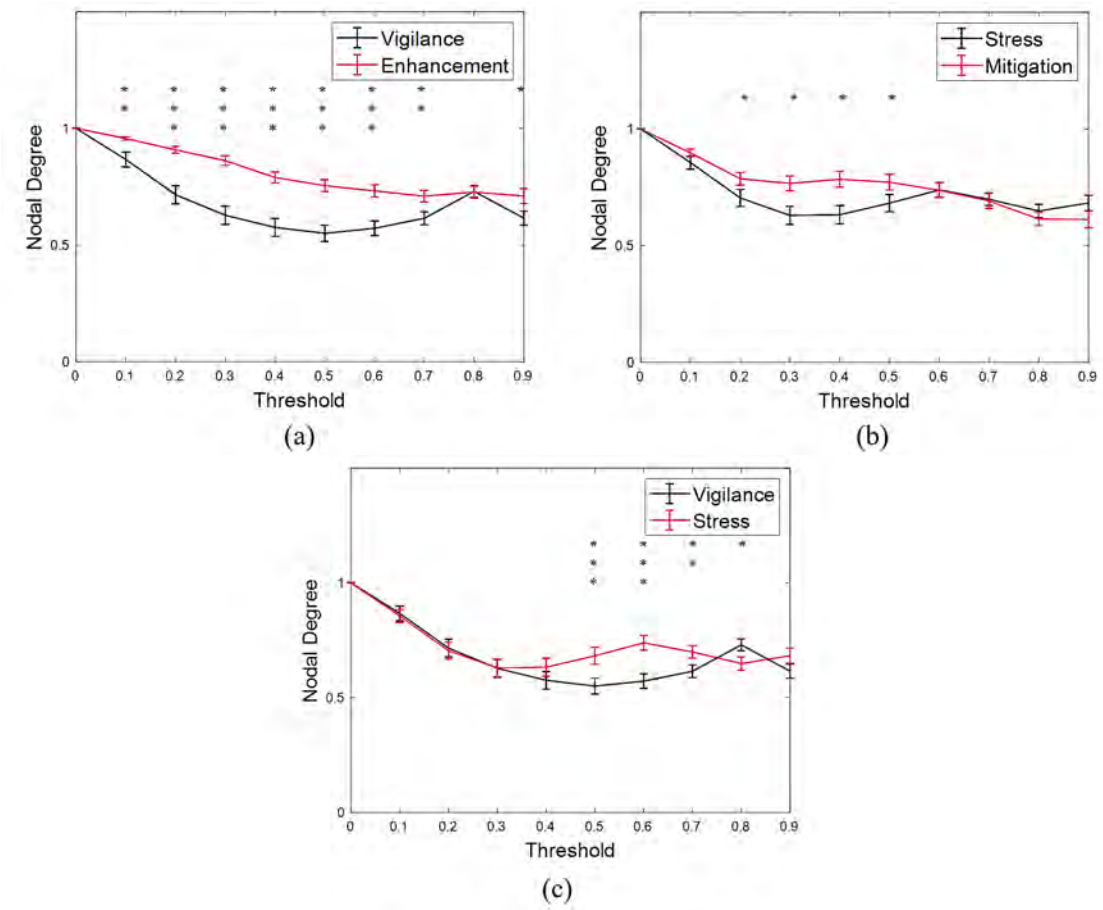

Figure 4.13: A comparison of the full-scale network's global node degree between the phases (a) Vigilance/Enhancement, (b) Stress/Mitigation and (d) Vigilance/Stress. The mean values among participants are shown, with error bars representing the standard error. The asterisks indicate that cognitive state has a substantial influence (*:p<0.05, **:p<0.01, ***:p<0.001).

threshold level to examine the statistical significance of differences between each two cognitive states. The asterisks on the graphs show that cognitive state has a significant influence (*:p<0.05, **:p<0.01, ***:p<0.001). ND values in the Enhancement phase were consistently high in Figure 4.13, showing a substantial effect for the BBS. In the threshold range (0.2-0.5), BBS was beneficial in mitigating stress (p<0.05), but it had no impact in the rest of the range (0.6-1). Additionally, ND showed no difference between the Vigilance and Stress phases for the threshold range (0-0.3) whereas it was significantly high in the Stress phases for the threshold range (0.4-0.7). Meanwhile, the only threshold value that exhibited a contrast effect for the ND between the two phases was the 0.8 threshold. As demonstrated in Figure 4.14, when network threshold rises, a slight decrease in the NS is noted throughout all four phases. This is to be expected because higher threshold levels account for a smaller number of edges. Additionally,

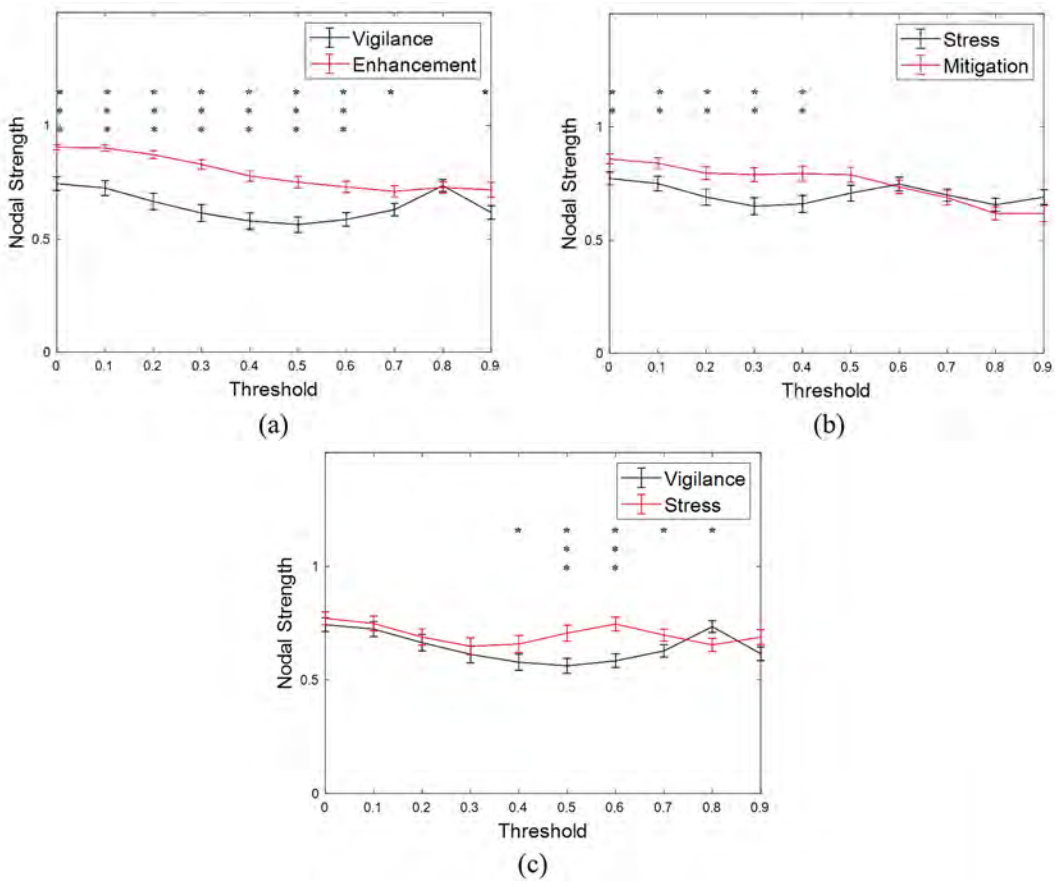

Figure 4.14: A comparison of the full-scale network's global node strength between the phases (a) Vigilance/Enhancement, (b) Stress/Mitigation and (d) Vigilance/Stress. The mean values among participants are shown, with error bars representing the standard error. The asterisks indicate that cognitive state has a substantial influence (*:p<0.05, **:p<0.01, ***:p<0.001).

the influence of the BBS on cognitive state was statistically significant throughout a low threshold range. Over the entire threshold range, the NS for the BBS phases (Enhancement and Mitigation) was substantially greater than that for the Vigilance and Stress phases. Meanwhile, statistical significance between the Vigilance and Stress phases became obvious for thresholds specified by 0.4-0.8. Figure 4.15 shows how the network's CC dropped significantly after the threshold value of 0.3. The clustering coefficients indicated substantial differences between Vigilance and Enhancement for the low and high threshold values (but not for the middle range values), while similar pattern was seen only for the first three thresholds between the Stress and Mitigation phases. On the other hand, across all thresholds, CC demonstrated no significant change between the Vigilance and Stress phases. Eventually, global efficiency findings showed the same effects by having a substantial influence on the BBS on increasing vigilance and reducing stress across many threshold values (mainly for the first half of the range).

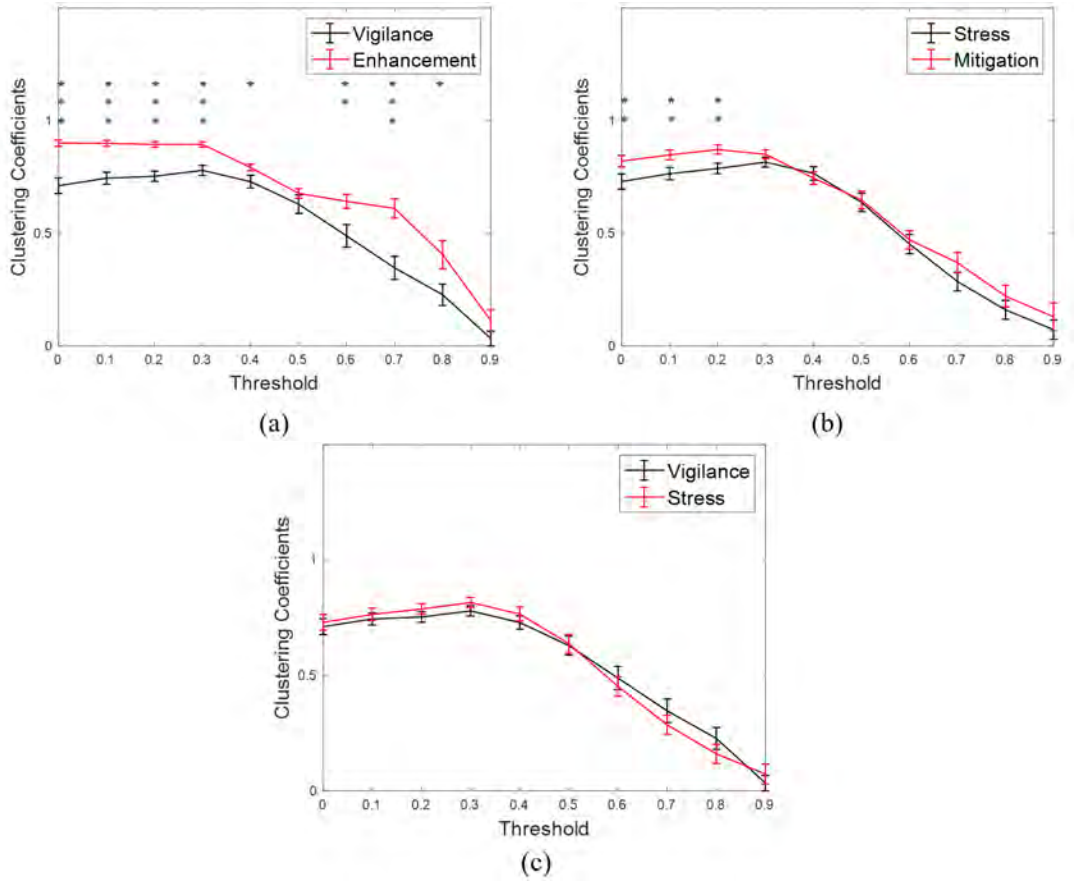

Figure 4.15: A comparison of the full-scale network's global clustering coefficients between the phases (a) Vigilance/Enhancement, (b) Stress/Mitigation and (d) Vigilance/Stress. The mean values among participants are shown, with error bars representing the standard error. The asterisks indicate that cognitive state has a substantial influence (*:p<0.05, **:p<0.01, ***:p<0.001).

When it came to the Vigilance and Stress phases, only 0.6 and 0.7 thresholds distinguished the NE from the rest of the group.

4.5.2 Local network analysis

The scalp maps of the full-scale local node degree, strength, clustering coefficient, and efficiency are shown in Figures 4.17–4.20. The mapped values are the overall average of all subjects. A paired sample t-test was used for each channel to evaluate the statistical significance of changes in local topology between the Vigilance/Enhancement and Stress/Mitigation phases. On the maps, asterisks (*) indicate a statistically significant difference ($p < 0.05$). The nodal degree for each phase is shown in Figure 4.17 for all twenty channels. Throughout the four phases, a high nodal degree was seen in the dorsolateral and left ventrolateral regions. Meanwhile, the significance of the negative t-test findings across many channels indicated a substantial difference between the Vigilance and Enhancement phases, suggesting the BBS'

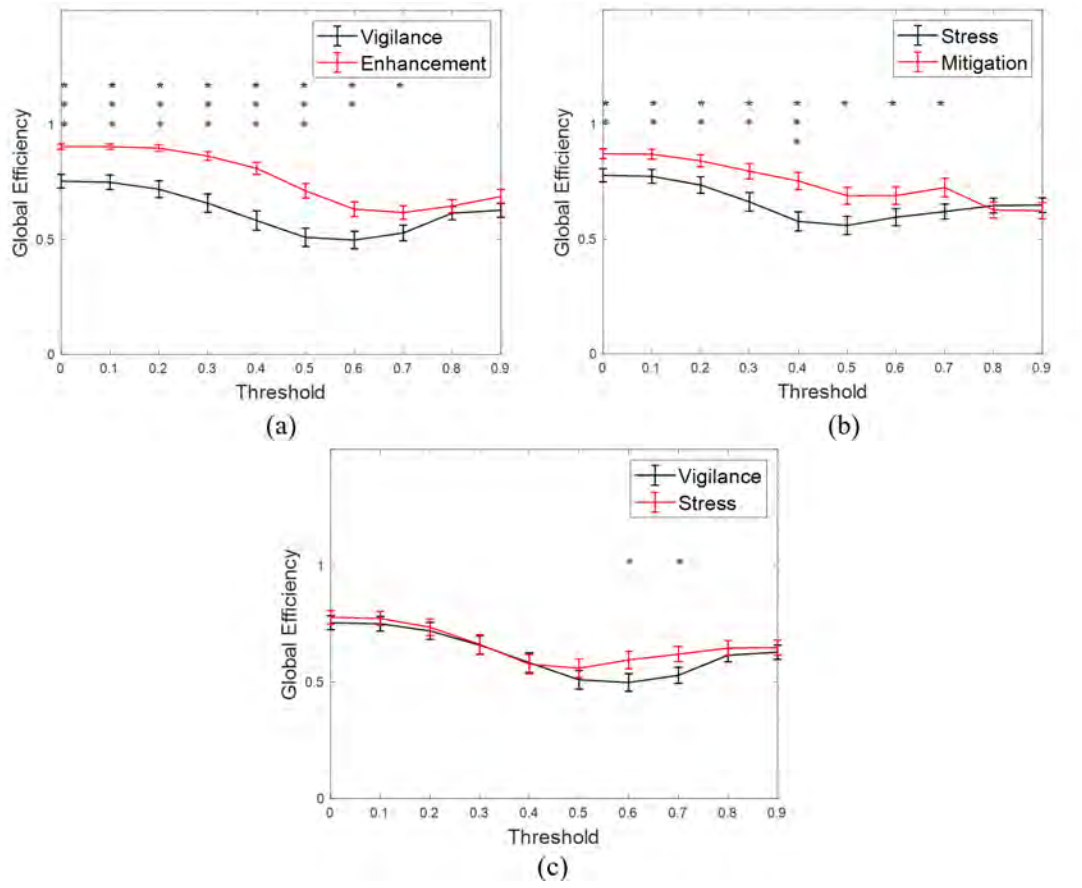

Figure 4.16: A comparison of the full-scale network's global node efficiency between the phases (a) Vigilance/Enhancement, (b) Stress/Mitigation and (d) Vigilance/Stress. The mean values among participants are shown, with error bars representing the standard error. The asterisks indicate that cognitive state has a substantial influence (*:p<0.05, **:p<0.01, ***:p<0.001).

essential function. Similarly, only three channels demonstrated this substantial impact of the BBS on relieving stress. The outcomes of the local nodal strength analysis are depicted in Figure 4.18, which show general full-scale increases in connectivity for the majority of channels over the four phases. Furthermore, under all conditions, there was substantial connectivity at the dorsolateral channels (i.e, 2, 8, 10 and 17). However, statistical analysis indicated a significant difference between the Vigilance and Enhancement phases for those channels, but not between the Stress and Mitigation phases. Almost all of the channels that shown a crucial difference in the local nodal degree between phases with/without BBS also demonstrated the same behavior with the local strength. Phase enhancement/mitigation demonstrated substantial increases in nearly all prefrontal brain channels using a paired sample t-test. According to paired t-test results, the full-scale local clustering coefficient decreased throughout the Enhancement stage in the channels (2, 8, 10, and 17) as shown in Figure 4.19.

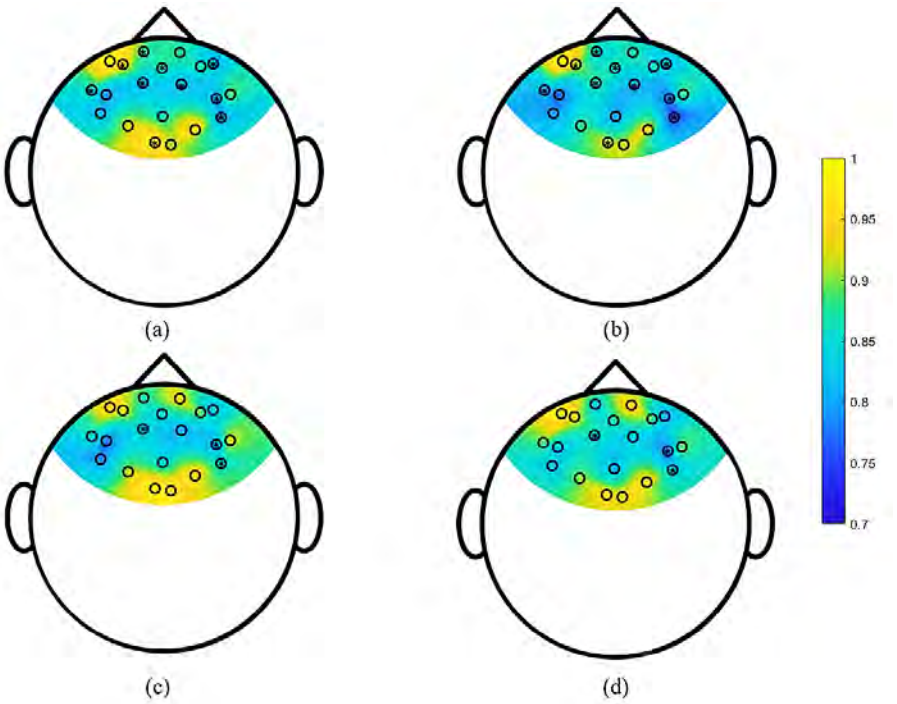

Figure 4.17: Scalp topography maps of local node degree in (a) Vigilance, (b) Enhancement, (c) Stress, and (b) Mitigation phases. The mapped values are the overall average of all subjects. The asterisks (*) indicate a statistically significant local difference ($p < 0.05$) between the two cognitive states.

Intriguingly, functional segregation was found to be larger between the Vigilance and Enhancement phases than between the Stress and Mitigation phases. Similarly, as illustrated in Figure 4.20, the local efficiency displayed an increasing connection trend that was BBS-specific.

4.6 Relationships between Functional Connectivity and Behavioral Responses

In this part, we compared the changes in connectivity strength (Nodal Strength) to reaction accuracy (response accuracy to SCWT stimuli) and Cortisol levels across the four phases. To begin, we calculated the changes in strength between the two phases by subtracting the Vigilance group's strength from the Enhancement group's strength, the Stress group's strength from the Mitigation group's strength, and lastly, the Vigilance group's strength from the Stress group's strength. These subtraction operations were based on the one-versus-all principle. In this case, the average strength of each subject in the vigilance group may be deducted from the average strength of all other individuals in the enhancement group. The ultimate strength was then calculated using the weighted sum. Positive strength difference implied network enhancement, whereas negative degree indicated network impairments or decline. Second, identical to what

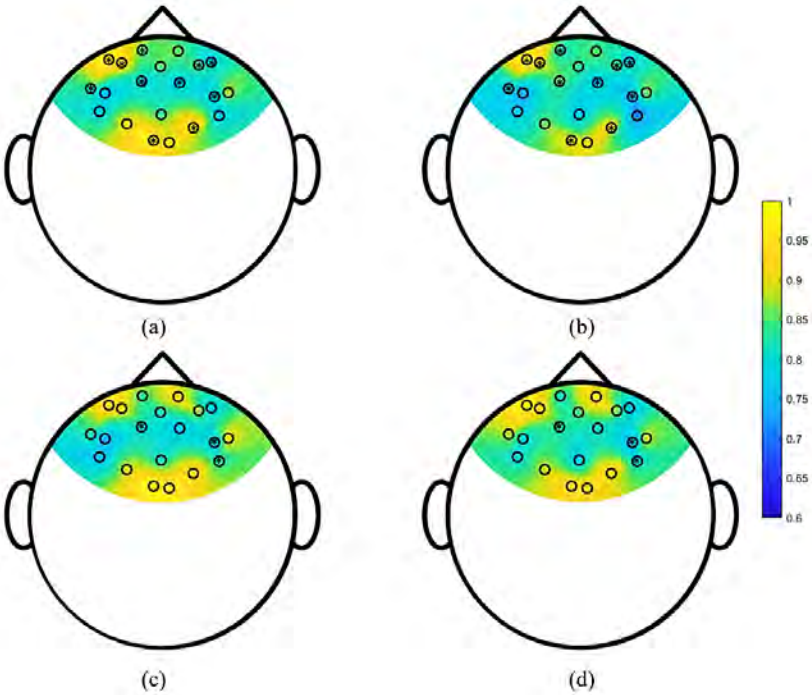

Figure 4.18: Scalp topography maps of local node strengths in (a) Vigilance, (b) Enhancement, (c) Stress, and (b) Mitigation phases. The mapped values are the overall average of all subjects. The asterisks (*) indicate a statistically significant local difference ($p < 0.05$) between the two cognitive states.

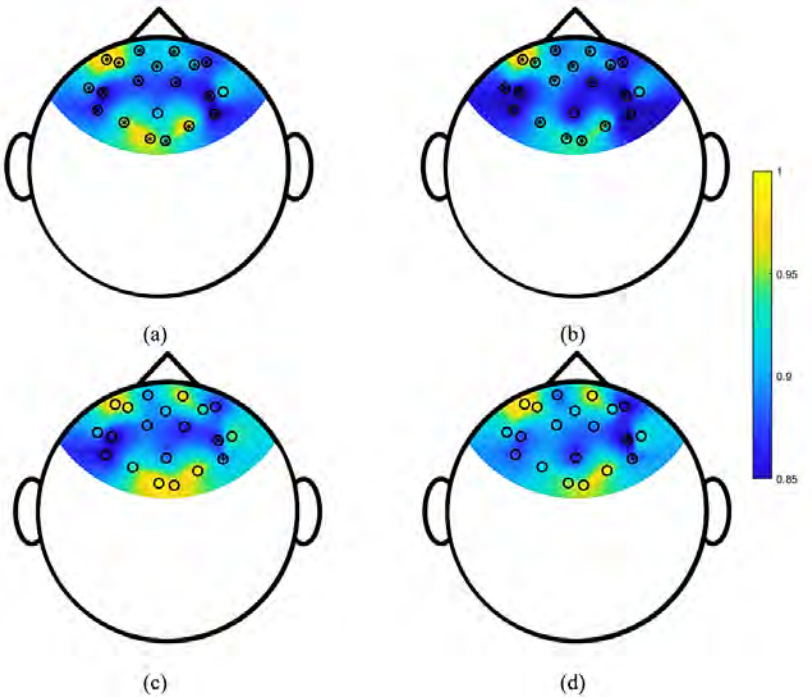

Figure 4.19: Scalp topography maps of local node clustering coefficients in (a) Vigilance, (b) Enhancement, (c) Stress, and (b) Mitigation phases. The mapped values are the overall average of all subjects. The asterisks (*) indicate a statistically significant local difference ($p < 0.05$) between the two cognitive states.

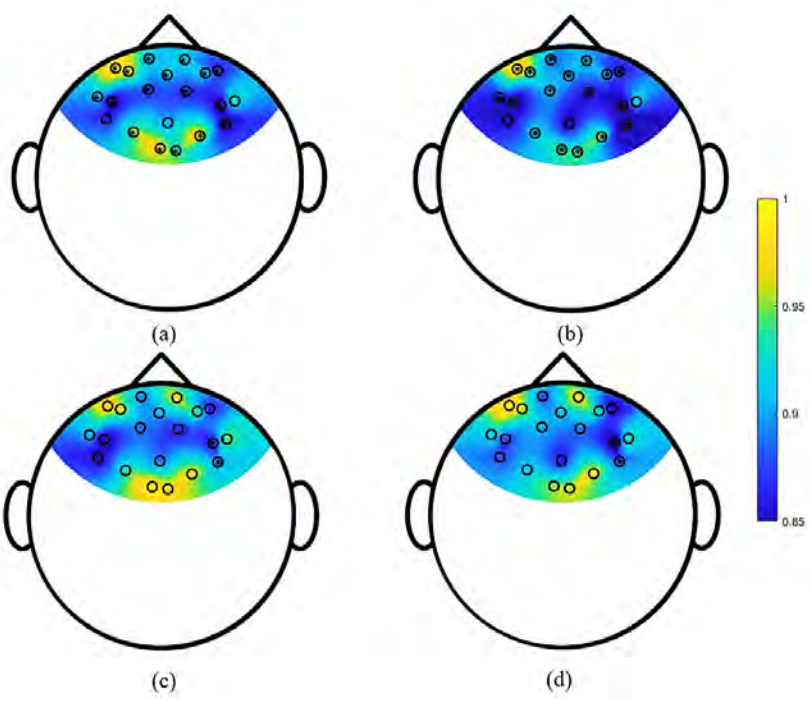

Figure 4.20: Scalp topography maps of local node efficiency in (a) Vigilance, (b) Enhancement, (c) Stress, and (b) Mitigation phases. The mapped values are the overall average of all subjects. The asterisks (*) indicate a statistically significant local difference ($p < 0.05$) between the two cognitive states.

was said previously, we determined the variations in SCWT accuracy by subtracting the recorded accuracy between each two phases. A positive difference in accuracy implied an improvement, whereas a negative difference suggested an impairment. Third, we determined the differences in cortisol levels between the two periods by subtracting the cortisol levels observed during each phase. Cortisol differences that are positive suggested deficits, whereas cortisol differences that are negative indicated enhancement. The results indicated that changes in strength were negatively correlated with cortisol levels and positively correlated with SCWT accuracy in the three instances investigated, as seen in Figures 4.21 and 4.22. The participants with the largest improvement in connection strength had a drop in cortisol levels and an increase in reaction accuracy to stimuli. This implies that the more connected the brain areas are, the greater the performance.

4.7 Convolutional Neural Network

The results acquired with Convolutional Neural Network (CNN) will be summarized in this section. To recap, three convolutional layers with fifteen filters were employed, as well as 5-fold-cross-validation (CV). The CNN was fed PDC matrices (each matrix

is 20×20 representing fNIRS channels × fNIRS channels) that also include stress phases (4 phases), frequencies (30 frequencies), SCWT blocks (10 blocks/trials), and subjects (30 subjects).

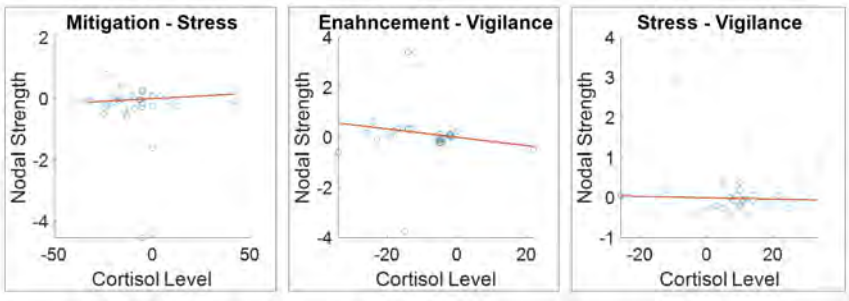

Figure 4.21: Correlation graphs between participants' cortisol levels and nodal strength. The vertical axis indicates the values of the various graph metrics, while the horizontal axis indicates the cortisol level.

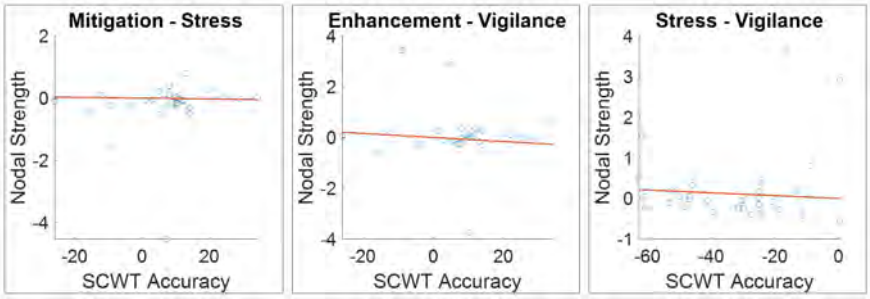

Figure 4.22: Correlation graphs between participants' response accuracy and nodal strength. The vertical axis indicates the values of the various graph metrics, while the horizontal axis indicates the SCWT accuracy.

CNN's analysis was conducted in three distinct ways. The initial analysis included CNN subject-independent analysis of all phases together (Vigilance, Enhancement, Stress and Mitigation). The PDC's six-dimensional matrix, which is 4×30×10×30×20×20 and represents task phases × subjects × blocks × frequencies × channels × channels, was translated to a three-dimensional matrix for each level. As a result, the Vigilance phase, for example, contained 9000 PDC maps (the 9000 came from the 30 subjects, 10 blocks and the 30 frequencies). Then four labels were used to indicate the four phases. The applied 5-fold CV results in 7200 PDC maps for training and 1800 PDC maps for validation for each phase. The accuracy, sensitivity, specificity, and precision obtained from training/testing the four phases are summarized in Table 4.2. Meanwhile, the confusion matrix for these results is depicted in Figure 4.23. The effectiveness of PDC and fNIRS to identify mental state is readily apparent when the largest portion of the

PDC maps is correctly matched to the phase associated. Likewise, the Vigilance and Mitigation phases produced the highest accuracy in correctly detecting the number of PDC maps that are supposed to be treated as Vigilance or Mitigation maps (out of the 9000) achieving 79.9% and 74.78%, respectively. This confirms the BBS's potential to enhance vigilance and reduce stress levels.

After that, CNN subject-independent analysis was used to compare each two phases together (binary analysis). Hence, the matrix for each phase had the same dimension as before which is 9000×20×20 that reflects 9000 PDC maps. The validation performance of the proposed CNN between each two phases is illustrated in Table 4.3. As indicated in the first two columns, the high records attained demonstrate BBS's capacity for enhancing vigilance and mitigating stress. Similarly, the Vigilance/Stress records indicate the SCWT's ability to induce stress as well as the fNIRS's ability to detect mental stress. The results depicted in Figures 4.24, 4.25, and 4.26 corroborate earlier findings by reaching the best accuracy for vigilance enhancement, stress reduction, and, to a lesser extent, stress induction/detection.

On the other hand, CNN architecture was used also to classify the four phases (Vigilance, Enhancement, Stress, and Mitigation) for each subject (subject-dependent analysis) utilizing PDC connectivity maps. Table 4.4 highlights the performance in terms of the number of PDC matrices that truly match the related phase. For each subject, the 30 frequency bands and the 10 SCWT blocks were combined to generate 300 PDC matrices per phase (where 240 of them were used for training and the 60 for validation). As a result, the maximum number of PDC matrices that can be recorded for any subject in each phase is 300. According to each subject's status, decisions were made in the areas of vigilance (V), enhancement (E), stress (S), and mitigation (M). The CNN results demonstrate the PDC's capacity to accurately reflect the nuances of each phase. The aforementioned findings corroborate the performance of BBS, SCWT, and fNIRS.

Table 4.2: 5-fold cross validation performance of proposed CNN between the four phases

Task phases	Accuracy (%)	Sensitivity (%)	Specificity (%)	Precision (%)
Vigilance Enhancement Stress Mitigation	70.62	68.39	90.76	71.16

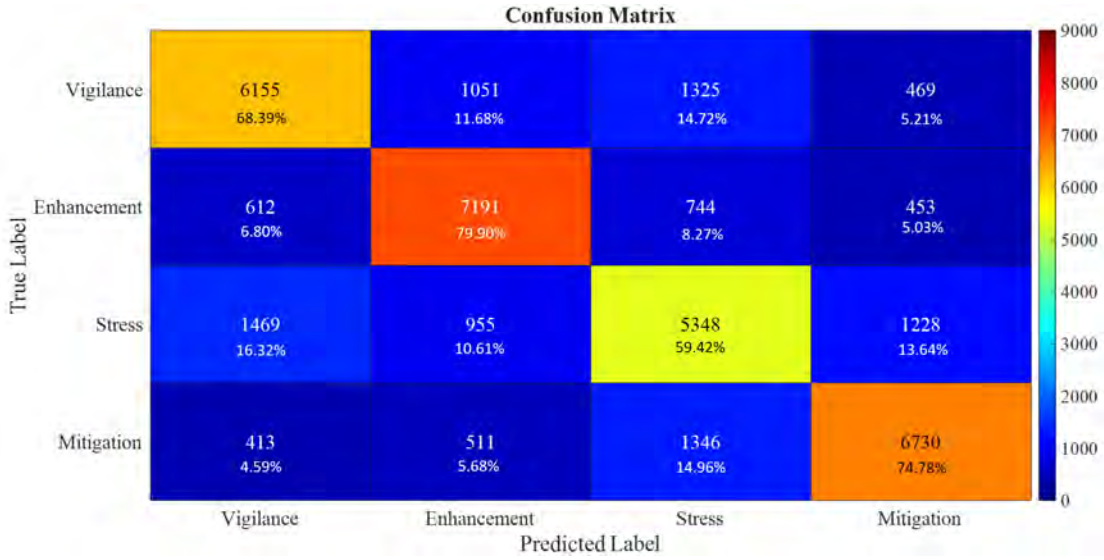

Figure 4.23: Confusion matrix for PDC matrices classification (9000 matrices per phase)

Table 4.3: 5-fold cross validation performance of proposed CNN between each two phases

	Vigilance Vs Enhancement	**Stress Vs Mitigation**	**Vigilance Vs Stress**
Accuracy (%)	96.42	94.39	93.36
Sensitivity (%)	95.96	94.33	93.57
Specificity (%)	96.89	94.44	93.10
Precision (%)	96.86	94.43	93.13

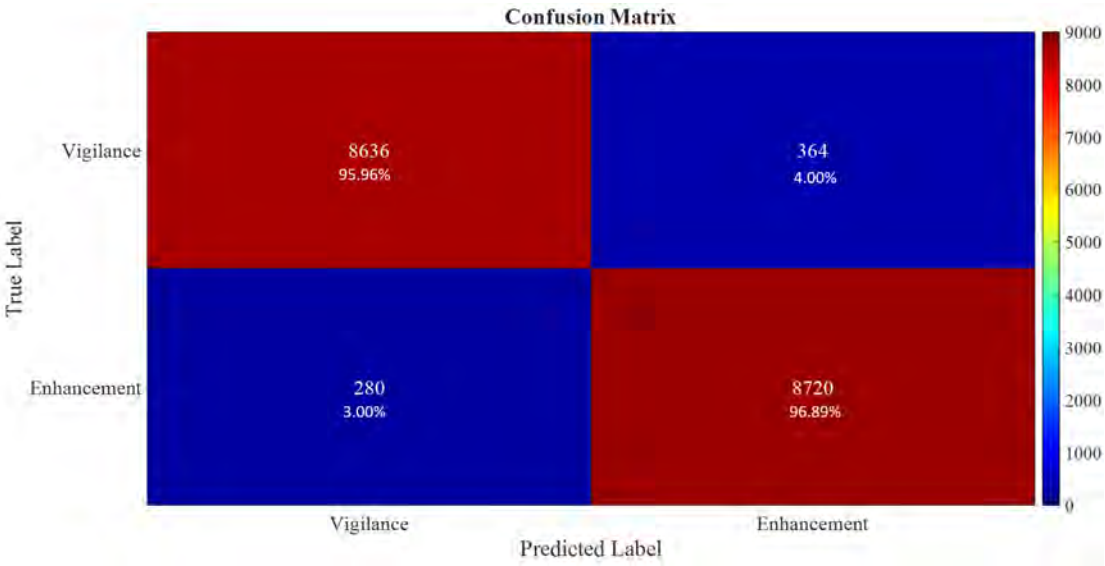

Figure 4.24: Confusion matrix for PDC matrices classification between Vigilance and Enhancement phases (9000 matrices per phase)

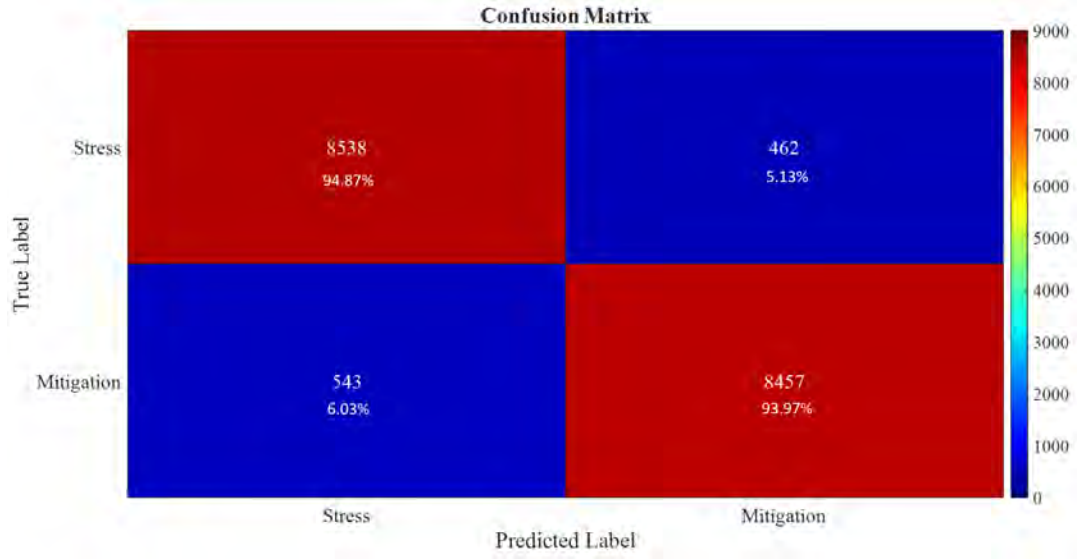

Figure 4.25: Confusion matrix for PDC matrices classification between Stress and Mitigation phases (9000 matrices per phase)

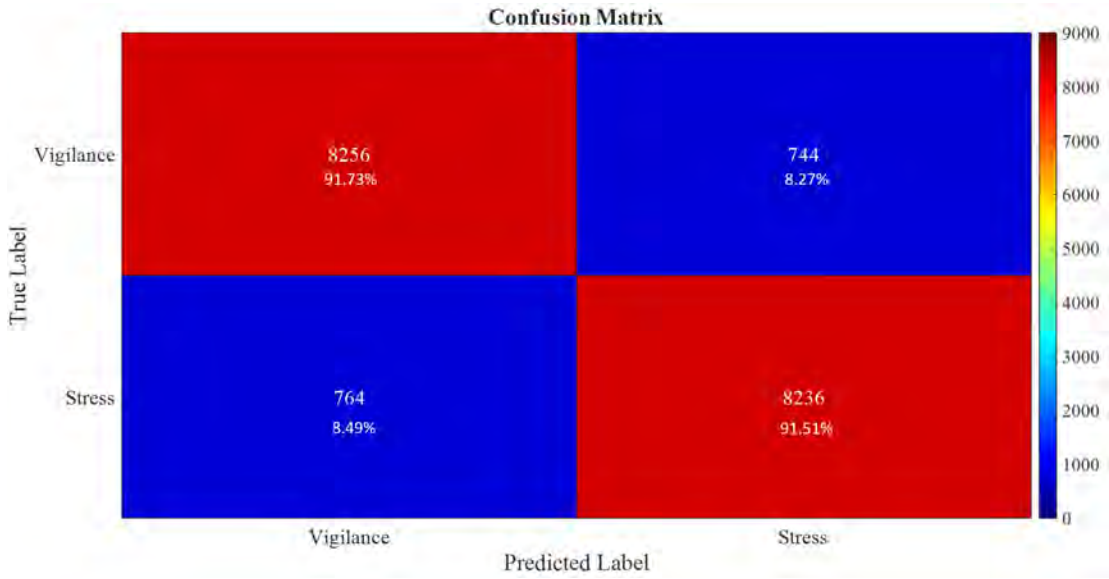

Figure 4.26: Confusion matrix for PDC matrices classification between Vigilance and Stress phases (9000 matrices per phase)

Table 4.4: CNN validation results for 300 PDC matrices per phase. Acc: Accuracy, Sen: Sensitivity, Spec: Specificity.

	# of PDC matrices (out of 300) identified as:												Acc (%)	Sen (%)	Spec (%)
Subject	**Vigilance**	**Acc (%)**	**Decision**	**Enhancement**	**Acc (%)**	**Decision**	**Stress**	**Acc**	**Decision**	**Mitigation**	**Acc**	**Decision**			
1	296	98.67	V	295	98.33	E	299	99.67	S	300	100.0	M	99.17	98.67	99.56
2	300	100.00	V	298	99.33	E	294	98.00	S	300	100.0	M	99.33	100.00	100.00
3	300	100.0	V	300	100.0	E	300	100.0	S	300	100.0	M	100.0	100.0	100.0
4	300	100.0	V	300	100.0	E	300	100.0	S	300	100.0	M	100.0	100.0	100.0
5	295	98.33	V	300	100.0	E	297	99.00	S	300	100.0	M	99.33	98.33	100.00
6	299	99.67	V	299	99.67	E	300	100.0	S	300	100.0	M	99.83	99.67	99.89
7	290	96.67	V	280	93.33	E	296	98.67	S	281	93.67	M	95.58	96.67	99.67
8	297	99.00	V	300	100.0	E	300	100.0	S	300	100.0	M	99.75	99.00	100.0
9	300	100.0	V	300	100.0	E	300	100.0	S	300	100.0	M	100.0	100.0	100.0
10	300	100.0	V	300	100.0	E	300	100.0	S	298	99.33	M	99.83	100.0	100.0
11	297	99.00	V	288	96.00	E	300	100.0	S	300	100.0	M	98.75	99.00	100.0
12	299	99.67	V	300	100.0	E	300	100.0	S	300	100.0	M	99.92	99.67	100.0
13	298	99.33	V	297	99.00	E	298	99.33	S	298	99.33	M	99.25	99.33	99.33
14	297	99.00	V	300	100.0	E	300	100.0	S	300	100.0	M	99.75	99.00	100.0
15	300	100.0	V	296	98.67	E	297	99.00	S	299	99.67	M	99.33	100.0	99.56

16	298	99.33	V	299	99.67	E	289	96.33	S	300	100.0	M	98.83	99.33	99.89
17	300	100.0	V	300	100.0	E	298	99.33	S	300	100.0	M	99.83	100.0	100.0
18	299	99.67	V	292	97.33	E	298	99.33	S	299	99.67	M	99.00	99.67	99.78
19	294	98.00	V	274	91.33	E	294	98.00	S	300	100.0	M	96.83	98.00	99.67
20	293	97.67	V	300	100.0	E	287	95.67	S	288	96.00	M	97.33	97.67	99.67
21	298	99.33	V	300	100.0	E	300	100.00	S	300	100.0	M	99.83	99.33	100.0
22	300	100.0	V	291	97.00	E	300	100.00	S	300	100.0	M	99.25	100.0	100.0
23	298	99.33	V	300	100.0	E	299	99.67	S	295	98.33	M	99.33	99.33	100.0
24	293	97.67	V	284	94.67	E	296	98.67	S	300	100.0	M	97.75	97.67	100.0
25	300	100.0	V	300	100.0	E	300	100.0	S	300	100.0	M	100.0	100.0	100.0
26	297	99.00	V	294	98.00	E	293	97.67	S	287	95.67	M	97.58	99.00	99.22
27	299	99.67	V	296	98.67	E	298	99.33	S	299	99.67	M	99.33	99.67	100.0
28	299	99.67	V	300	100.0	E	300	100.0	S	300	100.	M	99.92	99.67	100.0
29	298	99.33	V	300	100.0	E	300	100.0	S	300	100.	M	99.83	99.33	100.0
30	297	99.00	V	296	98.67	E	300	100.0	S	300	100.	M	99.42	99.00	100.0

Chapter 5. Conclusion and Future work

This thesis examined two significant stress-related issues that are prevalent in a range of operational and industrial contexts. To begin, a quantitative method to stress evaluation was suggested based on graph theory analysis of fNIRS functional connectivity. Second, the efficacy of auditory stimulation in improving vigilance performance and mitigating stress was examined. The fNIRS data collection technique was based on a computerized version of the Stroop Color-Word Task (SCWT). Four scenarios based on SCWT and Binaural Beat Stimulation (BBS) were suggested as part of the experimental protocol: Vigilance (SCWT with no audio), Enhancement (SCWT with BBS), Stress (SCWT under time pressure with no audio) and Mitigation (SCWT with time pressure and BBS). A 10-minutes SCWT triggered each of the four stages. Cortical connection was modelled using the partial directed coherence value statistic, which was used throughout the Vigilance and Stress phases as well as the Enhancement and Mitigation phases. The connectivity networks were then subjected to extensive graph theory research in order to measure and compare their many topological properties. Finally, we used deep learning using a convolutional neural network (CNN) to validate BBS's capacity to increase alertness and reduce stress, as well as fNIRS's ability to identify stress levels.

5.1 Major Findings

The purpose of this research was to explore a new technique of stress detection and reduction based on functional near infrared spectroscopy and binaural beat stimulation. Furthermore, when time pressure was applied, the experimental findings demonstrated that the ten-minutes SCWT successfully produced stress in the cortical connections. The PDC statistic responded well to changes in stress levels, increased alertness, and reduced stress. Studying prefrontal cortex PDC networks revealed that alterations in functional connectivity during mental stress were confined to cortical regions and fNIRS channels. During each of the 10 block designs of the SCW, participants received binaural beat stimulation in both ears at the same time. Simultaneously with the SCWT, we monitored individuals' hemodynamic responses, stress hormone levels, and behavioral reactions. Subject-independent classification revealed an accuracy of 96.42%, 94.39%, and 93.36% for detecting vigilance augmentation, stress mitigation,

and stress induction, respectively, utilizing GTA and PDC characteristics belonging to a single cortical area and frequency band. Cortical connection remained strong for the course of the audio-enhanced mental states. Additionally, substantial increases in participant performance were found when audio was used. BBS improved vigilance detection by an average of 11.51%, while stress mitigation detection improved by an average of 15.36%. Moreover, we discovered that stress raised salivary alpha amylase levels, which reduced after treatment with binaural beat stimulation. Similarly, we observed that accuracy in answering the SCWT question decreased substantially between Vigilance and Stress and rose significantly between Stress and Mitigation, suggesting gains in cognitive function. Stress hormone and behavioral responses show that the proposed binaural beat stimulation substantially reduces stress levels. Thus, the findings demonstrate that the proposed methodology is capable of quantifying many elements of cortical functional connectivity under a variety of stress conditions. To identify vigilance-enhancement and stress-mitigation with trustworthy accuracy, the topology of PFC connection patterns may be characterized as simple and dimension-reduced indices. Finally, the findings demonstrate that auditory stimulation may improve cognitive processing and behavioral performance.

5.2 Recommendations and Future Directions for Research

It is important to highlight that the study's primary drawback is its small sample size, and the number of individuals included was deemed small to overcome biases resulting from individual variations. Our results will be more robust if we had a bigger sample size to work with. The following are some suggestions for further research based on this study:

- The PDC has been shown to be effective in mental state discriminating settings as one of the best predictive functional connectivity estimators. While the PDC showed susceptibility to stress induction/mitigation, alternative estimators of functional connectivity may be worth investigating.
- This study relied heavily on the processing of fNIRS data for stress evaluation. FNIRS is a relatively novel neuroimaging technique that has been utilized in investigations of alertness, mental fatigue, and emotions. It is possible, though, that other physiological and neuroimaging modalities will reveal more about

vigilance/stress' brain and physiological processes. Thus, researching stress through a multimodal neuroimaging approach would be advantageous. If this is the case, applying feature fusion techniques is anticipated to enhance the accuracy of identifying and mitigating stress.

References

[1] H. Selye, "The stress syndrome," *The American Journal of Nursing*, vol. 65, no. 3, pp. 97-99, 1965.

[2] F. Al-Shargie, “Quantification of Mental Stress using fNIRS Signals”, 07-Apr-2019. [Online]. Available: engrxiv.org/um762.

[3] G. Giannakakis, D. Grigoriadis, K. Giannakaki, O. Simantiraki, A. Roniotis, and M. Tsiknakis, "Review on psychological stress detection using biosignals," *IEEE Transactions on Affective Computing*, pp. 1-22, 2019.

[4] O. V. Crowley, P. S. McKinley, M. M. Burg, J. E. Schwartz, C. D. Ryff, M. Weinstein, T. E. Seeman, R. P. Sloan, "The interactive effect of change in perceived stress and trait anxiety on vagal recovery from cognitive challenge," *International Journal of Psychophysiology*, vol. 82, no. 3, pp. 225-232, 2011.

[5] P. A. Thoits, "Stress and health: Major findings and policy implications," *Journal of Health Social Behavior*, vol. 51, no. 1_suppl, pp. S41-S53, 2010.

[6] Garg A, Chren M, Sands LP, et al, "Psychological stress perturbs epidermal permeability barrier homeostasis: implications for the pathogenesis of stress-associated skin disorders," *JAMA Dermatology*, vol. 137, no. 1, pp. 53-59, 2001.

[7] T. C.Adam and E. S.Epel, "Stress, eating and the reward system," *Physiology & Behavior*, vol. 91, no. 4, pp. 449-458, 2007.

[8] J. Bakker, M. Pechenizkiy, and N. Sidorova, "What's your current stress level? Detection of stress patterns from GSR sensor data," *2011 IEEE 11th International Conference on Data Mining Workshops*, 2011, pp. 573-580, doi: 10.1109/ICDMW.2011.178.

[9] T. W. Colligan and E. M. Higgins, "Workplace stress: Etiology and consequences," *Journal of Workplace Behavioral Health*, vol. 21, no. 2, pp. 89-97, 2006.

[10] X. Hou, Y. Liu, O. Sourina, Y. R. E. Tan, L. Wang, and W. Mueller-Wittig, "EEG based stress monitoring," *2015 IEEE International Conference on Systems, Man, and Cybernetics*, 2015, pp. 3110-3115, doi: 10.1109/SMC.2015.540.

[11] D. H. Hellhammer, S. Wüst, and B. M. Kudielka, "Salivary cortisol as a biomarker in stress research," *Psychoneuroendocrinology*, vol. 34, no. 2, pp. 163-171, 2009.

[12] A. Haag, S. Goronzy, P. Schaich, and J. Williams, "Emotion recognition using bio-sensors: First steps towards an automatic system," In: André E., Dybkjær L., Minker W., Heisterkamp P. (eds) Affective Dialogue Systems. ADS 2004. Lecture Notes in Computer Science, vol 3068. Springer, Berlin, Heidelberg. https://doi.org/10.1007/978-3-540-24842-2_4.

[13] J. A. Healey and R. W. Picard, "Detecting stress during real-world driving tasks using physiological sensors," *IEEE Transactions on Intelligent Transportation Systems,* vol. 6, no. 2, pp. 156-166, 2005.

[14] G. Otero, F. Pliego-Rivero, T. Fernández, and J. Ricardo, "EEG development in children with sociocultural disadvantages: a follow-up study," *Clinical Neurophysiology,* vol. 114, no. 10, pp. 1918-1925, 2003.

[15] T. L. Schultz, "Technical tips: MRI compatible EEG electrodes: advantages, disadvantages, and financial feasibility in a clinical setting," *The Neurodiagnostic Journal,* vol. 52, no. 1, pp. 69-81, 2012.

[16] M. Ferrari and V. Quaresima, "A brief review on the history of human functional near-infrared spectroscopy (fNIRS) development and fields of application," *Neuroimage,* vol. 63, no. 2, pp. 921-935, 2012.

[17] T. Wilcox and M. Biondi, "fNIRS in the developmental sciences," *Wiley Interdisciplinary Reviews: Cognitive Science,* vol. 6, no. 3, pp. 263-283, 2015.

[18] V. Dubljević, C. Venero, and S. Knafo, "What is cognitive enhancement?," in *Cognitive Enhancement*: Elsevier, 2015, pp. 1-9.

[19] A. F. Arnsten, "Stress signalling pathways that impair prefrontal cortex structure and function," *Nature Reviews Neuroscience,* vol. 10, no. 6, pp. 410-422, 2009.

[20] T. H. Holmes and R. H. Rahe, "The social readjustment rating scale," *Journal of Psychosomatic Research,* vol. 11, pp. 213-218, 1967.

[21] S. M. Monroe, "Modern approaches to conceptualizing and measuring human life stress," *Annu. Rev. Clin. Psychol,* vol. 4, pp. 33-52, 2008.

[22] G. C. Blackhart, J. A. Minnix, and J. P. Kline, "Can EEG asymmetry patterns predict future development of anxiety and depression?: A preliminary study," *Biological Psychology,* vol. 72, no. 1, pp. 46-50, 2006.

[23] T.-K. Liu, Y.-P. Chen, Z.-Y. Hou, C.-C. Wang, and J.-H. Chou, "Noninvasive evaluation of mental stress using by a refined rough set technique based on biomedical signals," *Artificial Intelligence in Medicine,* vol. 61, no. 2, pp. 97-103, 2014.

[24] G. S. Shields and G. M. Slavich, "Lifetime stress exposure and health: A review of contemporary assessment methods and biological mechanisms," *Social Personality Psychology Compass,* vol. 11, no. 8, pp. e12335, 2017.

[25] D. Carneiro, J. C. Castillo, P. Novais, A. Fernández-Caballero, and J. Neves, "Multimodal behavioral analysis for non-invasive stress detection," *Expert Systems with Applications,* vol. 39, no. 18, pp. 13376-13389, 2012.

[26] G. Giannakakis, D. Manousos, V. Chaniotakis, and M. Tsiknakis, "Evaluation of head pose features for stress detection and classification," in *2018 IEEE EMBS International Conference on Biomedical & Health Informatics (BHI),* 2018, pp. 406-409.

[27] D. F. Dinges *et al.*, "Optical computer recognition of facial expressions associated with stress induced by performance demands," *Aviation, Space, and Environmental Medicine,* vol. 76, no. 6, pp. B172-B182, 2005.

[28] D. Marazziti, A. Di Muro, and P. Castrogiovanni, "Psychological stress and body temperature changes in humans," *Physiology & Behavior,* vol. 52, no. 2, pp. 393-395, 1992.

[29] S. E. Rimm-Kaufman and J. Kagan, "The psychological significance of changes in skin temperature," *Motivation and Emotion,* vol. 20, no. 1, pp. 63-78, 1996.

[30] A. Nozawa and M. Tacano, "Correlation analysis on alpha attenuation and nasal skin temperature," *Journal of Statistical Mechanics: Theory and Experiment,* vol. 2009, no. 01, pp. 1-10, 2009.

[31] J. A. Levine, I. Pavlidis, and M. Cooper, "The face of fear," *The Lancet,* vol. 357, no. 9270, pp. 1757, 2001.

[32] I. Pavlidis and J. Levine, "Thermal image analysis for polygraph testing," *IEEE Engineering in Medicine and Biology Magazine,* vol. 21, no. 6, pp. 56-64, 2002.

[33] K. Hong and S. Hong, "Real-time stress assessment using thermal imaging," *The Visual Computer,* vol. 32, no. 11, pp. 1369-1377, 2016.

[34] E. Veronika, M. Arcangelo, and A. Joshua, "Exploring the use of thermal infrared imaging in human stress research," *PLoS One,* vol. 9, no. 3, pp. 125-136, 2014.

[35] D. Farina, P. Madeleine, T. Graven-Nielsen, R. Merletti, and L. Arendt-Nielsen, "Standardising surface electromyogram recordings for assessment of activity and fatigue in the human upper trapezius muscle," *European Journal of Applied Physiology,* vol. 86, no. 6, pp. 469-478, 2002.

[36] U. Lundberg *et al.*, "Psychophysiological stress and EMG activity of the trapezius muscle," *International Journal of Behavioral Medicine,* vol. 1, no. 4, pp. 354-370, 1994.

[37] J. T. Cacioppo and L. G. Tassinary, "Inferring psychological significance from physiological signals," *American Psychologist,* vol. 45, no. 1, pp. 16, 1990.

[38] J. Wijsman, B. Grundlehner, J. Penders, and H. Hermens, "Trapezius muscle EMG as predictor of mental stress," *ACM Transactions on Embedded Computing Systems (TECS),* vol. 12, no. 4, pp. 1-20, 2010

[39] E. Simoes, R. Roark, S. Berman, L. Esler, and J. Murphy, "Respiratory rate: measurement of variability over time and accuracy at different counting periods," *Archives of Disease in Childhood,* vol. 66, no. 10, pp. 1199-1203, 1991.

[40] D. McDuff, S. Gontarek, and R. Picard, "Remote measurement of cognitive stress via heart rate variability," in *2014 36th Annual International Conference of the IEEE Engineering in Medicine and Biology Society*, 2014, pp. 2957-2960.

[41] P. Grossman, "Respiration, stress, and cardiovascular function," *Psychophysiology,* vol. 20, no. 3, pp. 284-300, 1983.

[42] M. Singh and A. B. Queyam, "Stress detection in automobile drivers using physiological parameters: A review," *International Journal of Electronics Engineering,* vol. 5, no. 2, pp. 1-5, 2013.

[43] S. A. Hosseini and M. B. Naghibi-Sistani, "Classification of emotional stress using brain activity," *Applied Biomedical Engineering,* vol. 7, pp. 313-336, 2011.

[44] D. Giakoumis *et al.*, "Using activity-related behavioural features towards more effective automatic stress detection," *PloS One,* vol. 7, no. 9, pp. e43571, 2012.

[45] M.-h. Lee, G. Yang, H.-K. Lee, and S. Bang, "Development stress monitoring system based on personal digital assistant (PDA)," in *The 26th Annual International Conference of the IEEE Engineering in Medicine and Biology Society*, 2004, vol. 1, pp. 2364-2367.

[46] J. Blechert, M. Lajtman, T. Michael, J. Margraf, and F. H. Wilhelm, "Identifying anxiety states using broad sampling and advanced processing of peripheral physiological information," *Biomedical Sciences Instrumentation,* vol. 42, pp. 136-141, 2006.

[47] G. Giannakakis *et al.*, "Stress and anxiety detection using facial cues from videos," *Biomedical Signal Processing and Control,* vol. 31, pp. 89-101, 2017.

[48] V. Engert, A. Merla, J. A. Grant, D. Cardone, A. Tusche, and T. Singer, "Exploring the use of thermal infrared imaging in human stress research," *PloS One,* vol. 9, no. 3, pp. e90782, 2014.

[49] A. J. Camm *et al.*, "Heart rate variability: standards of measurement, physiological interpretation and clinical use. Task Force of the European Society of Cardiology and the North American Society of Pacing and Electrophysiology," *Circulation,* vol. 93, pp. 1043-1065, 1996.

[50] J. P. Saul, R. Rea, D. L. Eckberg, R. D. Berger, and R. J. Cohen, "Heart rate and muscle sympathetic nerve variability during reflex changes of autonomic activity," *American Journal of Physiology-Heart and Circulatory Physiology,* vol. 258, no. 3, pp. H713-H721, 1990.

[51] N. Hjortskov, D. Rissén, A. K. Blangsted, N. Fallentin, U. Lundberg, and K. Søgaard, "The effect of mental stress on heart rate variability and blood pressure during computer work," *European Journal of Applied Physiology,* vol. 92, no. 1-2, pp. 84-89, 2004.

[52] L. Finsen, K. Søgaard, C. Jensen, V. Borg, and H. Christensen, "Muscle activity and cardiovascular response during computer-mouse work with and without memory demands," *Ergonomics,* vol. 44, no. 14, pp. 1312-1329, 2001.

[53] A. R. Subhani, W. Mumtaz, M. N. Saad, N. Kamel, and A. S. Malik, "Machine learning framework for the detection of mental stress at multiple levels," *IEEE Access,* vol. 5, pp. 13545-13556, 2017.

[54] C. Kirschbaum and D. H. Hellhammer, "Salivary cortisol in psychoneuroendocrine research: recent developments and applications," *Psychoneuroendocrinology,* vol. 19, no. 4, pp. 313-333, 1994.

[55] K. Hanrahan, A. M. McCarthy, C. Kleiber, S. Lutgendorf, and E. Tsalikian, "Strategies for salivary cortisol collection and analysis in research with children," *Applied Nursing Research,* vol. 19, no. 2, pp. 95-101, 2006.

[56] V. Engert *et al.*, "Investigation into the cross-correlation of salivary cortisol and alpha-amylase responses to psychological stress," *Psychoneuroendocrinology,* vol. 36, no. 9, pp. 1294-1302, 2011.

[57] E. Koibuchi and Y. Suzuki, "Exercise upregulates salivary amylase in humans," *Experimental and Therapeutic Medicine,* vol. 7, no. 4, pp. 773-777, 2014.

[58] M. Zanetti *et al.*, "Multilevel assessment of mental stress via network physiology paradigm using consumer wearable devices," *Journal of Ambient Intelligence and Humanized Computing,* vol. 12, no. 4, pp. 1-10, 2019.

[59] Y. Tong and B. d. Frederick, "Time lag dependent multimodal processing of concurrent fMRI and near-infrared spectroscopy (NIRS) data suggests a global circulatory origin for low-frequency oscillation signals in human brain," *Neuroimage,* vol. 53, no. 2, pp. 553-564, 2010.

[60] C. M. Michel and M. M. Murray, "Towards the utilization of EEG as a brain imaging tool," *Neuroimage,* vol. 61, no. 2, pp. 371-385, 2012.

[61] R. Hari and R. Salmelin, "Magnetoencephalography: from SQUIDs to neuroscience: Neuroimage 20th anniversary special edition," *Neuroimage,* vol. 61, no. 2, pp. 386-396, 2012.

[62] M. Ullsperger and S. Debener, *Simultaneous EEG and fMRI: recording, analysis, and application*. Oxford University Press, 2010.

[63] M. Safi-Harb, S. Proulx, N. von Ellenrieder, and J. Gotman, "Advantages and disadvantages of a fast fMRI sequence in the context of EEG–fMRI investigation of epilepsy patients: a realistic simulation study," *Neuroimage,* vol. 119, pp. 20-32, 2015.

[64] Y. Shi, Y. Zhu, R. K. Mehta, and J. Du, "A neurophysiological approach to assess training outcome under stress: A virtual reality experiment of industrial shutdown maintenance using Functional Near-Infrared Spectroscopy (fNIRS)," *Advanced Engineering Informatics,* vol. 46, pp. 101153, 2020.

[65] F. Al-Shargie, "Fusion of fNIRS and EEG Signals: Mental Stress Study," Apr. 2019, [online] Available: https://engrxiv.org/kaqew.

[66] F. Al-shargie, T. B. Tang, N. Badruddin, and M. Kiguchi, "Simultaneous measurement of EEG-fNIRS in classifying and localizing brain activation to mental stress," in *2015 IEEE International Conference on Signal and Image Processing Applications (ICSIPA),* 2015, pp. 282-286.

[67] A. V. Medvedev, "Does the resting state connectivity have hemispheric asymmetry? A near-infrared spectroscopy study," *Neuroimage,* vol. 85, pp. 400-407, 2014.

[68] A. Villringer and U. Dirnagl, "Coupling of brain activity and cerebral blood flow: basis of functional neuroimaging," *Cerebrovascular and Brain Metabolism Reviews,* vol. 7, no. 3, pp. 240-276, 1995.

[69] D. A. Boas, A. M. Dale, and M. A. Franceschini, "Diffuse optical imaging of brain activation: approaches to optimizing image sensitivity, resolution, and accuracy," *Neuroimage,* vol. 23, pp. S275-S288, 2004.

[70] DA. Pizzagalli, "Electroencephalography and high-density electrophysiological source localization," *Handbook of Psychophysiology,* vol. 3, pp. 56–84, 2007.

[71] S. Duschek and R. Schandry, "Functional transcranial Doppler sonography as a tool in psychophysiological research," *Psychophysiology,* vol. 40, no. 3, pp. 436-454, 2003.

[72] R. K. Mehta and R. Parasuraman, "Neuroergonomics: a review of applications to physical and cognitive work," *Frontiers in human neuroscience,* vol. 7, pp. 889, 2013.

[73] T. Nozawa and T. Kondo, "A comparison of artifact reduction methods for real-time analysis of fNIRS data," in *Symposium on Human Interface*, 2009: Springer, pp. 413-422.

[74] T. Zama and S. Shimada, "Simultaneous measurement of electroencephalography and near-infrared spectroscopy during voluntary motor preparation," *Scientific Reports,* vol. 5, no. 1, pp. 1-9, 2015.

[75] Y. Zhu, C. Rodriguez-Paras, J. Rhee, and R. K. Mehta, "Methodological approaches and recommendations for functional near-infrared spectroscopy applications in HF/E research," *Human Factors,* vol. 62, no. 4, pp. 613-642, 2020.

[76] Y. Tomita, F.-B. Vialatte, G. Dreyfus, Y. Mitsukura, H. Bakardjian, and A. Cichocki, "Bimodal BCI using simultaneously NIRS and EEG," *IEEE Transactions on Biomedical Engineering,* vol. 61, no. 4, pp. 1274-1284, 2014.

[77] F. Wallois, M. Mahmoudzadeh, A. Patil, and R. Grebe, "Usefulness of simultaneous EEG–NIRS recording in language studies," *Brain and Language,* vol. 121, no. 2, pp. 110-123, 2012.

[78] S. Fazli *et al.*, "Enhanced performance by a hybrid NIRS–EEG brain computer interface," *Neuroimage,* vol. 59, no. 1, pp. 519-529, 2012.

[79] T. Liu, M. Pelowski, C. Pang, Y. Zhou, and J. Cai, "Near-infrared spectroscopy as a tool for driving research," *Ergonomics,* vol. 59, no. 3, pp. 368-379, 2016.

[80] Y. Shi, Y. Zhu, R. K. Mehta, and J. Du, "A neurophysiological approach to assess training outcome under stress: A virtual reality experiment of industrial shutdown maintenance using Functional Near-Infrared Spectroscopy (fNIRS)," *Advanced Engineering Informatics,* vol. 46, pp. 101153, 2020.

[81] M. Mücke, S. Ludyga, F. Colledge, U. Pühse, and M. Gerber, "Association of Exercise with Inhibitory Control and Prefrontal Brain Activity Under Acute Psychosocial Stress," *Brain Sciences,* vol. 10, no. 7, pp. 439, 2020.

[82] N. Z. Gurel, H. Jung, S. Hersek, and O. T. Inan, "Fusing near-infrared spectroscopy with wearable hemodynamic measurements improves classification of mental stress," *IEEE Sensors Journal,* vol. 19, no. 19, pp. 8522-8531, 2018.

[83] F. Al-shargie, T. B. Tang, and M. Kiguchi, "Mental stress grading based on fNIRS signals," in *2016 38th Annual International Conference of the IEEE Engineering in Medicine and Biology Society (EMBC)*, 2016, pp. 5140-5143.

[84] R. A. Shirvan, S. K. Setaredan, and A. M. Nasrabadi, "Classification of mental stress levels by analyzing fNIRS signal using linear and non-linear features," *International Clinical Neuroscience Journal,* vol. 5, no. 2, pp. 55, 2018.

[85] F. Al-Shargie, M. Kiguchi, N. Badruddin, S. C. Dass, A. F. M. Hani, and T. B. Tang, "Mental stress assessment using simultaneous measurement of EEG and fNIRS," *Biomedical Optics Express,* vol. 7, no. 10, pp. 3882-3898, 2016.

[86] R. Li, T. Nguyen, T. Potter, and Y. Zhang, "Dynamic cortical connectivity alterations associated with Alzheimer's disease: An EEG and fNIRS integration study," *NeuroImage: Clinical,* vol. 21, pp. 101622, 2019.

[87] Y. Minagawa-Kawai, H. Van Der Lely, F. Ramus, Y. Sato, R. Mazuka, and E. Dupoux, "Optical brain imaging reveals general auditory and language-specific processing in early infant development," *Cerebral Cortex,* vol. 21, no. 2, pp. 254-261, 2011.

[88] H. Bortfeld, E. Wruck, and D. A. Boas, "Assessing infants' cortical response to speech using near-infrared spectroscopy," *Neuroimage,* vol. 34, no. 1, pp. 407-415, 2007.

[89] R. N. Aslin and J. Mehler, "Near-infrared spectroscopy for functional studies of brain activity in human infants: promise, prospects, and challenges," *Journal of Biomedical Optics,* vol. 10, no. 1, pp. 011009, 2005.

[90] M. Hu, T. Shealy, J. Grohs, and R. Panneton, "Empirical evidence that concept mapping reduces neurocognitive effort during concept generation for sustainability," *Journal of Cleaner Production,* vol. 238, pp. 117815, 2019.

[91] M. Hu, T. Shealy, M. Hallowell, and D. Hardison, "Advancing construction hazard recognition through neuroscience: Measuring cognitive response to hazards using functional near infrared spectroscopy," in *Construction Research Congress 2018*, 2018, pp. 134-143.

[92] J. Du, Q. Zhu, Y. Shi, Q. Wang, Y. Lin, and D. Zhao, "Cognition digital twins for personalized information systems of smart cities: Proof of concept," *Journal of Management in Engineering,* vol. 36, no. 2, pp. 04019052, 2020.

[93] M. A. Yücel, J. J. Selb, T. J. Huppert, M. A. Franceschini, and D. A. Boas, "Functional near infrared spectroscopy: enabling routine functional brain imaging," *Current Opinion in Biomedical Engineering,* vol. 4, pp. 78-86, 2017.

[94] T. Huppert, J. Barker, B. Schmidt, S. Walls, and A. Ghuman, "Comparison of group-level, source localized activity for simultaneous functional near-infrared spectroscopy-magnetoencephalography and simultaneous fNIRS-fMRI during parametric median nerve stimulation," *Neurophotonics,* vol. 4, no. 1, pp. 015001, 2017.

[95] H. Obrig, "NIRS in clinical neurology—a 'promising'tool?," *Neuroimage,* vol. 85, pp. 535-546, 2014.

[96] S. Lloyd-Fox, A. Blasi, and C. Elwell, "Illuminating the developing brain: the past, present and future of functional near infrared spectroscopy," *Neuroscience & Biobehavioral Reviews,* vol. 34, no. 3, pp. 269-284, 2010.

[97] I. Miyai *et al.*, "Cortical mapping of gait in humans: a near-infrared spectroscopic topography study," *Neuroimage,* vol. 14, no. 5, pp. 1186-1192, 2001.

[98] V. Quaresima and M. Ferrari, "Functional near-infrared spectroscopy (fNIRS) for assessing cerebral cortex function during human behavior in natural/social situations: a concise review," *Organizational Research Methods,* vol. 22, no. 1, pp. 46-68, 2019.

[99] L. Xu, B. Wang, G. Xu, W. Wang, Z. Liu, and Z. Li, "Functional connectivity analysis using fNIRS in healthy subjects during prolonged simulated driving," *Neuroscience Letters,* vol. 640, pp. 21-28, 2017.

[100] D. Dong, L. K. Wong, and Z. Luo, "Assessment of Prospective Memory using fNIRS in Immersive Virtual Reality Environment," *Journal of Behavioral and Brain Science,* vol. 7, no. 06, pp. 247, 2017.

[101] S. B. Moro *et al.*, "A semi-immersive virtual reality incremental swing balance task activates prefrontal cortex: a functional near-infrared spectroscopy study," *Neuroimage,* vol. 85, pp. 451-460, 2014.

[102] A. De, S. Biswas, A. Konar, and L. Ghosh, "A Functional Near Infrared Spectroscopy Based Evaluation of Cognitive Lagging from Prefrontal Hemodynamics," *IEEE Sensors Letters,* vol. 4, no. 6, pp. 1-4, 2020.

[103] Y. L. Chan, W. C. Ung, L. G. Lim, C.-K. Lu, M. Kiguchi, and T. B. Tang, "Automated Thresholding Method for fNIRS-Based Functional Connectivity Analysis: Validation With a Case Study on Alzheimer's Disease," *IEEE Transactions on Neural Systems and Rehabilitation Engineering,* vol. 28, no. 8, pp. 1691-1701, 2020.

[104] M. Parent, V. Peysakhovich, K. Mandrick, S. Tremblay, and M. Causse, "The diagnosticity of psychophysiological signatures: Can we disentangle mental workload from acute stress with ECG and fNIRS?," *International Journal of Psychophysiology,* vol. 146, pp. 139-147, 2019.

[105] J. M. Baker, J. L. Bruno, A. Gundran, S. H. Hosseini, and A. L. Reiss, "fNIRS measurement of cortical activation and functional connectivity during a visuospatial working memory task," *PloS one,* vol. 13, no. 8, pp. e0201486, 2018.

[106] A. Saidatul, M. Paulraj, S. Yaacob, and N. M. Nasir, "Automated system for stress evaluation based on EEG signal: A prospective review," in *2011 IEEE 7th International Colloquium on Signal Processing and its Applications*, pp. 167-171, 2011.

[107] A. R. Subhani, L. Xia, and A. S. Malik, "EEG signals to measure mental stress," in *2nd International Conference on Behavioral, Cognitive and Psychological Sciences*, pp. 84-88, 2011

[109] B. Horwitz, "The elusive concept of brain connectivity," *Neuroimage,* vol. 19, no. 2, pp. 466-470, 2003.

[110] K. J. Friston, "Functional and effective connectivity in neuroimaging: a synthesis," *Human Brain Mapping,* vol. 2, no. 1-2, pp. 56-78, 1994.

[111] K. J. Friston, "Functional and effective connectivity: a review," *Brain Connectivity,* vol. 1, no. 1, pp. 13-36, 2011.

[112] E. Bullmore and O. Sporns, "Complex brain networks: graph theoretical analysis of structural and functional systems," *Nature Reviews Neuroscience,* vol. 10, no. 3, pp. 186-198, 2009.

[113] K. Lambourne and P. Tomporowski, "The effect of exercise-induced arousal on cognitive task performance: a meta-regression analysis," *Brain Research,* vol. 1341, pp. 12-24, 2010.

[114] R. Ballester, F. Huertas, E. Molina, and D. Sanabria, "Sport participation and vigilance in children: Influence of different sport expertise," *Journal of Sport and Health Science,* vol. 7, no. 4, pp. 497-504, 2018.

[115] H. R. Lieberman, C. M. Falco, and S. S. Slade, "Carbohydrate administration during a day of sustained aerobic activity improves vigilance, as assessed by a novel ambulatory monitoring device, and mood," *The American Journal of Clinical Nutrition,* vol. 76, no. 1, pp. 120-127, 2002.

[116] K. A. MacLean *et al.,* "Intensive meditation training improves perceptual discrimination and sustained attention," *Psychological Science,* vol. 21, no. 6, pp. 829-839, 2010.

[117] A. J. Johnson, "Cognitive facilitation following intentional odor exposure," *Sensors,* vol. 11, no. 5, pp. 5469-5488, 2011.

[118] E. Matsubara *et al.,* "Volatiles emitted from the leaves of Laurus nobilis L. improve vigilance performance in visual discrimination task," *Biomedical Research,* vol. 32, no. 1, pp. 19-28, 2011.

[119] H. R. R. N. Sheela and T. S. Ganpat, "Efficacy of Yoga for sustained attention in university students," *Ayu,* vol. 34, no. 3, pp. 270, 2013.

[120] S. Telles, R. K. Gupta, S. Verma, N. Kala, and A. Balkrishna, "Changes in vigilance, self rated sleep and state anxiety in military personnel in India following yoga," *BMC Research Notes,* vol. 11, no. 1, pp. 518, 2018.

[121] Y. Hirano and M. Onozuka, "Chewing and attention: a positive effect on sustained attention," *BioMed Research International,* vol. 2015, pp. 1-7, 2015.

[122] T. M. McLellan, G. H. Kamimori, D. M. Voss, D. G. Bell, K. G. Cole, and D. Johnson, "Caffeine maintains vigilance and improves run times during night operations for Special Forces," *Aviation, Space, and Environmental Medicine,* vol. 76, no. 7, pp. 647-654, 2005.

[123] I. P. Bodala, S. Kukreja, J. Li, N. V. Thakor, and H. Al-Nashash, "Eye tracking and EEG synchronization to analyze microsaccades during a workload task," in *2015 37th Annual International Conference of the IEEE Engineering in Medicine and Biology Society (EMBC),* pp. 7994-7997, 2015

[124] J. L. Szalma, T. Schmidt, G. Teo, and P. A. Hancock, "Vigilance on the move: video game-based measurement of sustained attention," *Ergonomics,* vol. 57, no. 9, pp. 1315-1336, 2014.

[125] J. Szalma, T. Daly, G. Teo, G. Hancock, and P. Hancock, "Training for vigilance on the move: A video game-based paradigm for sustained attention," *Ergonomics,* vol. 61, no. 4, pp. 482-505, 2018.

[126] J. T. Nelson, R. A. McKinley, E. J. Golob, J. S. Warm, and R. Parasuraman, "Enhancing vigilance in operators with prefrontal cortex transcranial direct current stimulation (tDCS)," *Neuroimage,* vol. 85, pp. 909-917, 2014.

[127] B. S. Löffler *et al.*, "Counteracting the slowdown of reaction times in a vigilance experiment with 40-Hz transcranial alternating current stimulation," *IEEE Transactions on Neural Systems and Rehabilitation Engineering,* vol. 26, no. 10, pp. 2053-2061, 2018.

[128] G. R. Arrabito, G. Ho, B. Aghaei, C. Burns, and M. Hou, "Sustained attention in auditory and visual monitoring tasks: Evaluation of the administration of a rest break or exogenous vibrotactile signals," *Human Factors,* vol. 57, no. 8, pp. 1403-1416, 2015.

[129] S. A. McBride, R. F. Johnson, D. J. Merullo, and R. E. Bartow Jr, "Effects of the periodic administration of odor or vibration on a 3-hr. vigilance task," *Perceptual and Motor Skills,* vol. 98, no. 1, pp. 307-318, 2004.

[130] S. Zhang, D. Wang, N. Afzal, Y. Zhang, and R. Wu, "Rhythmic haptic stimuli improve short-term attention," *IEEE Transactions on Haptics,* vol. 9, no. 3, pp. 437-442, 2016.

[131] C. E. Giurgea, "The nootropic concept and its prospective implications," *Drug Development Research,* vol. 2, no. 5, pp. 441-446, 1982.

[132] G. E. Prinsloo, H. L. Rauch, and W. E. Derman, "A brief review and clinical application of heart rate variability biofeedback in sports, exercise, and

rehabilitation medicine," *The Physician and Sportsmedicine,* vol. 42, no. 2, pp. 88-99, 2014.

[133] P. L. Schoenberg and A. S. David, "Biofeedback for psychiatric disorders: a systematic review," *Applied Psychophysiology and Biofeedback,* vol. 39, no. 2, pp. 109-135, 2014.

[134] A. R. Subhani, N. Kamel, M. N. M. Saad, N. Nandagopal, K. Kang, and A. S. Malik, "Mitigation of stress: new treatment alternatives," *Cognitive Neurodynamics,* vol. 12, no. 1, pp. 1-20, 2018.

[135] A. K. Bader, C. Reade, and F. J. Froese, "Terrorism and expatriate withdrawal cognitions: the differential role of perceived work and non-work constraints," *The International Journal of Human Resource Management,* vol. 30, no. 11, pp. 1769-1793, 2019.

[136] F. Al-Shargie, U. Tariq, H. Mir, H. Alawar, F. Babiloni, and H. Al-Nashash, "Vigilance decrement and enhancement techniques: a review," *Brain sciences,* vol. 9, no. 8, pp. 178, 2019.

[137] J. D. Lane, S. J. Kasian, J. E. Owens, and G. R. Marsh, "Binaural auditory beats affect vigilance performance and mood," *Physiology & behavior,* vol. 63, no. 2, pp. 249-252, 1998.

[138] J. A. Frederick, J. F. Lubar, H. W. Rasey, S. A. Brim, and J. Blackburn, "Effects of 18.5 Hz auditory and visual stimulation on EEG amplitude at the vertex," *Journal of Neurotherapy,* vol. 3, no. 3-4, pp. 23-28, 1999.

[139] S. A. Reedijk, A. Bolders, L. S. Colzato, and B. Hommel, "Eliminating the attentional blink through binaural beats: a case for tailored cognitive enhancement," *Frontiers in Psychiatry,* vol. 6, pp. 82, 2015.

[140] B. Isik, A. Esen, B. Büyükerkmen, A. Kilinc, and D. Menziletoglu, "Effectiveness of binaural beats in reducing preoperative dental anxiety," *British Journal of Oral and Maxillofacial Surgery,* vol. 55, no. 6, pp. 571-574, 2017.

[141] C. Beauchene, N. Abaid, R. Moran, R. A. Diana, and A. Leonessa, "The effect of binaural beats on verbal working memory and cortical connectivity," *Journal of Neural Engineering,* vol. 14, no. 2, pp. 026014, 2017.

[142] L. S. Colzato, H. Barone, R. Sellaro, and B. Hommel, "More attentional focusing through binaural beats: Evidence from the global–local task," *Psychological Research,* vol. 81, no. 1, pp. 271-277, 2017.

[143] D. Vernon, Human potential: Exploring techniques used to enhance human performance. Routledge, 2009.

[144] P. Goodin, J. Ciorciari, K. Baker, A.-M. Carrey, M. Harper, and J. Kaufman, "A high-density EEG investigation into steady state binaural beat stimulation," *PloS One,* vol. 7, no. 4, pp. e34789, 2012.

[145] S. Skau, I. H. Jonsdottir, A. Sjörs Dahlman, B. Johansson, and H. G. Kuhn, "Exhaustion disorder and altered brain activity in frontal cortex detected with fNIRS," *Stress,* vol. 24, no. 1, pp. 64-75, 2021.

[146] D. Rosenbaum *et al.,* "Insights from a laboratory and naturalistic investigation on stress, rumination and frontal brain functioning in MDD: An fNIRS study," *Neurobiology of stress,* pp. 100344, 2021.

[147] A. Olszewska-Guizzo *et al.,* "Hemodynamic Response to Three Types of Urban Spaces before and after Lockdown during the COVID-19 Pandemic," *International Journal of Environmental Research and Public Health,* vol. 18, no. 11, pp. 6118, 2021.

[148] E. Alyan, N. M. Saad, N. Kamel, and M. A. Rahman, "Workplace design-related stress effects on prefrontal cortex connectivity and neurovascular coupling," *Applied Ergonomics,* vol. 96, pp. 103497, 2021.

[149] E. Alyan, N. M. Saad, N. Kamel, S. S. Al-Bawri, M. A. Zakariya, and M. A. Rahman, "Identifying the Impact of Noise-Levels on Mental Stress: An EEG-fNIRS Study," *Journal of Physics: Conference Series,* vol. 1962, no. 1, pp. 012006, 2021.

[150] I. Park, Y. Kim, and S. K. Kim, "Athlete-Specific Neural Strategies under Pressure: A fNIRS Pilot Study," *International Journal of Environmental Research and Public Health,* vol. 17, no. 22, pp. 8464, 2020.

[151] M. Mirbagheri, N. Hakimi, E. Ebrahimzadeh, and S. K. Setarehdan, "Quality analysis of heart rate derived from functional near-infrared spectroscopy in stress assessment," *Informatics in Medicine Unlocked,* vol. 18, pp. 100286, 2020.

[152] E. Alyan, N. M. Saad, N. Kamel, and M. A. Rahman, "Investigating Frontal Neurovascular Coupling in Response to Workplace Design-Related Stress," *IEEE Access,* vol. 8, pp. 218911-218923, 2020.

[153] H. Santosa, A. Aarabi, S. B. Perlman, and T. Huppert, "Characterization and correction of the false-discovery rates in resting state connectivity using functional near-infrared spectroscopy," *Journal of Biomedical Optics,* vol. 22, no. 5, pp. 055002, 2017.

[154] G. Vergotte *et al.,* "Dynamics of the human brain network revealed by time-frequency effective connectivity in fNIRS," *Biomedical Optics Express,* vol. 8, no. 11, pp. 5326-5341, 2017.

[155] M. Causse, Z. Chua, V. Peysakhovich, N. Del Campo, and N. Matton, "Mental workload and neural efficiency quantified in the prefrontal cortex using fNIRS," *Sci. Rep,* vol. 7, no. 1, pp. 5222, 2017.

[156] J. Shin, K.-R. Müller, and H.-J. Hwang, "Near-infrared spectroscopy (NIRS)-based eyes-closed brain-computer interface (BCI) using prefrontal cortex activation due to mental arithmetic," *Scientific Reports,* vol. 6, pp. 36203, 2016.

[157] N. Naseer, N. K. Qureshi, F. M. Noori, and K.-S. Hong, "Analysis of different classification techniques for two-class functional near-infrared spectroscopy-based brain-computer interface," *Computational Intelligence and Neuroscience*, vol. 2016, pp. 1-11, 2016.

[158] K.-S. Hong, N. Naseer, and Y.-H. Kim, "Classification of prefrontal and motor cortex signals for three-class fNIRS–BCI," *Neuroscience Letters*, vol. 587, pp. 87-92, 2015.

[159] H.-J. Hwang, J.-H. Lim, D.-W. Kim, and C.-H. Im, "Evaluation of various mental task combinations for near-infrared spectroscopy-based brain-computer interfaces," *Journal of Biomedical Optics*, vol. 19, no. 7, pp. 077005, 2014.

[160] L. Zhang, J. Sun, B. Sun, Q. Luo, and H. Gong, "Studying hemispheric lateralization during a Stroop task through near-infrared spectroscopy-based connectivity," *Journal of Biomedical Optics*, vol. 19, no. 5, pp. 057012, 2014.

[161] G. Durantin, J.-F. Gagnon, S. Tremblay, and F. Dehais, "Using near infrared spectroscopy and heart rate variability to detect mental overload," *Behavioural Brain Research*, vol. 259, pp. 16-23, 2014.

[162] C.-M. Lu, Y.-J. Zhang, B. B. Biswal, Y.-F. Zang, D.-L. Peng, and C.-Z. Zhu, "Use of fNIRS to assess resting state functional connectivity," *Journal of Neuroscience Methods*, vol. 186, no. 2, pp. 242-249, 2010.

[163] P. Valdez, C. Ramírez, A. García, J. Talamantes, P. Armijo, and J. Borrani, "Circadian rhythms in components of attention," *Biological Rhythm Research*, vol. 36, no. 1-2, pp. 57-65, 2005.

[164] F. Scarpina and S. Tagini, "The stroop color and word test," *Frontiers in Psychology*, vol. 8, pp. 557, 2017.

[165] D. A. Washburn, "The Stroop effect at 80: The competition between stimulus control and cognitive control," *Journal of the Experimental Analysis of Behavior*, vol. 105, no. 1, pp. 3-13, 2016.

[166] F. Gutiérrez-Martínez, M. Ramos-Ortega, and J. Ó. Vila-Chaves, "Executive efficacy on Stroop type interference tasks. A validation study of a numerical and manual version (CANUM)," *Anales de Psicología*, vol. 34, no. 1, pp. 184-196, 2018.

[167] W. Van der Elst, M. P. Van Boxtel, G. J. Van Breukelen, and J. Jolles, "The Stroop color-word test: influence of age, sex, and education; and normative data for a large sample across the adult age range," *Assessment*, vol. 13, no. 1, pp. 62-79, 2006.

[168] M. J. Kane and R. W. Engle, "Working-memory capacity and the control of attention: the contributions of goal neglect, response competition, and task set to Stroop interference," *Journal of Experimental Psychology: General*, vol. 132, no. 1, pp. 47-70, 2003.

[169] F. Al-Shargie, U. Tariq, O. Hassanin, H. Mir, F. Babiloni, and H. Al-Nashash, "Brain Connectivity Analysis Under Semantic Vigilance and Enhanced Mental States," *Brain Sciences,* vol. 9, no. 12, pp. 1-29, 2019.

[170] M. L. Schroeter, S. Zysset, and D. Y. von Cramon, "Shortening intertrial intervals in event-related cognitive studies with near-infrared spectroscopy," *Neuroimage,* vol. 22, no. 1, pp. 341-346, 2004.

[171] R. T. Chatterton Jr, K. M. Vogelsong, Y. c. Lu, A. B. Ellman, and G. A. Hudgens, "Salivary α-amylase as a measure of endogenous adrenergic activity," *Clinical Physiology,* vol. 16, no. 4, pp. 433-448, 1996.

[172] N. Rohleder, U. Nater, J. M. Wolf, U. Ehlert, and C. Kirschbaum, "Psychosocial stress-induced activation of salivary alpha-amylase," *Annals of the New York Academy of Sciences,* vol. 1032, no. 1, pp. 258-263, 2004.

[173] L. Chaieb and J. Fell, "Binaural Beat Stimulation," *Theory-Driven Approaches to Cognitive Enhancement*, L. S. Colzato Ed. Cham: Springer International Publishing, pp. 167-181, 2017

[174] V. Thakur, "What Are Binaural Beats?," vol. 1024*544, ed. Science ABC, 2020.

[175] S. G. Hart and L. E. Staveland, "Development of NASA-TLX (Task Load Index): Results of empirical and theoretical research," *Advances in Psychology*, vol. 52, pp. 139-183, 1988

[176] H. Santosa, X. Zhai, F. Fishburn, and T. Huppert, "The NIRS brain AnalyzIR toolbox," *Algorithms,* vol. 11, no. 5, pp. 1-33, 2018.

[177] A. Sassaroli and S. Fantini, "Comment on the modified Beer–Lambert law for scattering media," *Physics in Medicine & Biology*, vol. 49, no. 14, pp. N255-N257, 2004.

[178] F. M. Al-Shargie, O. Hassanin, U. Tariq, and H. Al-Nashash, "EEG-Based Semantic Vigilance Level Classification Using Directed Connectivity Patterns and Graph Theory Analysis," *IEEE Access,* vol. 8, pp. 115941-115956, 2020.

[179] C. R. Buchanan *et al.*, "The effect of network thresholding and weighting on structural brain networks in the UK Biobank," *NeuroImage,* vol. 211, pp. 116-443, 2020.

[180] N. Langer, A. Pedroni, and L. Jäncke, "The problem of thresholding in small-world network analysis," *PloS One,* vol. 8, no. 1, pp. 1-9, 2013.

[181] S. Achard and E. Bullmore, "Efficiency and cost of economical brain functional networks," *PLoS Computational Biology*, vol. 3, no. 2, pp. 0174-0183, 2007.

[182] M. Jalili and M. G. Knyazeva, "Constructing brain functional networks from EEG: partial and unpartial correlations," *Journal of Integrative Neuroscience*, vol. 10, no. 02, pp. 213-232, 2011.

[183] M. Rubinov and O. Sporns, "Complex network measures of brain connectivity: uses and interpretations," *Neuroimage,* vol. 52, no. 3, pp. 1059-1069, 2010.

[184] G. Fagiolo, "Clustering in complex directed networks," *Physical Review E*, vol. 76, no. 2, pp. 026-107, 2007.

[185] D. Choi, Y. Noh, and R. Jin Sung, "Work pressure and burnout effects on emergency room operations: a system dynamics simulation approach," *Service Business*, vol. 13, no. 3, pp. 433-456, 2019.

[186] M. Sniedovich, "Dijkstra's algorithm revisited: the dynamic programming connexion," *Control and Cybernetics*, vol. 35, pp. 599-620, 2006.

[187] W. Shu-Xi, "The improved dijkstra's shortest path algorithm and its application," *Procedia Engineering*, vol. 29, pp. 1186-1190, 2012.

[188] E. Alpaydin, *Introduction to machine learning*. MIT press, Cambridge, MA, USA, 2020.

[189] S. C. Wang, "Artificial neural network," in *Interdisciplinary Computing in Java Programming*, Boston, MA:Springer, pp. 81-100, 2003.

[190] Roffo, Giorgio. "Ranking to learn and learning to rank: On the role of ranking in pattern recognition applications." *CoRR*, vol. abs/1706.05933, pp. 1-245, 2017.

[191] Y. LeCun, Y. Bengio, and G. Hinton, "Deep learning," *Nature*, vol. 521, no. 7553, pp. 436-444, 2015.

[192] M. Paluszek and S. Thomas, *Practical MATLAB Deep Learning: A Project-Based Approach*. Apress, 2020.

[193] T. Nguyen et al., "Utilization of a combined EEG/NIRS system to predict driver drowsiness", *Sci*. Rep., vol. 7, pp. 1-10, 2017.

[194] M. J. Khan and K.-S. Hong, "Passive BCI based on drowsiness detection: an fNIRS study," *Biomedical Optics Express*, vol. 6, no. 10, pp. 4063-4078, 2015.

[195] S. Ahn, T. Nguyen, H. Jang, J. G. Kim, and S. C. Jun, "Exploring neuro-physiological correlates of drivers' mental fatigue caused by sleep deprivation using simultaneous EEG, ECG, and fNIRS data," *Frontiers in Human Neuroscience*, vol. 10, pp. 1-14, 2016, doi: 10.3389/fnhum.2016.00219

[196] Y.-H. Kwon, S.-B. Shin, and S.-D. Kim, "Electroencephalography based fusion two-dimensional (2D)-convolution neural networks (CNN) model for emotion recognition system," *Sensors*, vol. 18, no. 5, pp. 1-13, 2018, doi: 10.3389/fnhum.2016.00219

[197] D. M. Khan, N. Yahya, N. Kamel, and I. Faye, "Effective Connectivity in Default Mode Network for Alcoholism Diagnosis," *IEEE Transactions on Neural Systems and Rehabilitation Engineering*, vol. 29, pp. 796-808, 2021.

[198] S. Albawi, T. A. Mohammed, and S. Al-Zawi, "Understanding of a convolutional neural network," *2017 International Conference on Engineering and Technology (ICET)*, 2017, pp. 1-6, doi: 10.1109/ICEngTechnol.2017.8308186.

[199] S. i. Tamura and M. Tateishi, "Capabilities of a four-layered feedforward neural network: four layers versus three," *IEEE Transactions on Neural Networks,* vol. 8, no. 2, pp. 251-255, 1997.

[200] A. Delorme and S. Makeig, "EEGLAB: an open source toolbox for analysis of single-trial EEG dynamics including independent component analysis," *Journal of Neuroscience Methods,* vol. 134, no. 1, pp. 9-21, 2004.

Vita

Rateb Katmah was born in 1996, in Homs, Syria. He received his primary and secondary education in Homs, Syria. He received his B.Sc. degree in Biomedical Engineering from the Jordan University of Science and Technology in 2018. From 2018 to 2020, he worked as a teacher in Genius Academy, Jordan.

In January 2020, he joined the Biomedical Engineering master's program in the American University of Sharjah as a graduate research assistant. During his master's study, he authored "A Review on Mental Stress Assessment Methods Using EEG Signals" and "Connectivity Analysis under Mental Stress using fNIRS" papers. His research interests are in assessment and mitigation of mental stress via fNIRS/EEG neuroimaging techniques, eye tracking, and binaural beat stimulation.